

Design and Demonstration of a Spark Ignition Engine Operating in a Stratified-EGR Mode

by

Sangmyeong Han

S.B., Mechanical Engineering
Seoul National University (1985)

S.M., Mechanical Engineering
Seoul National University (1987)

Submitted to the Department of Mechanical Engineering
in partial fulfillment of the requirements for the Degree of

Doctor of Philosophy

at the

MASSACHUSETTS INSTITUTE OF TECHNOLOGY

May 1997

© Massachusetts Institute of Technology
All rights reserved

Signature of Author _____
Department of Mechanical Engineering
May 1997

Certified by _____
Wai K. Cheng
Associate Professor, Department of Mechanical Engineering
Thesis Adviser

Accepted by _____
Ain A. Sonin
Chairperson, Department Graduate Committee

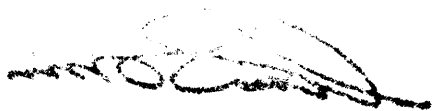
MASSACHUSETTS INSTITUTE
OF TECHNOLOGY

JUL 21 1997

eng.

LIBRARIES

(This page was intentionally left blank)

A handwritten signature in black ink, appearing to be a stylized name, possibly "M. J. ...".

Design and Demonstration of a Spark Ignition Engine Operating in a Stratified-EGR Mode

by
Sangmyeong Han

Submitted to the Department of Mechanical Engineering
on May 19, 1997 in partial fulfillment of the requirements for
the Degree of Doctor of Philosophy

Abstract

The use of substantial amount of exhaust gas recirculation (EGR) via the technique of flow stratification in-cylinder was investigated to improve the fuel economy of spark ignition engines under part load. The fuel economy gain is achieved by reducing the pumping loss with EGR while the stratification enables stable combustion at high levels of EGR. By doing so, the ability to control NO_x emissions using the three-way catalytic converter is also retained. To realize this goal, a new method of supplying EGR to achieve in-cylinder stratification was incorporated and experiments were performed to demonstrate the concept.

A new transparent engine facility was constructed to assist the development of the stratified EGR strategy. In order to minimize the mixing in intake port, to maintain the stratification in cylinder, and to obtain fast burn, an intake flow control system was realized by using solenoid valve-controlled EGR injection. Qualitative measurements of in-cylinder flow motion at motoring condition were carried out with visualization techniques such as planar laser-induced fluorescence (PLIF) and Mie scattering to obtain information on the mixing process during intake and compression. The engine was operated at firing condition to assess the engine performance operating in a stratified-EGR mode. Cylinder pressure measurements were used to gain information about the combustion process. A new combustion model incorporating mixing and flame stretch factor, which is believed to be significant, especially under the diluted mixture condition, was developed to examine flame propagation properties under the stratified condition.

The visualization results of PLIF showed that the stratification between air/fuel mixture and EGR gas was relatively well established during the intake stroke. There was, however, significant mixing in the late part of the compression stroke. This process may be explained by that large scale tumble motion was introduced into the cylinder during the intake stroke, and that the organized motion broke into small eddies during the compression stroke and hence resulted in the substantial mixing then. Performance comparison between the engine operating with the homogeneous mixture and with the stratified mixture illustrated that the stratified mode had greatly improved fuel consumption and had provided stable combustion at high dilution ratio. The observed trend on the burning process could be reproduced reasonably well by the model.

Thesis Advisor

Wai K. Cheng
Associate professor of Mechanical Engineering

Acknowledgments

“Where there is a will, there is a way.”, which has encouraged me to challenge and to explore a new world through my life. This work is another accomplishment of those words.

This page is not enough space to fully acknowledge all the people who helped me confront adversities in MIT life. To those who helped but are not mentioned by name here, my apologies go.

First, I especially would like to express my gratitude to my advisor, Prof. Wai K. Cheng for his understanding and support. I appreciate all discussion about automotive industry as well as my research. I would like to thank Prof. John B. Heywood for encouragement and suggestion on my research. Prof. J.L. Smith, Jr., a member of committee, deserves my thanks for his suggestion.

I would like to thank my office mates for their friendship, especially Mike Shelby for the help on the visualization test, Robert Meyer, Norman Peralta, Brad VanDerWege, Mark Dawson, Haissam Haidar, Carlos Herrera. We talked about too many things including our research, engines and life, sometimes over drinking beer. I want to mention the students of Sloan Automotive Lab, Tung-Ching Tseng, Wolf Bauer, J.R. Linna, Bouke Noordzij and Tian Tian. I also want to thank Brian Corkum, Nancy Cook and Dr. Victor Wong for their help.

Special thanks go to Korean friends, Kyoungdug Min, Daeyup Lee, Youngchul Ra, Byeongjin Lim and the members of KGSA ME. My sincere gratitude goes to Younggy Shin and his family for their friendship and help.

My parents, brothers, sisters and sisters-in-law deserve my special appreciation for their love, support and sacrifice to get me where I am. They have been always there for me.

I would like to express my gratitude to my parents-in-law for their support.

I would like to dedicate this thesis to my wife, Kyoungja. She has been a best friend and advisor through the good times and bad times. Even though she is always busy to take care of everything at home, she willingly made time to correct my English writings. My sons, Changhee and Unghee, always have been waiting for me to have time with, which I could not make. They deserve my deepest appreciation for their love and devotion. Without their endurance and patience, this work would never have been finished.

I would like to thank people in DAEWOO who helped me study here. This work has been supported by DAEWOO MOTOR CO., Ltd.

Table of Contents

	Page
Title Page	1
Abstract	3
Acknowledgments	4
Table of Contents	5
List of Tables	8
List of Figures	9
CHAPTER 1 Introduction	14
1.1 Previous studies.....	14
1.1.1 Lean burn engine.....	15
1.1.2 Engine operating at high level of charge dilution.....	15
1.2 Objective and approach.....	16
1.3 The engine concept.....	17
1.4 Engine development procedure.....	18
CHAPTER 2 Apparatus and diagnostics	20
2.1 Experimental procedure.....	20
2.1.1 The transparent engine.....	20
2.1.2 Artificial EGR gas supply and control of mixing.....	22
2.1.3 Instrumentation and data acquisition.....	22
2.1.4 Experimental setup for visualization.....	25
2.1.4.1 Mie scattering flow visualization.....	25
2.1.4.2 Planar Laser Induced Fluorescence(PLIF) flow visualization.....	26
2.1.4.3 Shadowgraph flame visualization.....	26
2.1.4.4 System synchronization.....	27
2.1.5 Experimental setup for firing test.....	27
2.2 Experiments.....	27

2.2.1	Engine motoring.....	27
2.2.2	Flow visualization.....	28
2.2.2.1	Mie scattering flow visualization.....	28
2.2.2.2	PLIF flow visualization.....	29
2.2.2.3	Shadowgraph flame visualization.....	30
2.2.3	System performance.....	30
2.2.4	Engine performance.....	30
CHAPTER 3 System performance analysis.....		32
3.1	Analysis of pressure data.....	32
3.2	Heat release analysis and statistics.....	33
3.2.1	Individual cycle variables.....	34
3.2.2	Misfires, partial burn cycles and operating limits.....	36
3.2.3	Sample size and uncertainty.....	36
3.2.4	Statistics.....	37
3.3	Image processing and calibration.....	37
CHAPTER 4 Engine development.....		40
4.1	Effects of tumble motion on combustion.....	40
4.1.1	Tumble enhancement by intake port partitions through the tumble adapter.....	40
4.2	Realization of charge stratification.....	41
4.2.1	In-cylinder visualization results.....	42
4.2.2	Phasing of artificial EGR injection and its effect on combustion..	43
4.3	Effects of the charge stratification on engine performance.....	47
4.3.1	Reference operation.....	47
4.3.2	Lean limit extension.....	47
4.3.3	Dilute limit extension.....	49
4.3.4	Comparison between lean burn and EGR.....	51
4.4	Identifying the design performance limit and its improvement.....	53
4.4.1	Charge mixing in the intake port and during the intake stroke.....	53
4.4.2	Charge mixing during the compression stroke.....	53
4.4.3	Charge mixing during the flame propagation phase.....	54
4.5	Discussion on engine implementation.....	54

CHAPTER 5 Model for lean/dilute combustion in the stratified EGR engine.....	56
5.1 Overview.....	56
5.2 Modeling assumptions and approach.....	57
5.3 Combustion model.....	57
5.3.1 Eddy burning model.....	57
5.3.2 Laminar flame speed.....	59
5.3.3 Modeling of strain rate factor I_0	60
5.3.3.1 Model I : general approach.....	60
5.3.3.2 Model II : eddy burning approach.....	64
5.3.3.3 Model III: general approach without turbulence effect...	65
5.3.4 Inert gas stratification and mixing model.....	67
5.4 Turbulence model.....	68
5.5 Heat transfer model.....	70
5.6 NOx formation model.....	72
5.6.1 Models for burned gas temperature for NO calculation.....	72
5.6.2 NO kinetics.....	74
5.7 Results and discussion.....	76
5.7.1 Model calibration.....	76
5.7.2 Combustion in the EGR dilution.....	77
5.7.3 Lean burn.....	80
5.7.4 System performance on engine NOx emissions.....	81
5.7.5 System performance prediction at different engine speed.....	81
CHAPTER 6 Summary and conclusions.....	83
References.....	86

List of Tables

		Page
Table 2.1	Engine geometry and specifications.....	90
Table 2.2	Tumble adapter design and velocity ratio.....	90
Table 2.3	Data on acetone properties.....	91
Table 2.4	Experimental conditions.....	91
Table 4.1	Design target, design parameters and test required.....	92
Table 4.2	System performance requirement of each stroke.....	92
Table 4.3	Test results summary of the tumble adapter performance.....	92
Table 4.4	Test results summary of the supplementary gas supply timing control.....	92
Table 4.5	Engine operation for baseline.....	93
Table 4.6	Reference test results for lean burn and EGR test.....	93
Table 4.7	Test results summary of lean burn operation.....	94
Table 4.8	Test results summary of EGR operation.....	94

List of Figures

	Page
Figure 1.1	Engine configuration. (a) concept of stratified_EGR flow configuration, (b) intake system design for stratified_EGR system..... 95
Figure 2.1	Engine assembly view. (a) Intake side view, (b) Exhaust side view..... 96
Figure 2.2	Side view of the transparent engine assembly..... 97
Figure 2.3	Front view of the transparent engine assembly..... 97
Figure 2.4	Support bar and cylinder mount bolt drawing..... 98
Figure 2.5	Support plate drawing..... 99
Figure 2.6	Spacer drawing..... 100
Figure 2.7	Cylinder liner drawing..... 100
Figure 2.8	Cylinder liner support bracket drawing..... 100
Figure 2.9	Calibration curve of the intake pressure sensor..... 101
Figure 2.10	The schematic of the experimental setup..... 102
Figure 2.11	The schematic of the experimental setup. (a) Mie scattering, (b) PLIF..... 103
Figure 2.12	The flow chart of laser and camera timing control for PLIF test..... 104
Figure 2.13	Temperature variation on the bottom of the piston and the quartz wall at motoring condition. Comparison between wide open throttle and throttle closed..... 105
Figure 2.14	Outside wall temperature of the metal cylinder with the difference of cylinder pressure. Data for no compression was obtained by removing the spark plug..... 105
Figure 2.15	Shadowgraph images of combustion. 1000 rpm, $\lambda = 1$, part load..... 106
Figure 3.1	Intake mass flow rate and pressure characteristics at motoring condition (a) mass flow rate vs. intake pressure. (b) intake pressure vs. crank angle. (c) cylinder pressure vs. crank angle. 1000 rpm..... 107
Figure 3.2	Image Correction for background and cylinder wall curvature..... 108
Figure 3.3	Calibration image for cylinder wall contraction. The small scale is 1 mm. 109

Figure 4.1	Effect of tumble on combustion. Comparison between production condition and tumble enhancement condition. (a) Cylinder pressure vs. crank angle (b) Mass fraction burn rate vs. crank angle. 1000 rpm, $\lambda=1$, MBT spark timing.....	110
Figure 4.2	Effect of tumble on burn duration. Comparison between production condition and tumble enhancement condition. Burn angle $\theta_{10-90\%}$ vs. burn angle $\theta_{0-10\%}$. 1000 rpm, $\lambda=1$, MBT spark timing.....	111
Figure 4.3	In-cylinder flow motion at motoring. Mie scattering test results. 1000 rpm, WOT.....	112
Figure 4.4	The cycle by cycle variation of in-cylinder flow motion during the intake stroke. 1000 rpm, motoring, 120 deg ATDC, WOT.....	113
Figure 4.5	The cycle by cycle variation of in-cylinder flow motion during the compression stroke. 1000rpm, motoring, 90 deg BTDC, WOT.....	114
Figure 4.6	Engine front and side view including combustion chamber.....	115
Figure 4.7	Images of PLIF to show overall mixing process. (a) intake stroke (b) compression stroke. 1000 rpm, WOT, motoring.....	116
Figure 4.8	Mixing comparison at 45 deg ; The distribution of acetone concentration. (a) intake stroke, (b) compression stroke.....	117
Figure 4.9	Mixing comparison at 90 deg ;The distribution of acetone concentration (a) intake stroke, (b) compression stroke.....	118
Figure 4.10	Cycle by cycle variation of mixing process during the intake stroke. (a) front view (b) side view, 90 deg ATDC.....	119
Figure 4.11	The effect of supply timing on combustion performance at lean operation. 1000 rpm, $\lambda=1.4$, spark timing = 35 deg BTDC. Horizontal axis is CA at which injection commences. IVO at 505. (540 deg is TDC intake).....	120
Figure 4.12	The effect of supply timing on combustion performance at lean operation. 1000 rpm, $\lambda=1.55$, spark timing = 30 deg BTDC.....	121
Figure 4.13	The effect of supply timing on combustion performance at EGR operation. 1000 rpm, $\lambda =1$, EGR ratio=30 %, spark timing = 45 deg BTDC.....	122
Figure 4.14	The effect of supply timing on combustion performance at EGR operation. 1000 rpm, $\lambda=1$, EGR ratio=30 %, spark timing=50 deg BTDC.	123

Figure 4.15	Performance comparison between the supply timing control strategies. (a) IMEP and COV of IMEP vs. supply angle, (b) Pmax vs. supply angle. 1000 rpm, $\lambda=1$, EGR ratio=40 %, spark timing=50 deg BTDC.....	124
Figure 4.16	Burn angle comparison with the difference of supply timing. 1000 rpm, $\lambda=1$, EGR ratio=40 %, spark timing=50 deg BTDC.....	125
Figure 4.17	The effect of supply timing on combustion performance at lean burn condition with the narrow gap of supply angle. 1000 rpm, $\lambda=1.4$, spark timing=35 deg BTDC.....	126
Figure 4.18	The engine performance comparison of reference test. (a), (c) $\lambda=1$, spark timing=30 deg BTDC, (b), (d) $\lambda=1$, spark timing=25 deg BTDC.....	127
Figure 4.19	Engine performance comparison at lean burn operation. 1000 rpm, $\lambda=1.55$, spark timing=35 deg BTDC, part throttle.....	128
Figure 4.20	Engine performance comparison at lean burn operation. 1000 rpm, $\lambda =1.5$, spark timing =35 deg BTDC, WOT.....	130
Figure 4.21	Engine performance comparison at EGR operation. 1000 rpm, $\lambda=1$, EGR ratio=38 %, spark timing=50 deg BTDC, part throttle.....	131
Figure 4.22	Combustion properties of cycles of the same 50 deg cycles of $\theta_{0-10\%}$. 1000 rpm, $\lambda=1$, EGR ratio=38%, spark timing=50 deg BTDC, part throttle.....	133
Figure 4.23	Engine performance comparison at EGR operation. 1000 rpm, $\lambda=1$, EGR ratio = 31 %, spark timing = 45 deg BTDC, WOT..	134
Figure 4.24	Combustion properties of cycles of the same 45 deg of $\theta_{0-10\%}$. 1000 rpm, $\lambda=1$, EGR ratio=31%, spark timing = 45 deg BTDC, WOT....	136
Figure 4.25	The comparison of IMEP as a function of $\theta_{0-50\%}$ 1000 rpm, $\lambda=1$, (a), (b) : 38 % EGR ratio, 50 deg BTDC, (c), (d): 31 % EGR, 45 deg BTDC.....	137
Figure 4.26	Performance comparison between the homogeneous mixture and the stratified mixture including the lean burn and EGR burn. (a) IMEP vs. dilution ratio, (b) COV of IMEP vs. dilution ratio, (c) σ_{imep} vs. dilution ratio, (d) ISFC vs. dilution ratio.....	138
Figure 4.27	Effect of stratification strategy on variations in flame initiation $\theta_{0-2\%}$ and development angle $\theta_{0-10\%}$. Comparison between the homogeneous mixture and the stratified mixture in average value.....	139

Figure 4.28	Effect of stratification strategy on variations in flame initiation $\theta_{0-2\%}$ and development angle $\theta_{0-10\%}$. Comparison between the homogeneous mixture and the stratified mixture in detail.....	140
Figure 4.29	Effect of stratification strategy on variations in flame development angle $\theta_{10-90\%}$. Comparison between the homogeneous mixture and the stratified mixture in average value.....	142
Figure 5.1	Fractional reduction in laminar flame speed as a function of EGR fraction.....	143
Figure 5.2	The comparison of the mixing function; linear mixing, sinusoidal mixing, step mixing.....	143
Figure 5.3	Non dimensional parameters affecting on the flame stretch factor. $\lambda=1$, EGR ratio=31%, spark timing=45 deg BTDC, homogeneous mixture.....	144
Figure 5.4	The effect of flame stretch factor on combustion. $\lambda=1$, EGR ratio=31%, spark timing=45 deg BTDC.....	145
Figure 5.5	The effect of initial mass fraction burned on combustion. $\lambda=1$, EGR ratio=31%, spark timing=45 deg BTDC.....	146
Figure 5.6	Computed engine performance as a function of initial residual fraction with the different mixing functions. $\lambda=1$, EGR in overall=36. %, external EGR supplied=31 %, spark timing=45 deg BTDC, WOT.....	147
Figure 5.7	The effect of mixing function on combustion parameters. $\lambda=1$, Initial EGR gas fraction=0.33, Overall EGR gas fraction=0.36, spark timing=45 deg BTDC.....	148
Figure 5.8	Engine performance comparison with the homogeneous mixture. Marked line for the simulation result of linear mixing model. $\lambda=1$, Initial EGR gas fraction=0.33, Overall EGR gas fraction=0.36, spark timing=45 deg BTDC.....	149
Figure 5.9	Engine performance comparison with the stratified mixture. Marked line for the simulation result of linear mixing model. $\lambda=1$, Initial EGR gas fraction=0.33, Overall EGR gas fraction=0.36, spark timing=45 deg BTDC.....	140
Figure 5.10	The effect of EGR fraction on engine performance. Engine performance variation as a function of EGR fraction. 1000 rpm, $\lambda=1$, spark timing=45 deg BTDC.....	151

Figure 5.11	The engine performance comparison between mixture stratification and turbulence enhancement as a function of EGR fraction. 1000 rpm, $\lambda=1$, spark timing=45 deg BTDC.....	152
Figure 5.12	Computed engine performance as a function of initial fuel/air ratio. 1000 rpm, $\phi=0.64(\lambda=1.56)$ in overall, spark timing=35 deg BTDC.....	154
Figure 5.13	The effect of stratification of unburned gas mixture and burned gas temperature on NOx formation at EGR mixture. 1000 rpm, $\lambda = 1$, EGR ratio = 30%, spark timing = 45 deg BTDC.....	155
Figure 5.14	The effect of stratification of unburned gas mixture and burned gas temperature on NOx formation at lean mixture. 1000 rpm, $\phi=0.64(\lambda=1.56)$ in overall, spark timing=35 deg BTDC.....	156
Figure 5.15	Comparison of combustion performance between with EGR and without EGR operation at constant BMEP. WOT for 30 % EGR and intake pressure = 0.79 bar for base w/o EGR. BMEP=695.5 Kpa, MBT spark timing, $\lambda=1$, 10 % initial stratification effect of overall residual fraction with linear mixing model.....	157
Figure 5.16	Engine performance improvement with the stratification strategy. 1500 rpm. MBT, $\lambda=1$, 10 % initial stratification effect of overall residual fraction with linear mixing model.....	158

CHAPTER 1 Introduction

Fuel economy improvement has been a challenge for engineers working on engine engineering. There have been tremendous efforts in this area since the birth of internal combustion engines. Diesel and lean burn technologies for fuel economy improvement are well established. Severe requirements on engine emissions, however, have limited the application of these combustion systems because the current three way catalytic converter cannot be used for NO_x reduction in oxygen rich condition. Although under intense development, NO_x catalyst with high conversion efficiency under lean condition does not appear to be feasible in the near future due to the difficulty of the technology. Therefore, there is a significant interest in improving the fuel economy of SI engines running under overall stoichiometric condition.

The objective of this thesis is to assess the feasibility of operating an engine under very high extent of external EGR. The overall charge would thus remain stoichiometric and thus the exhaust is amenable to three way catalytic treatment. To alleviate the unstable combustion under very dilute condition, a stratified charge strategy is explored: the external EGR and the fresh charge (which is stoichiometric) are kept separate in the cylinder through the appropriate design of the charge motion. Ideally, if there is no mixing between these two parts of the charge, the flame would propagate only in the undiluted fresh and hence there would be no combustion problem. In practice, there would always be mixing and the overall combustion behavior needs to be examined.

In the following, some background on various lean/dilute combustion strategies is first discussed. Then the subject of this thesis- study of a stratified EGR strategy for SI engine - is introduced.

1.1 Previous studies

The major fuel economy benefit via using a lean or dilute combustion strategy comes from the reduced pumping loss in part load operation; there is also thermodynamics benefit in terms of the lower level of dissociation in the burned gas and of the higher specific heat ratio particularly for the lean burn case. The lean and dilute strategies are briefly reviewed in the following.

1.1.1 Lean burn engine

Improvement in fuel economy has long been the primary factor driving lean burn development. A theoretical analysis showed that heat capacity effect and pumping work effect were the primary incentives [1,2]. The stable and complete combustion at the very lean air/fuel ratio is essential for lean burn implementation.

As the mixture is leaned from a stoichiometric condition, the energy required for combustion initiation increases. Much effort has been applied to the ignition of highly lean air mixtures. The flame speed also reduces significantly. Dual or multiple spark improved the fuel economy by about 5 % by reducing combustion duration [3-5].

Extension of the lean combustion limit could be achieved through the appropriate enhancement of the turbulent motion in the engine. Controlled charge motion and turbulence generation are used to realize a fast burn combustion system with a conventional ignition system. High swirl was generated by adopting the swirl control valve and optimizing the intake port design [6]. When an advanced engine management system and a variable-swirl system with a variable valve timing/lift mechanism were applied, the fuel economy improvement of 12 % was achieved with lean, homogeneous charge engine.

Another approach to intensify turbulence and to extend lean limit was using the tumble motion in cylinder. By using the effects of turbulence enhancement and the charge stratification realized by tumble, a significant combustion improvement could be realized in the extremely lean conditions such as the air fuel ratio of 30 [7]. The fuel distribution and flow structure in cylinder was optimized by intake port partitions and tumble control piston [8].

1.1.2 Engine operating at high level of charge dilution

The increase of the amount of EGR gas does help the fuel economy. The improvement in fuel consumption at part load condition with increasing EGR gas at constant brake load is mainly due to the reduced pumping work. There are also other beneficial effects of EGR; reduced heat loss to the walls because burned gas temperature decreases remarkably, and the reduction in the degree of dissociation in the high-temperature burned gases [9,10].

There are attempts to increase the amount of EGR gas usage through different methods without combustion degradation. One research has shown charge separation in cylinder by using a swirl motion supplied through an additional induction port [11]. The gain in fuel economy was

shown to be 10 % increase in the experimental engine. The gain is largely due to the decrease in pumping loss with EGR gas increased. The geometry of that research engine, however, was too complex to be applied to a real engine even if there are promising results in fuel economy.

Recently, the concept of EGR gas stratification was applied to the modern four valve engine [12,13]. This research was based on an engine geometry with two intake ports; one intake port was used for the fuel-air mixture and the other one for the EGR gas at part load condition. Therefore the flow stratification in cylinder was introduced through the intake flow separation. Experimental results showed that the engine could operate at over 25 % EGR rate and under certain condition nearly 40 % EGR rate. The spark plug of the research engine was located off-center or two spark plugs were required for the proper flame propagation. This arrangement was necessary because only the half of cylinder was supposed to be filled with combustible mixture under part-load condition.

1.2 Objective and approach

The objective of this thesis is to assess the feasibility of operating an engine under the very high extent of external EGR. The strategy is to use a stratified charge concept so that the fresh mixture is separated from the EGR gas which forms the remaining part of the charge. This separation would enable robust combustion in the fresh mixture, while the EGR gas would serve as a "buffer" in the charge. Therefore efficient part load operation may be possible by controlling the amount of EGR gas, rather than by the throttling the induction flow. It would be better if we could use air rather than the EGR gas as filling substance in the cylinder. But the additional air to the stoichiometric mixture makes the overall air-fuel ratio lean and prevents the usage of three-way catalytic converter for NO_x control. The EGR gas is definitely required in order to meet NO_x regulation in the future. The availability of EGR gas for improving fuel economy can be fully obtained in addition to the NO_x control if a substantial amount of EGR gas can be used in cylinder.

With the limited research on the relation between stratified EGR gas and combustion properties, it is not clear how much benefit on the fuel economy from stratified EGR could be expected, but the effect of different non-uniformity on combustion properties with arbitrary controlled EGR mixing is able to be investigated.

1.3 The engine concept

The concept of the stratified_EGR combustion system for part load operation is shown in Fig. 1.1a and b. The intake system is set up to induce the strong tumble motion which persists through the combustion process. The purpose of the strong tumble is to maintain a separation of the mass elements of the charge across the cylinder bore by trapping them in the strong vertical vortex, while at the same time, providing good mixing in the axial direction within the cross-section of the vortex to promote combustion.

In the proposed system, stratification is to have the fresh mixture at the center part of the barrel vortex and EGR at two sides. With this configuration, the spark plug would conveniently be located at the center of the combustion chamber. Other benefits of such a system are that the heat transfer to the walls is less because combustion gas is buffered by EGR regions, and that hydrocarbon emissions are less because the piston crevice is less exposed to the fresh mixture.

The EGR stratification is obtained by partitioning the Siamese intake port, shown in Fig. 1.1b, so that the fresh mixture would enter the center of the cylinder through the center half of the intake valves; and EGR would enter the two sides of the fresh mixture. Several design issues of the intake system are critical to the success of the combustion system.

- The intake system should provide enough tumble motion to maintain a barrel stratification. This requirement is different from that of the usual tumble design engine. In the latter, the tumble is designed to break up into small scale turbulent eddies at the start of the combustion process so as to promote turbulent burning. The current configuration requires that the large scale tumble motion persist throughout much of the combustion process to maintain stratification. The requirement is especially difficult at low rpm and low load at which Reynolds number is small.
- The combustion within the stratified vortex should be fast to have a satisfactory performance. Thus the turbulence within the barrel vortex should be high to promote combustion. This is a requirement in contradiction to the previous one and compromise is required.
- The EGR induction system has to be controlled so that there is pressure balance between the exhaust gas flow and the flow of the fresh mixture to prevent mixing during the intake

process. Also because the supply pipe in the intake port does not form a complete gas seal, the EGR has to be switched off when the valve is closed to prevent backflow of the EGR into the fresh charge part of the system.

1.4 Engine development procedure

A critical element in this research is dependent on the realization of the flow stratification in cylinder in order to increase the amount of EGR gas through the optimum flow control. With this approach, the three-way catalytic converter could be retained for NO_x emission control and fuel economy also can be improved. The critical issues in the application of this method were defined.

The objective was achieved by demonstrating the feasibility of stratified EGR engine concept by constructing and operating such engine. The approach is described in the following :

1. Design and development of engine with visualization feature and firing capability

A quartz transparent liner was developed for visualization and a metal cylinder was used for firing; although the firing could be done with the quartz cylinder as well. Key features of the production engine were maintained as much as possible in developing a transparent engine.

2. Assess system performance in terms of flow stratification during the induction and compression period with PLIF and Mie scattering technique

Laser diagnostics were applied to assess the system performance. Recently, the planar laser induced fluorescent (PLIF) technique has become an important tool for engine research, as it can provide spatially-resolved measurements of species concentration. Using acetone as the tracer gas, the technique characterizes stratification and mixing in the engine. Mie scattering technique was applied to investigate the formation of tumble motion from the intake flow and its subsequent decay into small eddies during the intake and the compression stroke.

3. Evaluate the system performance at a firing condition

The engine performance was evaluated with a firing test at selected system operation conditions.

4. Combustion model for the stratified-EGR engine

The flame propagation, which is not easily measured during combustion, was assessed by using a quasi-dimensional model to examine its effects on the engine output.

CHAPTER 2 Apparatus and diagnostics

2.1 Experimental procedure

Because charge separation is essential for the successful operation of the stratified EGR concept, a transparent engine was designed so that the in-cylinder flow field could be visualized. Of vital interest is the mixing between the fresh mixture and the EGR gas. Another critical element is the design of the intake system that introduces an artificial external EGR to the engine. The followings are the detail description of experimental apparatus and diagnostics.

2.1.1 The transparent engine

The key issues in the transparent engine design are to keep as much as production engine condition and obtain a full stroke view. This concept was achieved by using production piston, piston rings and operating with limited lubrication for motoring and firing as well as using whole cylinder liner of glass. The engine performance could be assessed on the same engine simply by replacing cylinder liner for each experimental purpose including visualization and firing.

The single cylinder engine was designed for lean/stratified_EGR mode operation and to give a good optical access while maintaining most of the features of a typical production engine. Engine specification is shown in Table 1. The production engine was modified to a single cylinder engine by operating one of 4 cylinders of a DAEWOO four-cylinder 1,500 cc engine. Figure 2.1a and b are intake side view and exhaust side view respectively. Figure 2.2- 2.3 show the overall assembly view.

The engine head was raised from the block and supported by six columns and plates, which are shown in Figure 2.4 and Figure 2.5 for details. Extended cylinder liner for visualization and firing purpose was fitted in between them. The piston was connected by a spacer to the original piston. Figure 2.6 contains the detail for the spacer. In this manner the full displacement volume could be accessed optically. Piston ring gap was increased to around 1mm, which is larger than that of the production engine around 0.15 mm range because the larger thermal expansion of piston and ring than quartz at a high temperature operation caused the excessive scratch on the wall.

The cylinder liner for visualization was made of quartz (Fused Quartz GE Type 125). This quartz has over 90 % transmittance at over 300 nm wave length and lower mechanical strength than sapphire, which is a preferred material used in transparent engines [14]. Quartz was selected for this research because it is not expensive, and easy to machine and polish compared to sapphire. Since the transparent engine was operated in motoring condition for the most part and firing for the limited time, the mechanical property of this material is not as critical. The 7 mm thickness of liner was calculated to be sufficient for mechanical strength. The cylinder liner for firing test was made of mild steel with the same thickness as the glass cylinder. The dimensions for the cylinder liner are shown in Figure 2.7.

The cylinder liner was fastened to the cylinder head by four head bolts and a support bracket, which are shown in Figure 2.8 for details . This configuration allows easy assembly and disassembly of the liner without taking the head off in order to clean the liner surface during the experiment. The contacting surface between the quartz cylinder and the aluminum cylinder head and the support bracket was cushioned by a rubber gasket.

Lubrication oil, which was bypassed from oil pump, was supplied onto the bottom of the extended piston. Since engine oil was supplied at a high pressure, the oil jet hit on the bottom of the piston and splashed onto the cylinder liner, which made oil distribution relatively even on the liner as much as possible . The oil supply valve was turned off after a small amount of oil was supplied for motoring test to keep the window condition clean. But for firing test with metal cylinder, continuous supply was kept for lubrication and cooling purpose. In order to prevent oil splash to outside, four pieces oil splash guard was mounted between bracket and cylinder block. For oil return into oil sump, two holes were incorporated in the bottom piston. Oil drain performance was not enough during engine operation due to the piston movement and the oil supplied but not drained continuously contributed to lubrication until the engine stopped. Two suction lines were mounted on the guard plate to take out the blow by gas.

Valve timing system was developed because the original belt driving system could not be used to make enough room for the extended cylinder liner. The new cam sprockets and crank gear of production engine were replaced with new ones: the gear for cam drive(Gates P80-5M-25) has 38 teeth and crankshaft gear(Gates P40-5M-25) has 19 teeth. In order to maintain enough belt tension, an auto tensioner supplied with the production engine was used. And an idler was

installed between crankshaft gear and exhaust gear to hold enough wrap angle. The cam driving belt(Gates 16905M25) has the same tooth profile and width (25mm) with gears.

Later one transparent acrylic panel was mounted near the quartz cylinder on the front side for safety, which is strongly recommended for firing test to prevent any injury due to explosion. As previously described, quartz itself with 7 mm thickness is strong enough for firing. But when the quartz cylinder was used for a long time, the scratch on the wall made the mechanical properties of quartz weaker and high pressure after misfiring or some knocking conditions caused explosion.

2.1.2 Artificial EGR gas supply and control of mixing

Since it is not easy to change the casting of the cylinder head, an adapter was made and inserted into the intake port. The adapter has two functions: one is to generate in-cylinder tumble motion; the other is to divert the flow of EGR gas and fuel-air mixture into the intended region of the cylinder respectively to minimize mixing during the supply stage.

The fuel-air mixture was inducted to the intake port close to the cylinder center with the main flow pipe and EGR gas was inducted to the remaining area through the adapter of EGR pipe as shown in Fig 1.1. Thus the fresh fuel-air mixture is located around the center part of the combustion chamber and EGR gas forms a buffer at each side of fuel-air mixture. This configuration has the advantage that it would allow a centrally located spark plug to be used. By buffering much of the piston crevice with EGR gas, the crevice HC mechanism also could be reduced.

EGR gas supply pipe was divided into two branches at the intake port to supply EGR gas to each branch of the runner in the Siamese port. Shear between the EGR gas flow and the fuel-air mixture flow is minimized to prevent mixing between them. EGR gas supply was controlled by solenoid valves to be synchronous with the intake event.

The adapter design was based on the geometric limitation of the intake port and performance. Table 2.2 shows the dimension of tumble adapter and velocity ratio.

2.1.3 Instrumentation and data acquisition

Dynamometer and speed control: DC dynamometer was installed on the test bed. Engine was mounted on test bed with rubber damping and coupled to the dynamometer through a universal

joint. A motor was connected to the water pump to circulate coolant and closed loop cooling circuit was adopted for dynamometer cooling. A thermocouple is mounted in the coolant reservoir to monitor the coolant temperature. Dynamometer controller (Digalog Model 1022A-STD) was connected to the dynamometer and installed on the engine control panel outside engine room.

Engine cooling: Another motor was mounted on the test bed to operate the engine coolant pump. Engine originally has a coolant pump mounted in the engine front side. However the pump was modified in order to operate the belt driving system. Water cooling was not needed for this work in order to keep uniform temperature around the combustion chamber as much as possible because the cylinder liner cooling depends on air convection.

Crank angle and piston positioning: An optical shaft encoder, BEI motion systems Model H24E-F18-SS-360, connected to the crankshaft, was used to indicate crank angle. For compression BDC reference signal, an optic sensor and a rotor with slot were installed at the end of the exhaust camshaft, where a production distributor was mounted. This sensor generates one pulse per rotation. The signal combination of the shaft encoder and the optic sensor was used to set the reference signal for the bottom dead center before compression stroke.

Mixture preparation and metering: Air passing through the laminar flow element and the air cleaner element was inducted into the mixing tank. Air flow rate was measured with a laminar flow element (Meriam 50MW20-2, 40 CFM@8" H₂O accuracy \pm 0.5% of full scale): the pressure drop across a matrix of small flow channel in which the flow is laminar is related to the volume flow rate.

Propane was continuously supplied to the mixing tank. The supply pressure of propane was kept to 20 psi and the flow rate was controlled with valve for the required amount of each test condition. Throttle valve was mounted between mixing tank and intake manifold. Since only one cylinder was used and intake manifold was modified, a plenum with 10 times as much as engine displacement was added to minimize the induction pressure pulsation effect due to the long induction system. Intake manifold temperature and pressure were measured to monitor an operating condition. Figure 2.9 shows the calibration curve of intake pressure sensor (Model Tanyx SA 25, 0-25 psi range)

Exhaust gas A/F was measured with a broad band AFR analyzer (Horiba Model MEXA-110λ). With this A/F value, fuel flow rate was calculated. Output signal was also connected to the data acquisition computer.

Spark ignition: Spark timing is set at a specified value with a reset counter (DCI model 304). Spark trigger signal was sent to ignition driver. In order to reduce ignition signal noise and ignition malfunction, photo power TR was used. There was a significant ignition problem and pressure signal noise when the spark plug with pressure transducer (Kistler Model 6117A) was used. The reason for ignition problem with this spark plug was assumed as this spark plug did not carry any resistance inside due to space limitation for pressure transducer mount. Some improvement was made when 20 K ohm resistance was inserted between spark plug and high tension cable. But still abnormal misfiring occurred. This spark plug was replaced with a conventional spark plug (Champion Model BRK6E)

Cylinder pressure measurement: The spark plug type pressure transducer was used initially because no modification in the cylinder head to mount transducer was needed. As mentioned above, that pressure transducer had significant noise problem due to the spark plug malfunction. Therefore another pressure transducer (Kistler Model 6051A) was mounted in the cylinder head and used together with a dual mode charge amplifier (Kistler Model 5010) to measure cylinder pressure.

EGR(inert gas) flow rate: High pressure inert gas supply was required to meet mass flow rate needed for the experiment at a large dilution rate. Air is inert gas for lean burn and Nitrogen (N₂) gas for EGR operation. Two solenoid valves (Kip Inc. Model 241015-02, 1/8" orifice) were used. For supply system configuration, refer to Figure 2.10. Another laminar flow element (Meriam 50MW20-1-1/2", 22 SCFM @ 8" H₂O) was installed to measure the flow rate. Hereafter external EGR means N₂ gas.

Cylinder wall temperature and exhaust gas temperature were monitored during engine operation to prevent engine overheating.

Data acquisition: For firing test, cylinder pressure, intake pressure and exhaust A/F signal were acquired in IBM compatible PC, in which Global Lab data acquisition interface card and its

associated software were installed. Data were recorded on a 1 deg crank angle interval by using the pulse per crank angle from the shaft encoder as an external clock. The bottom dead center of compression stroke was added to the pressure signal to get cycle reference. At least over 600 cycles were gathered at each test condition and about 100 consecutive cycles per test were acquired. Figure 2.10 contains major components of the experimental setup.

2.1.4 Experimental setup for visualization

Since the tumble adapter for main fresh mixture flow was designed to generate a strong tumble, LDV test or other technique to quantify the turbulence intensity or flow velocity at each location might be needed in order to assess the performance of adapter. However, it is expected that the adapter, designed based on generally accepted knowledge for strong tumble generation should introduce higher level of tumble strength than base level. Even though the tumble ratio might not be optimum for this test condition, its contribution to stratification in the cylinder could be assessed with visualization test. Therefore visualization test was adopted to assess the system performance in terms of tumble motion and stratification..

Two kinds of visualization technique were used to get flow field information during induction and compression stroke at motoring condition. Experiment was done at the same condition as that of firing condition: the engine was operated at 1000 rpm and WOT by supplying high pressure(20 psi) inert gas, which makes 30 % inert gas fraction.

2.1.4.1 Mie scattering flow visualization

The purpose of this test was to visualize the tumble motion introduced and formed in the cylinder. Baby powder was used for tracer for flow visualization, the particle size of which is less than 10 μm . The particles were supplied into one of inert gas supply lines to have clear streak line with a small amount of tracer. The tracer was illuminated with Argon-Ion laser, Model 95 Lexel, of continuous beam with a power output of 2.5W at a wavelength of 514 μm . Laser sheet with 1 mm thickness was formed with cylindrical lens and passed through the center line of one of intake valves. Intensified CCD camera (Model 576SE) was used to take pictures of scattered particles. The camera was connected to a camera control unit to synchronize with engine operation. Images were transferred to IBM compatible PC with 16 bit, slow scan (1 frame per 8 cycle). The images with the resolution of 576 x 386 Pixels were monitored on screen with data acquisition software, Winview, supplied by Princeton Instruments, which was used for image analysis.

Figure 2.11a shows the schematic of the experimental setup. Since the laser emits the continuous beam, the camera and seed supply was synchronized to take pictures at the intended crank angles.

2.1.4.2 Planar Laser Induced Fluorescence(PLIF) flow visualization

This test was to estimate the level of stratification and mixing process during induction and compression stroke. The laser utilized in this test was an XeCl-excimer laser(Lamda Physik Compex 102) with a power output of approximately 112 mJ at a wavelength of 308 nm and a exit beam size(7x22 mm). The laser beam was formed into a thin sheet (0.7 x 38 mm) with two cylindrical lenses and slit and directed through the quartz cylinder. The camera operation and data acquisition in PLIF test are the same way described in 2.1.4.1. Acetone (Dimethyl ketone, or 2-Propanone) $\text{CH}_3\text{-CO-CH}_3$ was used for the fluorescence tracer because it is easy to vaporize it even with motoring condition owing to the low boiling point (58 °C). It absorbs over a broad band of wavelengths (225-320nm) with a maximum between 270 and 280 nm. The fluorescence emission is broadband in the blue (350-550nm) with peaks at 445 and 480 nm and a short lifetime of less than 4ns. Details are given in Table 2.3. Since the wavelength of XeCl-excimer laser is 308 nm, the absorption efficiency is not good [15-16], but in this test, the sufficient amount of acetone was supplied through one of inert gas supply lines by Venturi effect and gravity to have enough fluorescence light intensity. Acetone has been used for a tracer for the measurements of planar fuel distributions and the progress of turbulent mixing formation by planar laser-induced fluorescence [15,17].

The schematic of the experimental setup for PLIF is shown in Figure 2.11b. The camera, laser and seed supply were synchronized together.

2.1.4.3 Shadowgraph flame visualization

Flame propagation was supposed to be measured with Shadowgraph technique. The setup for this experiment is the same as that of typical Shadowgraph test [18], which consists of two spherical mirrors and 350W mercury arc lamp as a light source. Cylindrical lens was tried to improve the aberration problem due to the curvature of cylinder and the area near the side wall was not considered for experiment because this area was expected to be distorted or expanded due to the aberration.

2.1.4.4 System synchronization

Since the supply of inert gas was controlled with solenoid valve timing, the dynamic characteristic of solenoid valve should be assessed to have a precise control of supply timing. Simple rig test was done to examine it. The results showed 8 ms time delay for opening and 26 ms duration for closing.

Figure 2.12 shows the process chart of the control of laser and camera for PLIF test. Considering the travel distance of trigger signal and light, the exposure time(15 μ s) covers all fluorescence lifetime (4ns) but not phosphorescence lifetime (200 μ s).

2.1.5 Experimental setup for firing test

Most experiments were performed at the constant engine load based on conditions and the constant engine speed, 1000 rpm, which are generally used for the experimental engine test for performance and visualization together. Since engine was operated at air cooling condition with the metal cylinder, engine was needed to be cooled down to prevent overheat, which becomes less than 3 min.

Propane was used for fuel because gas fuel enables us to assess the flow motion effect separately without consideration of fuel vaporization effect. Homogeneous mixture was made in mixing tank by supplying inert gas, air and fuel. For stratified mixture, air and fuel were completely mixed before the mixture arrived at the intake port and inert gas was supplied through solenoid valve.

2.2 Experiments

2.2.1 Engine motoring

Since the engine was cooled down via convection rather than water cooling, the duration of engine operation was limited to prevent any possible damage on quartz liner due to overheating. Even though engine lubrication oil was supplied into the piston, its main purpose is to prevent a solid contact between the piston ring and the wall but it did not contribute to cooling the engine. Therefore the duration of engine operation had to be confirmed. Engine was motored to see the temperature variation of outside of the quartz wall and bottom of the piston. The temperature of the piston was measured to estimate the temperature of inner wall of quartz. Since quartz is weak to the big temperature gradient, the gradient was monitored. No fan to cool down the cylinder

was used to maintain a uniform temperature because quartz does become stronger as it gets hotter and uniformly hot operation is preferable.

Figure 2.13 shows temperature variation of the bottom of the piston and the outside wall of quartz cylinder. Since the thermocouple for the outside wall of quartz cylinder was mounted near the cylinder head, temperature was expected to be highest value. The heat generation during motoring is largely due to compression pressure and friction between the piston ring and the wall. The temperature increase on the wall is less than that of the piston, which indicates the low conduction characteristic of quartz material.

The temperature variation of the outside wall of the metal cylinder is illustrated in Figure 2.14. Compared with Figure 2.13, the temperature gradient in the metal wall was smaller than that of the quartz cylinder.

2.2.2 Flow visualization

Several measures were taken to improve the quality of obtained images. All experiments for visualization were targeted for the qualitative assessment on tumble motion and stratification.

2.2.2.1 Mie scattering flow visualization

A lot of trials were needed to obtain good pictures. The biggest problems were to keep window clean and to have enough image intensity. Once particles were supplied into the cylinder and stuck on the cylinder wall, it was hard to take them out even though most particles in air were removed from the cylinder during exhaust stroke. Engine oil did help clean the window a little bit, but it was not enough to maintain a clear view because the camera could take only one picture per 8 cycles. When the amount of particles was small, the scattered light intensity was not enough to see flow motion. Smaller particles around $1\mu\text{m}$ size were tried. But the light intensity was also not enough even though the problem of maintaining the clean window was lessened. The bigger particles around $50\mu\text{m}$ were investigated to enhance the light intensity, but with the possible damage on the quartz wall considered, it was not tried.

Pictures were taken with baby powder at 75, 120 deg ATDC of the intake stroke and 90 BTDC compression stroke. In order to capture the streak line, the exposure time of the camera was $333\mu\text{sec}$ (2 deg).

2.2.2.2 PLIF flow visualization

The engine with quartz cylinder was operated at motoring condition. Usually the flow characteristic differences between motoring and firing results from the residual gas back flow dynamics and its impact on intake flow. When induction flow was guided by the pressure difference between intake port and cylinder, backflow dynamic could make a big difference between them. However, it is expected that even though supplementary inert gas flow was affected by the back flow dynamics, the inert gas flow would keep the same flow response characteristic at motoring as firing flow response because it was supplied with high pressure. Engine was operated at WOT and 1000 rpm, 1500 rpm with 30 % EGR supply. Since the difference between front and side view of cylinder was supposed to indicate the level of stratification, the pictures for both side were taken.

Each data set has at least 10 frames; the first 1 - 3 frames are for the background and later frames for the data. The reason for taking the background on each data set is that the amount of engine oil or other fluorescent material attached on the cylinder wall was different, which made the different level of background noise. Before gathering the data at different condition, engine was motored at least 1 minute to remove all acetone remaining in the cylinder after each test. Pictures were taken at 30, 45, 60, 90, 120, 150, 180 ATDC of the intake stroke, which includes intake stroke and exhaust stroke.

Rig test for calibration was done. Since there was a strong background noise, it was required to make calibration on the data. The followings are the procedures to take pictures for calibration:

- Step 1 Fill acetone in the cylinder and stay for more than 10 minutes
- Step 2 Take pictures at 30, 45, 60, 90 and 120 deg crank angle
- Step 3 Take out all acetone from the cylinder with the vacuum pump and take pictures at the same angle for the background image

Another calibration test was to assess image deformation due to the curvature of the cylinder wall. The scale with 1mm unit was inserted into the quartz cylinder and pictures were taken.

2.2.2.3 Shadowgraph flame visualization

Rig test was carried out to examine the aberration effect due to the cylinder wall curvature and thickness. The results indicated that the wall was found to act like lens with multiple focuses. Since the vertical direction was not distorted so much, firing test was carried out hopefully to take a picture on the flame profile. Figure 2.15 shows that it was hard to figure out images due to the resolution limit of the camera and the engine oil images on the wall. The trial to take a picture on the flame through the curvature glass with Schlieren or Shadowgraph technique could be found in literature [19-20].

The conclusion from this trial is that pictures should be taken with the wall dry without any lubrication oil because engine oil made a significant problem on clear images and a special equipment or modification is demanded to improve the aberration problem.

2.2.3 System performance

Intake port pressure was measured to monitor pressure wave characteristics. Differences in pressure between the intake port and the cylinder drive the flow through the intake valves. The pressure characteristic was supposed to indicate the difference of the injection strategy.

The pressure in the volume of supplementary inert gas was measured. The purpose of the pressure measurement was to confirm whether the pressure wave characteristic possibly affects the flow rate when a different solenoid valve timing was applied. The performance of the solenoid valve was confirmed. Since the solenoid valve has its own response time, the system response time including the flow rate, pressure wave characteristics and so on was required to be measured to make precise control as much as possible.

2.2.4 Engine performance

Since pumping loss is heavily involved in part load condition, the system performance would be better at part load condition. However, the induction momentum of air/fuel mixture and supplementary inert gas could not be strong enough to maintain the stratification strategy. Therefore combustion stability would be worse.

Engine firing test was carried out to directly measure the performance of the system at each case. Even though the purpose of this work is to investigate the strategy of stratified-EGR mode operation, the lean burn test also was done because the stratification strategy could be applied to extend lean limit. Air in lean condition is also inert gas, but excess oxygen will contribute to combustion positively compared with nitrogen. Therefore the comparison between lean burn and

EGR burn in terms of the performance of stratification strategy was another interest. For performance comparison, the experiment for reference condition was done first. Emission test for HC was carried out to examine the engine operation condition including leakage etc.

However, from the beginning, it was recognized that attempts to assess the performance improvement with this concept by directly measuring the performance at each condition would be difficult and not central to the study at hand. It was decided, therefore, to conduct a set of experiments comparing two cases; one where mixture was homogeneously mixed, and the other with stratified mixture in the cylinder.

The experimental conditions executed are shown in Table 2.4. For each experiment and each case, cylinder pressure was collected for a large number of cycles. When the wall temperature reaches 80 deg °C, data collection was started. During operation, the fuel flow rate was maintained as a constant value by supplying fuel at higher than atmospheric pressure. Spark timing was swept to have the maximum engine performance at each experiment. In order to have the maximum performance at each experimental condition, engine was operated at MBT (Maximum spark timing for Best Torque) spark timing.

CHAPTER 3 System performance analysis

In this chapter, system performance analysis techniques are described. The analysis is based on the following. i) The pressure data; results are used to evaluate the difference between the stratified EGR and the homogeneous lean burn analysis. ii) The image data from LIF measurement; the data are used to evaluate the in-cylinder mixing process during the intake stroke.

3.1 Analysis of pressure data

Since the performance of engine is based on the processing of cylinder firing pressure, pressure data analysis and interpretation of the statistics of the results are the engine diagnostic tools. In this work, the primary objective is to extend the misfiring limit of the usage of the charge dilution further than could be achieved in a conventional way. The cyclic variation of combustion is significantly involved when the engine was operated close to combustion limit; frequent misfiring mass occurs.

Intake pressure was used to set the reference pressure of the cylinder pressure in every cycle to eliminate the effects of possible signal drift. Figure 3.1 illustrates the mass flow rate, intake pressure wave characteristic and cylinder pressure at motoring condition. The trend in Fig. 3.1a is not linear and these trends change with the engine speed and the valve timing. Each curve of Fig 3.2b shows the intake pressure wave characteristic at each average intake pressure, shown in the legend. The nonlinear flow rate is largely due to the pressure wave characteristic during the intake stroke. Sudden pressure increase when the intake valve is opened, which is clear when intake pressure is low, seems due to the backflow of the cylinder mass into the intake port. For the reference pressure of cylinder pressure, the average pressure value of the intake pressure was used.

Pressure data was used to calculate work transfer from gas to piston. The gross indicated mean effective pressure (IMEP), gross indicated work per cycle normalized by the displacement volume, was used to indicate the engine performance. The gross indicated work was defined as the work which is delivered to the piston over the compression and the expansion strokes only. The maximum cylinder pressure, crank angle at which the peak cylinder pressure occurs and the rate of pressure rise ($dP/d\theta$) were investigated because these pressure-related parameters can easily be measured through the pressure transducer.

3.2 Heat release analysis and statistics

In order to obtain the information about the fundamental characteristics of burning process, the cylinder pressure analysis is necessary to separate the effect of combustion from the effect of volume change, heat transfer, leakage, etc. Such analysis is referred as a heat release analysis and is based on applying the first law of thermodynamics to cylinder contents, in which the pressure changes can be related directly to the amount of fuel chemical energy released by combustion.

The two most common approaches to calculate the mass fraction burned from the measured cylinder pressure data in a spark ignition engine are one zone model and two zone model. One zone model is based on the assumption that combustion chamber contents are treated as a single zone. In two zone model the combustion chamber is divided into burned and unburned zone. The advantage of two zone model is that the thermodynamic properties of the cylinder contents can be quantified more accurately because it is obviously based on a more realistic picture of the combustion process than one zone model. The disadvantages are that the geometric location of each zone must be estimated, and in order to decide the composition of the gas flowing into the crevice additional assumptions are needed.

To simplify heat release analysis, one zone model was applied to all the cylinder pressure data collected for each experiment. This model has been developed and used for various applications within Sloan Laboratory [21-23].

Since details of the one zone model have been described in [21], the essential basics used for this work are the subject of this section.

By applying the first law of thermodynamic law to the combustion chamber, one can obtain an equation for the chemical or gross heat release that may be solved using a measured pressure-time data from an engine, a model for heat transfer, and a model for crevice mass flux:

$$\delta Q_{ch} = \frac{\gamma}{\gamma - 1} p dV + \frac{1}{\gamma - 1} V dp + \delta Q_{ht} + (h' - u + c_v T) dm_{cr} \quad (3.1)$$

The first two terms of Eq. (3.1) together represent work and the sensible internal energy changes of the charge, which would be heat release if no losses were present.

The heat transfer model to calculate heat loss to walls is based on Woschni's correlation for the heat transfer coefficient h [22]. This correlation is described in detail in the following Sec.5.5.

$$\delta Q_{ht} = Ah(T - T_w) \quad (3.2)$$

The last term of Eq.3.1 is the energy loss of the chamber due to the flow into the crevice regions; h' is evaluated at cylinder condition if the crevice flow is out of the cylinder or at the condition in the crevice volume if the flow is into the cylinder. The mass flow into the crevice is,

$$dm_{cr} = \frac{V_{cr}}{RT_w} dp \quad (3.3)$$

Leakage or blow-by effect was not included separately in this model because the metal cylinder was used for firing and the leakage condition was not much different from the production engine. The total crevice volume for a warm-up condition was assumed to be 1 % of the clearance volume.

Appropriate functions of temperature to determine the ratio of specific heat γ were suggested by Chun and Heywood [22], in which a table of γ values is provided for several different equivalence ratios and three residual fractions. Although there may be uncertainty as to whether the effective γ value for a homogeneous charge is applicable to the stratified charge situation, quantifying this uncertainty is beyond the scope of this work and the γ value based on the overall charge is used. For the compression and the expansion stroke, γ is approximated by linear functions and a constant value for combustion stroke. In order to ensure a smooth transition from compression to combustion and from combustion to expansion, a 5 deg transition region was added in the beginning and at the end of combustion. Since γ varied with the fuel-air equivalence ratio, residual fraction and fuel types, the accuracy of γ depends on the appropriate values of mixture composition. In order to predict the amount of residual gas fraction x_r , the model developed by Fox [25] was used. The model relates x_r to engine speed, inlet pressure, valve overlap, and fuel-air equivalence ratio.

3.2.1 Individual cycle variables

From the detailed analysis of the pressure trace from each cycle, several parameters were determined in characterizing cyclic variations in combustion. The following variables were determined on cycle-by-cycle bases:

0-2% Mass fraction burned angle, $\theta_{0-2\%}$: This is the angle of crank rotation when 2% of the mass in the chamber is burned, referred to as the flame initiation angle.

0-10% Mass fraction burned angle, $\theta_{0-10\%}$: This is the crank angle between the spark and the point when 10% of the mass in the chamber is burned, referred to as the flame development angle, which is the measure of the time required to develop a fully turbulent propagation flame.

0-50% Mass fraction burned angle, $\theta_{0-50\%}$: The angle between the spark and the point where 50% of the mass in the chamber is burned

0-90% Mass fraction burned angle, $\theta_{0-90\%}$: The angle between the spark and the point where 90% of the mass in the chamber is burned

10-90% Mass fraction burned angle, $\theta_{10-90\%}$: The angle between the points when 10% and 90% of the mass in the chamber is burned. Also referred to as the flame propagation angle, it is the measure of the time required for a fully developed flame to propagate through the majority of mixture.

Coefficient of variation of IMEP, COV_{IMEP} : The coefficient of variation is defined as the standard deviation normalized by the average value. The COV of IMEP was used to describe engine stability, since it directly relates to engine torque variations.

Peak Pressure, P_{max} : The peak pressure per cycle is the maximum pressure of the cycle.

Peak pressure location, θ_{pmax} : θ_{pmax} is defined as the crank angle at which the peak pressure occurs, measured from the piston top dead center.

Peak mass burning rate, $\dot{x}_{b(max)}$: This is the peak rate of mass burning during the combustion cycle, normalized by the total mass in the cylinder.

Peak mass burning location, $\theta_{\dot{x}_{b(max)}}$: This is the crank angle at which $\dot{x}_{b(max)}$ occurs, measured from the spark crank angle.

Heat transfer fraction, Q_{htf} : The heat transfer fraction is defined as the fraction of fuel enthalpy in the mixture lost to the combustion chamber walls through heat transfer.

Peak mass fraction burned, $x_{b(max)}$: This is the peak value of mass fraction burned for each cycle at the end of combustion.

The mass fraction burned was taken relative to the computed mass fraction burned at spark; the 2 %, 5%, etc. are not necessarily the absolute points.

3.2.2 Misfires, partial burn cycles and operating limits

Misfires: Misfires are defined as the cycles for which the gross IMEP is less than zero, which implies that the flame does not propagate at all in these cycles. There will not be any significant amount of fuel burned. Means and standard deviations for cycle variables are computed by omitting both misfired cycles and those immediately following a misfire. The cycles following a misfire were removed because these cycles are abnormal too, in the sense that their burned gas fraction is lower than that of all the other cycles.

Partial burn cycles: Partial burn cycles are defined as the cycles whose gross IMEP is between zero and one-half of the mean value of the total sample with positive IMEP. These cycles are engine cycles where at the time of exhaust valve open a significant amount of the fuel is still unburned, even though a propagating flame has been developed.

Operation limits: Operation limits are limits within which acceptable engine operation is obtained. In general 10 % COV_{IMEP} has been used for the criterion of engine operation limits. In case of heavy dilution condition, the engine experiments were carried out at over 10 % COV of IMEP to have information on combustion and compare two systems even though those operation conditions are not used in real engines.

3.2.3 Sample size and uncertainty

The appropriate sample size depends on operating conditions because in general the higher the degree of cyclic variability is, the greater are the number of cycles required to define the behavior under those conditions. Since it was hard to sustain a steady state operation with this engine, the average values of overall cycles could not show the performance value at each condition. Around 600 cycles were obtained for analysis at each experiment. The average of

variables was done per 100 consecutive cycle and its trend on overall data analysis was analyzed. The analysis of cycle-by-cycle was limited due to the sample size.

3.2.4 Statistics

Since it is impossible to look at and evaluate all pressure tracers, the statistical behavior of parameters should be considered. Several statistical results including the sample mean, coefficient of variation (COV) , were determined for the cycles corresponding to each sample of pressure data recorded. For certain data, correlation coefficients between the combinations of individual cycle parameters were computed to allow investigation of the relationship between certain variables for a single experiment.

The correlation coefficient (R) to describe the relationship between two variables x and y is defined as

$$R = \frac{\sum_i^N (x_i - \bar{x}) \cdot (y_i - \bar{y})}{\sqrt{\sum_i^N (x_i - \bar{x})^2} \sqrt{\sum_i^N (y_i - \bar{y})^2}} \quad (3.4)$$

where N is the number of cycles, \bar{x} and \bar{y} are the mean values of x and y . A value of $R=0$ corresponds to no correlation between the variables, while a value of ± 1 means that there is a perfect one-to-one correspondence between them.

Box distribution was used to show the distribution of data scattered. The box contains 50 % of the data population and the line in the box indicates the medium of the data.

3.3 Image processing and calibration

To eliminate noise in the fluorescence signal requires an image post-processing. Disturbances needed to be taken into account include fluorescence from the oil spots on windows, background light scattering, laser intensity variation over space, optical distortion, and operating gain conditions of the intensifier etc.

The raw images of the acetone distribution in the cylinder were post-processed in order to eliminate the artifacts. Scattered laser light caused a strong background noise due to the fluorescence species, especially engine oil attached on the cylinder wall.

The image is corrected by subtracting a mean background image from each of the images of interest. The calibration and background corrections are made on the basis of mean laser sheet characteristics to take into account the shot noise and pulse-to-pulse fluctuations in the laser sheet. The reason for the background difference between raw data and calibration is largely due to the oil distribution difference on the cylinder inner wall.

$$\begin{aligned} I(x, y)_{image} &= I(x, y)_{raw} - I(x, y)_{background, raw} \\ I(x, y)_{calibration} &= I(x, y)_{raw, calibration} - I(x, y)_{background, calibration} \end{aligned} \quad (3.5)$$

, where $I(x, y)$ is image intensity at (x, y) location. x is radial direction and y is also cylinder axial direction.

In addition to the background correction, the curvature correction of the raw image is needed.

$$\begin{aligned} I(x, y)_{calibration} &= f_1(x, y) \cdot I_{uniform} \\ I(x, y)_{image} &= f_2(x, y) \cdot I(x, y)_{real, data} \end{aligned} \quad (3.6)$$

where f_1, f_2 are the function of the wall curvature effect including aberration, etc. $I_{uniform}$ is the image intensity of the uniform acetone distribution

Since the fluorescence signal is proportional to the mole fraction[15], it follows that

$$\frac{I_{real, data}(x, y)}{I_{uniform, cal}} = \frac{I_{image}(x, y)}{I_{calibration}(x, y)} \cdot \frac{f_1(x, y)}{f_2(x, y)} = f_n \cdot \frac{X_{data}}{X_{uniform, cal}} \quad (3.7)$$

where the factor f_n corrects the difference in the temperature and the pressure between data and calibration condition. The image of acetone distribution in the cylinder normalized by calibration intensity can be achieved by the following relation.

$$\frac{I_{real,data}(x, y)}{I_{uniform,cal}} = \frac{I(x, y)_{raw} - I(x, y)_{background,raw}}{I(x, y)_{raw,calibration} - I(x, y)_{background,calibration}} \cdot \frac{f_1(x, y)}{f_2(x, y)} \quad (3.8)$$

If the acetone concentration represented in the calibration image and f_n were known, the acetone mole distribution in the cylinder could be calculated by the following relation.

$$\frac{X_{data}}{X_{uniform,cal}} = \frac{I(x, y)_{raw} - I(x, y)_{background,raw}}{I(x, y)_{raw,calibration} - I(x, y)_{background,calibration}} \cdot \frac{f_1(x, y)}{f_n \cdot f_2(x, y)} \quad (3.9)$$

However, since the seed concentration (acetone) in the calibration gas can not be determined with a sufficient accuracy because of the difficulty of maintaining the known value and it is not easy to obtain the factor f_n , images under different conditions can be compared qualitatively.

Figure 3.2 illustrates one of typical calibrated results. The local image near the wall shows that light intensity was over the saturation limit of the camera. Once the intensity is beyond the saturation limit, the image correction is not possible. Therefore the calibrated image of those areas is not available to get the mixture distribution information. In order to improve this situation, the less power of laser light was tried, then the light intensity of other areas was not enough. Locally saturated spots were shown in all image analysis results because of a necessary trade off required. The horizontal lines on the calibrated image were caused by the scratch on the wall due to the piston ring travel. The vertical lines were due to the fluorescence of the wall reflection of the laser beam and its variations.

The image contraction in a radial direction was shown in Figure 3.3. The small scale marks 1 mm and the overall scale in the cylinder shows 75 mm. The 5 mm near the wall was clearly shown as dislocated non linearly. This image contraction was not calibrated because the level of contraction was considered to be relatively small.

The influence of cyclic variations was taken into account by averaging images.

CHAPTER 4 Engine development

This chapter is to describe the development procedure, which includes the verification of a design concept by constructing and operating the engine and to assess the system performance with experiment results. The design concept of the stratified-EGR mode operation is to reduce the fuel consumption by maintaining the stable combustion with high EGR. In order to achieve the goal, more precise flow control into the cylinder is essential. Detail experiments were carried out to achieve the design target shown in Table 4.1.

The level of stratification between fresh mixture and lean/dilute gas was investigated by seeking the system performance required during each engine stroke. Table 4.2 shows the system requirement at each engine stroke.

4.1 Effects of tumble motion on combustion

4.1.1 Tumble enhancement by intake port partitions through the tumble adapter

As described in Section 3.3.1, a tumble adapter was mounted in the intake port to enhance the tumble motion. In order to confirm the effectiveness of the tumble adapter, a comparison test was conducted with the metal cylinder. The engine was operated at part load condition, 75 kpa intake pressure, 35 deg BTDC spark timing, stoichiometric condition. The production condition was known to be a low tumble engine with the tumble ratio 0.45 compared with the typical values for good combustion characteristics in the range of 0.7 - 1. Since the level of tumble enhancement with the tumble adapter was not measured, the quantitative comparison in terms of the charge motion was not possible, but the condition with the tumble adapter was expected to be high tumble. The effectiveness of the configuration was evaluated by comparing the engine behavior in the original configuration with the engine behavior with the adapter.

Table 4.3 shows the test summary. The high tumble illustrates more stable combustion and fast burning. It is generally understood that the tumble has a strong effect on flame propagation angle $\theta_{10-90\%}$ rather than flame development angle $\theta_{0-10\%}$. This trend was shown in Table 4.3.

Figure 4.1 shows the comparison of pressure and mass fraction burn rate, which was averaged with 100 cycles. The spark timing (35 BTDC) is assumed to be slightly retarded compared with MBT. The comparison of burning characteristics is shown in Figure 4.2. The results showed that the tumble adapter formed a high turbulence and made a stable combustion. All these results lead to the conclusion that the tumble adapter meets its target to increase the burn rate.

The in-cylinder flow motion under motoring condition is illustrated in Figure 4.3. Since the seed was supplied through one of supplementary gas lines as shown in Fig 2.11a and the pictures were taken at the plane passing through the intake valve stem offset from the cylinder center line, the pictures did not include the overall tumble motion generated in the center plane. And the view was limited by the camera even though the laser sheet covers the whole stroke. Figure 4.3a and b show the flow motion at 70 deg ATDC and 120 deg ATDC during the intake stroke, respectively. The dark wide stripe, which covers the lower left side of view, was due to the scratch on the wall and the dark side of upper right was due to the particle accumulation on the wall. Large scale motion in Fig 4.3 is clearly shown. During compression stroke, the tumble motion was found to be broken into the small scale turbulence[26]. Figure 4.3 c shows the small scale motion at 90 deg BTDC compression stroke even though the tumble rotation seems to be sustained. The breakdown of the large scale motion into irregular small eddies enhances in-cylinder mixing. Figure 4.4 and 4.5 show the cycle by cycle variation at 120 deg ATDC intake stroke and at 90 deg BTDC compression stroke respectively. The large scale motion shown in Fig. 4.4 illustrates less cycle by cycle variation than the small eddies during compression stroke shown in Fig. 4.5. The small scale eddies in Fig. 4.5 had not only a large cyclic variation, but also was relatively well distributed. The characteristic of small eddy distribution and mixing was discussed in Section 4.2 in detail.

4.2 Realization of charge stratification

The charge stratification between the air/fuel mixture and the supplementary inert gas to simulate external EGR was generated in the intake port and supplied into the cylinder. The inflow momentum of air/fuel mixture and inert gas is driven by the piston induction as well as by the inert gas supply control mode. Since the geometric shape of the cylinder head, pentroof design, is good for maintaining the tumble motion, the high tumble motion itself is not hard to be sustained through the intake stroke.. It was expected that each side of the inert gas flow should

have an equal momentum to minimize mixing and form the stratified mixture in the cylinder. Unless the momentum balance of inert gas flow is maintained, the unbalanced momentum creates a swirl motion which could destroy the tumble motion and caused mixing between fresh mixture and critical EGR. Even though the flow hit the valves, the velocity of supplementary gas is more significant than that of air-fuel mixture as addressed in Section 2.1.2. Therefore the large velocity gradient that exists at interface between two flows could also increase mixing.

4.2.1 In-cylinder visualization results

The mixing process during the intake and compression stroke was discussed in this section . Since the view covered around 40 % of the window of overall stroke, the overall mixing process in the cylinder was not shown in image data. Figure 4.6a and b illustrate the engine side and front view at 90 deg ATDC of the intake stroke. The upper part is the combustion chamber in the cylinder head, which was not accessible to visualization. The lower part is not completely accessible to visualization due to the limitation of the laser beam size.

Figure 4.7 illustrates the overall mixing process during the intake and compression stroke. The seed was supplied through the right supplementary gas supply line. The mixing process measured through the window illustrates that the level of mixing across the cylinder increases as the piston goes down. The boundary lines were expected to be formed by the large scale motion in the cylinder as discussed in Section 4.1.1. As the piston goes up after the bottom dead center, the tumble motion is getting to be broken due to the flat top piston and compression. When the piston reaches 60 deg BTDC, a significant mixing has already been occurred. Considering the mixing of the left side, substantial amount of mixing was expected at around 45 - 50 deg BTDC of the compression stroke, MBT spark timing. Since the tumble motion has three dimensional nature, one sectional view might not reveal enough information on mixing process, but these results indicate that an additional mechanism is needed to maintain the stratification during the compression stroke.

Figure 4.8 shows the comparison of intensity profiles at the same piston position, 45 deg ATDC of intake stroke and 45 deg BTDC of compression stroke. The radial profile in Fig. 4.8a, the intake side, clearly indicates the stratification of supplementary gas even though the overall image was distorted due to disturbances. However the significant mixing during the compression stroke was shown in Fig. 4.8b. Figure 4.9 illustrates mixing characteristic at the same piston

position, 90 deg. The mixing trend in the intake side is similar to that of 45 deg of Fig. 4.8a. The notable intensity gradient at 90 deg BTDC during compression is shown in Fig. 4.9b, which indicates that the substantial mixing occurred during the later part of the compression stroke as mentioned before. The mixing profile difference of axial direction at the same piston location illustrates the decay of the large scale motion during the compression stroke.

The comparison of cycle-by-cycle variation in mixing is shown in Figure 4.10a and b. The front and side views of 90 deg ATDC intake stroke are shown together. The image was calibrated with the background only, not intensity, to minimize image distortion. As the Mie scattering result of the front view is shown in Fig. 4.3, the tumble motion could be observed in this side view if the seed follows the strong tumble motion. However as shown in Fig. 4.10a, it is hard to observe the tumble motion with the image of PLIF. The possible reason may include that the shutter exposure time was too short to show any streak line or the seed did not reach the cylinder center line, where the laser sheet is passing through. The cycle-by-cycle variation of the mixture distribution of the front view also is worse than that of the side view. It is not clear that the tumble motion causes the cycle variation in mixing characteristic. In order to maintain supplementary gas in each corner of the cylinder, the tumble generated by supplementary gas might not be needed.

The mixing characteristics by changing the engine speed and the acetone supply location, on the left side of the part, were also examined. There was a similar mixing trend. Therefore, the result is not included here. Although the images were distorted due to the noise related to the engine operation, visualization test results illustrated a significant information on the flow motion, the mixing process in the cylinder during the intake and compression stroke. However this information was not reflected on the design improvement, which required the major change of the piston etc.

4.2.2 Phasing of artificial EGR injection and its effect on combustion

The proper synchronized timing control of the supplementary gas supply is a means to achieve a stable combustion at the dilute limit by maintaining stratification in the cylinder. In the EGR strategy, one extreme is a complete mixing between air-fuel mixture and inert gas (homogeneous charge), and the other limit is a complete stratification between them. When the EGR injection in the port occurs at close-valve, there is substantial mixing between the fresh

charge and the artificial EGR in the port and the charge approximates that of the homogeneous configuration. In open valve injection, the momentum of the EGR jet contributes to the tumble motion in the charge and tends to maintain the separation between the fresh mixture and the artificial EGR. Therefore by controlling the supply timing, the extent of mixing could be varied. Another point is to find out the optimum operating condition of the solenoid valve and to assess the relative performance. The solenoid valve opening duration was adjusted to 18 ms so as to meet the air/fuel ratio requirement.

Figure 4.11 shows the combustion behavior at lean condition with the difference of air supply timing by controlling the solenoid valve. Different cases are labeled by the CA at the start of EGR injection. For example, the 520 case is defined as that with opening timing of the solenoid valve at 520 deg so that it is in synchronization with the intake stroke¹. The others are shifted to 180 deg out of phase with the intake period; the 340 means that air is supplied during the exhaust stroke. IMEP and COV of IMEP are shown in Fig. 4.11a. The mixing control in the intake port did not show any significant improvement at this particular operation condition; λ is 1.4, spark timing is 35 deg BTDC. Fig. 4.11b illustrates the statistical distribution in IMEP. The box in each case contains 50 % data and the center line is for a median value. The 520 case shows wider data spread into higher IMEP largely due to the faster burning compared with the others. It is generally accepted that the maximum cylinder pressure occurs at about 16 deg after the top dead center for MBT timing [27]. In that point of view, the spark timing 35 deg BTDC for 520 case, is a little advanced for MBT timing possibly owing to the fast burning characteristic, which is also illustrated in Fig. 4.11c, e and f. Since the spark timing was maintained at a constant value, the performance improvement with the help of the mixing control strategy was not much shown in Fig. 4.11a and b.

The effect of supply control on engine performance was investigated at much leaner condition. When there was a significant cycle by cycle variation in engine performance, the setting of MBT spark timing was not a simple work because the misfire and after-misfiring cycles were alternating. Therefore the engine was operated at λ of 1.55 and the spark timing of 30 deg BTDC, which was assumed to be MBT in terms of uniform IMEP. Figure 4.12 illustrates that the mixing control in the intake port made a significant improvement in combustion, about 14 % increase in IMEP and stable combustion. The effect of stratification by optimizing supply

angle is clearly shown in Fig. 4.12b on the flame propagation angle $\theta_{10-90\%}$. Whether the stratification has a bigger effect on the flame propagation angle than the flame development angle $\theta_{0-10\%}$ could not be deduced from the data. The variation of the maximum cylinder pressure of the 520 case, which is shown Fig. 4.12c, was larger than the others, but most of cycles have higher pressure and the crank angles of the maximum pressure were less scattered and stayed around MBT timings as shown in Fig. 4.12d.

Figure 4.13 shows the effect of the supply angle on combustion at WOT, 30 % EGR and stoichiometric operation with MBT spark timing (45 deg BTDC). The results show the similar trend with lean burn condition. Since the 700 case has more time for mixing in the intake port, this could have worse combustion behavior than the 160 and 340 cases in terms of dilution effect on combustion. However Fig. 4.13 did not show those trends, which means that less mixing but non uniformity in mixture of the 160 and 340 could make a negative effect on combustion. The spark timing of non synchronized cases seems not to be MBT as shown in Fig.4.13d. Therefore in order to assess the effect of the spark timing on combustion performance, an experiment was done with 5 deg advance (50 deg ATDC). Figure 4.14 shows the comparison of peak pressure and IMEP with the peak pressure location. All other cases show a typical slow burning characteristic, whereas the 520 case indicated less partial burning. Comparing Fig. 4.13 and Fig. 4.14, the further spark advance increased the flame development angle $\theta_{0-10\%}$ and reduced the flame propagation angle $\theta_{10-90\%}$. These changes improved the combustion stability of non synchronized cases.

Figure 4.15 illustrates the comparison on the combustion behavior at the part load with the operation condition of 40 % dilution ratio, stoichiometric and 50 deg BTDC spark timing. Since mixture was heavily diluted by EGR gas, the normal operation with less than 10% COV of IMEP was hard to be achieved. The 520 case brought about more stable combustion and higher maximum combustion pressure with small improvement in IMEP as shown Fig. 4.15a and b. The burn angles are statically compared in Figure 4.16 because the cycle average of those angles is not enough to understand the combustion performance. The 520 case shows the narrow distribution in the flame initiation angle $\theta_{0-2\%}$ and $\theta_{0-10\%}$.

¹ The solenoid valve was opened at 20 deg BTDC in 520 case.

In order to examine the effect of less dilution ratio and supply control on engine performance, the engine was run at WOT condition with 20% EGR ratio, stoichiometric and 40 deg BTDC spark timing. Table 4.4 shows the summary of the test result. The difference in IMEP could be regarded as a experimental data scattering range. In this operation condition, the dilution effect on combustion could be regarded negligible even with the relatively large EGR ratio. These results can be achieved with the help of a high tumble.

The narrow angle spacing of supply angle around 520; 430 deg (520-90 deg) and 610 deg (520+90 deg) was tried to confirm whether the 520 deg is a relatively optimum condition. The 430 deg case supplies supplementary air during the early intake stroke and the 610 deg case does it during the later intake stroke. Figure 4.17 shows performance comparison. Since the spark timing was not adjusted for MBT timing, the comparison of IMEP and COV_{imep} does not imply the system performance exactly. Peak pressure and peak pressure location $\theta_{peak\ pressure}$ indicate that the spark timings for 520 and 610 are too advanced, which shows the fast burning as shown in $\theta_{0-10\%}$ and $\theta_{10-90\%}$. A possible explanation for this characteristic is that the early supplementary air supply before intake valves open with 340 deg gave much time to be mixed in the intake port and the part of air supplied during the early intake stroke also had time to be mixed and did not have enough momentum to make stratification during the intake and compression stroke. The mixing in the intake port with the 610 case is similar when intake valves are closed, but the supplied air during the later intake stroke seemed to be able to make mixture stratification during the last cycle.

Therefore the full synchronization with the intake stroke is found to be a better way to supply supplementary air.

Two conclusions can be drawn with regard to the phasing control of supplementary gas; first, the duration of supplementary gas in the intake port with the early injection before the intake valve open did not contribute to more mixing in the intake port at a low dilution situation, but at a high dilution, less duration and mixing in the intake port did improve combustion. The cycle by cycle variation in mixing dynamics due to the pressure interaction between dilute gas and air/fuel mixture should also be considered. And second, there was a substantial reduction in IMEP fluctuations with the synchronized supply control at a high dilution condition.

4.3 Effects of the charge stratification on engine performance

The effect of the charge stratification on engine performance was addressed more in this section by comparing the homogeneous charge supply with the stratified (the 520 case) charge supply. There might be an optimal operation condition in supplementary gas supply in each load condition. However too many experiments are needed to find all those conditions, which is beyond the work scope of this research. Therefore two conditions were compared; one is WOT and the other is part load. Fuel flow rates are kept at a constant value.

4.3.1 Reference operation

Engine was run at a stoichiometric condition without EGR to have reference data. First in order to check combustion efficiency HC was measured. Table 4.5 shows the test results. Since unburned hydrocarbon levels in the exhaust of a spark-ignition engine under normal operating conditions are typically in the range 1000 to 3000 ppm C₁, the measurement was expected to be done at a normal operation condition considering the level of HC in Table 4.5.

In order to have the reference data for the system performance comparison, engine firing pressure data was obtained and analyzed with the burn analysis program. Figure 4.18 shows the comparison of IMEP and P_{max} vs. θ_{Pmax} and $\theta_{10-90\%}$ vs. $\theta_{0-10\%}$ at two operating conditions. Table 4.6 is the summary of test results. The flame development angle $\theta_{0-10\%}$ was more affected by load increase than the flame propagation angle $\theta_{10-90\%}$, probably due to the influence of the amount of residual gas amount in the cylinder with the difference of load.

The fuel flow rates for each load condition were kept a constant level for load comparison. The part_1 of Table 4.6 was used for the reference for the part throttle test of lean and dilution condition and the part_2 was for WOT, where WOT is to indicate the throttle position rather than to mean the full load performance.

4.3.2 Lean limit extension

The combustion performance in the lean mixture condition was already introduced and discussed in section 4.2.2. In this section, the combustion properties were addressed. In order to understand the contribution of stratification strategy to combustion, each parameter was analyzed by comparing combustion of homogeneous and stratification mixture together. Table 4.7 illustrates the lean burn test summary.

Figure 4.19 shows the comparison of lean burn between the homogeneous mixture and the stratified mixture combustion. As shown in Table 4.7 and Fig. 4.19a, there was a significant IMEP variation in the homogeneous mixture. When the flame development angle $\theta_{0-10\%}$ is less than around 35 deg, near the top dead center of compression stroke, the peak pressure location moves to the later crank angle with the increase of $\theta_{0-10\%}$, shown in Fig. 4.19e and f. As $\theta_{0-10\%}$ is higher than 35 deg, which means that most burning occurs during the expansion stroke, IMEP drops steeply, as shown in Fig.4.16 c. Most of the stratified mixture was burned at less than 35 deg of $\theta_{0-10\%}$. However a significant amount of homogeneous mixture was burned at higher than 35 deg. Another point to make is that IMEP of homogeneous mixture is more sensitive to $\theta_{0-10\%}$ change, which means that the less the flame development angle $\theta_{0-10\%}$ is, the bigger IMEP is. Since the burn angle $\theta_{10-90\%}$ is proportional to the burn angle $\theta_{0-10\%}$ as shown in Fig. 4.19g and h, once the stratification strategy reduces the flame development angle $\theta_{0-10\%}$, the effect also decreases the flame propagation angle $\theta_{10-90\%}$. Figure 4.19i and j show the statistical distribution of frequency of $\theta_{0-10\%}$ and $\theta_{10-90\%}$. The cycle-by-cycle variation of $\theta_{10-90\%}$ is bigger than that of $\theta_{0-10\%}$. Fast flame development produced higher peak pressure, which is shown in Fig 4.19k and l. The trend of peak pressure as a function of $\theta_{0-10\%}$ is similar between two cases but the stratified strategy made a fast burn.

Next analysis is on the engine operation of less air dilution ratio at WOT, which creates more turbulence generated by a strong tumble motion. As shown in Table 4.7, IMEP of homogeneous mixture is bigger. Comparing burn angles, the stratified mixture has a fast burning characteristic. Therefore there seems not much improvement with the stratification strategy results. Even though there is a difference in lamda value even with the same fuel flow rate, overall operation conditions can be regarded similar due to the limit of engine operation. Figure 4.20 illustrates the results in detail. As illustrated in Fig. 4.20a, the homogeneous mixture seems to be operated around MBT spark timing. Considering this fact, the stratification strategy improved combustion a little by reducing the burn angle. And the general trend shows that with the same flame development angle $\theta_{0-10\%}$, the flame propagation angle $\theta_{10-90\%}$ is reduced with the help of stratification.

4.3.3 Dilute limit extension

The typical modern production engine has the tolerance on EGR dilution ratio up to about 20% [27]. As the amount of EGR gas increases after normal operation limit, there are a rapid IMEP drop and a significant combustion instability. In this section, the effect of stratification strategy on the combustion of highly EGR diluted mixture was addressed. Table 4.8 shows the summary of test results.

In order to understand the stratification effect on combustion, the data analysis was statistically analyzed because at part throttle operation there are significant partial burning and IMEP fluctuation. Figure 4.21 shows the individual cycle parameters. Fig. 4.21a and c illustrate that there are highly IMEP variations due to the cyclic behavior of slow burn and after slow burn². Even with the stratification strategy, the level of COV_{imep} is too big for engine operation as shown in Fig. 4.21b and d. Considering the peak pressure location and IMEP distribution in Fig. 4.21, the spark timing, 50 deg BTDC, might not be controlled enough for MBT timing, even though Fig. 4.21e and f indicate that the peak pressure location seems to be advanced. However those spark characteristics were reflected on peak pressure value in Fig. 4.21a and b.

Another interesting behavior in burn parameter $\theta_{0-10\%}$ is that there is a significant IMEP variation around the 50 deg of $\theta_{0-10\%}$. Since this location is the piston top dead center, if the flame had not been developed to the top dead center, the possibility of misfiring would be quite high. This issue was discussed in Section 4.3.2, but the trend in this operation condition is much different. As shown in Fig. 4.21g and h, there are two groups with a different trend. With the stratification strategy, the group with a long duration was diminished, which could make it possible to have less cycle by cycle variation.

In both figures 4.21g and h, there are substantial IMEP variations for cycles with approximately the same $\theta_{0-10\%}$ of around 50 deg. With spark timing at 50 deg BTDC, the 10 % burn point of these cycles thus occurred at around TDC. This data is consistent with those in figures 4.21i and j, which show that for the same $\theta_{0-10\%}$ duration, there is a substantial variation in the peak pressure location. The implication is that although the early parts (0 - 10% burn) of

² After-slow burn cycle showed relatively higher IMEP due to the internal residual gas containing some fuel from the previous partial burn cycle.

combustion in these cycles are similar, there are substantial differences in the later part of the burning process.

To investigate this observation further, cycles with $\theta_{0-10\%}=50$ deg are selected out from Fig. 4.21 and are explored in Fig.4.22. In Fig. 4.22a and b, the IMEPs of these cycles are proportional to the mass fraction burn.³ The group in the homogeneous mixture has a different combustion characteristic compared with the cycles in the stratified mixture as well as the slow burning cycles. The higher pressure(temperature) of these cycles contributed to larger heat loss as shown in Fig. 4.22c and d. The correlation between IMEP versus $\theta_{10-90\%}$ shown in Fig. 4.22e and f is not strong, which indicates that the cycle by cycle variation of fuel in mixture largely caused by the partial burn is a dominant factor in combustion; Since 10% of the fuel burned of each cycle does not have to be the same amount of fuel, the amount of fuel of each cycle has a large cycle variation even with constant fuel supply.

The conclusion from this issue is that the level of stratification at this operation condition reduced the partial burning, but not enough to make a fully developed stable flame, which requires the angle $\theta_{0-10\%}$ to be less than 50 deg after ignition as shown in Fig. 4.21.

Figure 4.23 shows burn parameters at WOT engine operation with EGR dilution. It indicates that engine was operated with a relatively stable combustion. The stratification strategy reduced the number of slow burn cycles. In this operation condition, the frequency of the cycle of after slow burn is also relatively small. The burn characteristics in Fig.4.23c and d indicate that a small variation of $\theta_{0-10\%}$ of the homogeneous mixture make a larger variation of IMEP than that of stratified mixture and IMEP of stratified mixture is less dependent on the variation of $\theta_{0-10\%}$. Considering a poor correlation between $\theta_{0-10\%}$ and $\theta_{10-90\%}$ and a good correlation between peak mass burn rate vs. $\theta_{10-90\%}$, peak mass burn rate seems governed by the flame propagation angle $\theta_{10-90\%}$, as shown in Fig. 4.23g-l, rather than the flame development angle $\theta_{0-10\%}$. The homogeneous mixture and stratified mixture seems to follow the same trend of peak mass burn rate at given $\theta_{10-90\%}$.

The same approach was tried to get the information about the reason of variation of IMEP at fixed 45 deg of $\theta_{0-10\%}$ shown in Fig. 4.23e and f. Figure 4.24 shows a similar trend in all burn

parameters. The variation in IMEP can be regarded as a typical combustion variation influenced by mixture composition and flow. One point to be addressed here is that the IMEP decrease with the increase of $\theta_{10-90\%}$ has a steeper slope in homogeneous mixture as indicated Fig. 4.24e and f, which could be regarded as the indicator of the effectiveness of stratification strategy.

In order to characterize the observed IMEP variations, the use of $\theta_{0-50\%}$ was suggested to relate individual cycle IMEP values to some measure of their burn history because this includes the dependence on both flame development and propagation details [21]. Figure 4.25 shows the comparison of IMEP vs. $\theta_{0-50\%}$ at two operation conditions. $\theta_{0-50\%}$ seems not to be a good characteristic parameter to see any correlation between IMEP and $\theta_{0-50\%}$ for this engine and operation conditions. It is well known that IMEP is relatively insensitive to phasing changes around the MBT spark timing. A typical combustion shows that half the charge is burned at about 10 deg after TC or the maximum pressure occurs at about 16 deg after TC [2]. Even though Fig 4.21 a-b and 4.23 a-b show that peak pressure occurs less than 16 deg ATC, Fig 4.25 indicates that spark timing seems not advanced enough due to slow burning. Since the setting of MBT timing is not a simple work here, the cycle variation caused by not MBT phasing is needed to be considered.

4.3.4 Comparison between lean burn and EGR

The reduction of laminar flame speed for given values of unburned temperature and pressure due to the addition of burn gas is much greater than the reduction due to the addition of excess air because (i) the burn gas has a higher heat capacity, and (ii) the oxygen in the excess air helps combustion, whereas the EGR diluent just absorbs energy and impedes the diffusion of chemical species and heat[28]. Figure 4.26 shows the performance comparison between lean burn and EGR. The comparison is based on the dilution ratio described in Table 4.7 and Table 4.8. The stratification strategy did improve engine performance in terms of overall view. The effectiveness of this strategy is getting better as the dilution ratio increases. The combustion variability was significantly improved up to a certain dilution ratio, where the amount of internal residual gas has a dominant effect on laminar flame speed. In order to fully assess the performance, the comparison of indicated specific fuel consumption shown in Fig. 4.26d might

³ In these figures, values of $x_b > 1$ arise from the fact that following a partial burn cycle, the fuel mass in the cylinder is higher than the fuel mass of the average cycle.

not be enough. As expected, the fuel consumption was improved at the lean burn condition with the stratification strategy.

The effect of the stratification strategy on variations of flame initiation and development angles is given in Figure 4.27. The results less than 40 deg of $\theta_{0-10\%}$ are from lean burn data. Figure 4.27a indicates that there is a linearity between mean $\theta_{0-2\%}$ and mean $\theta_{0-10\%}$, and flame initiation and development were reduced with the stratification strategy. However Fig. 4.27b and c illustrate notable results. Even though the stratification strategy has reduced the flame initiation angle at a given operating condition, the trend in Fig. 4.27b indicates that the cycle variability of this angle was worsened with the stratification strategy at the fixed $\theta_{0-10\%}$. But this trend was reversed at Fig. 4.27c.

In order to examine this issue, the correlation between $\theta_{0-2\%}$ and $\theta_{0-10\%}$ for the various operating conditions including the homogeneous mixture and stratification mixture is shown in Figure 4.28. There is a significant difference between lean burn and EGR in the general shape. Except the fast combustion of the stratification strategy in lean burn, it appears that there is a good linear correlation between $\theta_{0-2\%}$ and $\theta_{0-10\%}$ that is shown Fig. 4.28e - f. The correlation of EGR illustrated in Fig. 4.28a - d is more complex than that of lean burn; there are two slopes in a and b largely due to the slow burn at the high dilution ratio and the correlation between c and d shows a different shape. How does the stratification strategy affect the flame initiation and development? The effect of this strategy on $\theta_{0-2\%}$ is not so clear. The flame initiation angle $\theta_{0-2\%}$, also called a ignition delay, is strongly influenced by ignition performance [27]. Once the flame was initiated, this strategy reduced the flame development angle $\theta_{0-10\%}$; the shorter $\theta_{0-2\%}$ was, the faster the flame was developed in Fig. 4.28d. Since the flame development angle $\theta_{0-10\%}$ was affected by the laminar flame speed, which is enhanced by the stratification of diluent, this result supports the effectiveness of the system partially.

Figure 4.29 shows the effect of the stratification strategy on variations of flame development angles. The stratification strategy effectively reduced the mean and variation of the flame development angle. Even though the flame development angle $\theta_{0-10\%}$ was reduced with the difference of engine operation condition, the flame propagation angle $\theta_{10-90\%}$ maintains the same level in both cases except one small dilution condition. The dilution ratio has a stronger effect on the flame development angle $\theta_{0-10\%}$ than the flame propagation angle $\theta_{10-90\%}$.

4.4 Identifying the design performance limit and its improvement

In this experiment, propane was used for fuel to minimize the effect of fuel vaporization and to have a uniform air/fuel mixture. When liquid fuel was injected into the cylinder, the possibility of fuel distribution near the spark plug is expected to be high with the stratification strategy, which could improve the flame development. The engine speed 1000 rpm, which is limited by an experimental setup, is not generally used for engine performance assessment. It is also not certain whether the stratification strategy was fully assessed in this test operation condition and whether this system will work at other operating conditions even if the system worked successfully at this condition. There are also optimization issues involved, which needs a tremendous amount of work. Therefore the discussion of the effect of different engine speeds and load conditions on system performance will not be included here even though those effects are really important for the system assessment.

4.4.1 Charge mixing in the intake port and during the intake stroke

The need to supply supplementary gas during the induction stroke as a synchronized condition was discussed in Section 4.2.2.

Since the air induction motion is controlled by the intake valves and the piston motion, the supply control of supplementary gas with a specified angle should be optimized with the cam phasing. Because of the test setup limitation, supplementary air was supplied in jet form, which enhances mixing due to the nearby gas entrainment into jet stream. Another important factor in mixing during the intake stroke is an induction momentum imbalance.

As shown in Fig. 4.7, stratification was maintained relatively well during the intake stroke. Since the residual gas back flowed into the intake port is also inducted, it is expected that the relative amount of inert gas external of internal is another factor. This is closely related to engine load control. As discussed in the previous sections, the efficiency of stratification strategy is getting rapidly worse largely due to the amount of inert gas uncontrollable. Also this issue was further investigated in Section 5.

4.4.2 Charge mixing during the compression stroke

When the piston goes up after the bottom dead center, the tumble motion breakup starts due to the geometry in the cylinder. In order to preserve the tumble momentum and stratification momentum formed during the intake stroke, there must not be much restriction in the flow direction. The cylindrical shape is expected to be better. The piston flat top was modified as an

attempt to maintain the momentum [8]. Considering the rigorous mixing during the compression stroke shown in Fig. 4.7, the design of flat top piston is required to be improved.

Another issue is that there seems a tradeoff between stratification requirement and turbulence generation. Tumble motion should be broken into the small eddy motion at certain crank angle during the compression stroke in order to be able to assist combustion. However the breakup of tumble motion could enhance the mixing due to the increase of mixing surface area and eddy motions.

4.4.3 Charge mixing during the flame propagation phase

Even though there is a perfect stratification between air/fuel mixture and inert gas, the mixing due to the diffusion or the expansion of burned gas during the flame propagation phase is expected and it would have a certain effect on the flame propagation. The possible way to control mixture distribution during the combustion phase is to set spark timing, which is limited for MBT for performance.

With the complex motion in the cylinder, it might not be easy to be able to figure out the each contribution on flame development of propagation. Therefore the possible level of mixing and mixture distribution and their effect on combustion is addressed in Section 5.6.1.2.

4.5 Discussion on engine implementation

There are several issues in order to implement the concept of stratified_EGR mode operation to the production engine. Considering the information from the concept development results, the suggestion on production engine implementation are as follows.

- EGR distribution system

In order to supply the dilute gas into the targeted area of in-cylinder, the mixing between fresh mixture and dilute gas in intake port should be minimized. The even distribution to each cylinder will be critical to maintain a uniform cylinder-to-cylinder power output. Two functional requirements are needed to be considered; one is to minimize the pressure fluctuation in EGR distribution system and the other to synchronize with the induction period throughout engine operation range. Since the supply source of EGR gas is from exhaust system and the pressure is maintained around atmospheric pressure, plenum is recommended to meet the amount of EGR gas required at each operation condition and to minimize pressure wave motion. An EGR distributor mechanically driven by cam mechanism is also recommended.

- Piston top design

The rapid mixing during the compression stroke is largely due to the geometry of cylinder wall and piston top design. In order to keep the tumble momentum and the stratification during the compression stroke, the piston top is recommended to be a curved shape.

- Control mechanism

The EGR gas supply from the exhaust system to the intake system is needed to be controlled to meet the EGR gas requirement. An electronically controlled EGR valve is recommended. Since the internal EGR gas is substantial at low load, more precise control on the amount of external EGR based on the engine operation condition is needed. A lot of calibration work is expected to setup the optimum operation condition.

CHAPTER 5 Model for lean/dilute combustion in the stratified EGR engine

5.1 Overview

The objective of the modeling is to develop a quantitative description of flame propagation properties in a highly diluted mixture and the resulting engine performance. The following issues are of particular interest.

- Flame initiation & development under the influence of flame stretch effect at high level of dilution.
- Burned gas and unburned fresh mixture mixing in the end gas and its effect on combustion

As shown in the previous chapter, at the same level of dilution, the stratified charge configuration has a substantially smaller cycle by cycle variation (CCV) of IMEP than the homogeneous configuration. One of the objective of the modeling effect is to explain this difference. There are a lot of different factors contributing to cyclic variations [27]. The approach here is to examine the sensitivity of the engine performance (e.g. IMEP) to the various factors via the model.

The MIT engine simulation program [29] was used as the base code. This program is based on a quasi-dimensional model. The engine combustion chamber is divided into burned and unburned zone, and the interface between them is the flame front, which is taken to be thin, spherical surfaces intersecting the combustion chamber walls and centered at the spark location. The burned gas zone consists of an adiabatic core and thermal boundary layers to take account of the heat transfer effect. In this base code, the fuel, air and residual gas are uniformly premixed and overall balances of mass, energy, chemical species are applied to each zone. A closed set of simultaneous ordinary differential equation with time dimension yields the temporal variation of temperature, pressure and other relevant variables in each zone. This program can account for turbulence, flame propagation, heat transfer, etc. and thus incorporate a reasonably complete description of the relevant physics.

The present investigation involves the development of turbulence and combustion models in order to incorporate the effects of mixing of dilution gas, strong tumble and stratification on the flame propagation.

5.2 Modeling assumptions and approach

Even though there is a strong organized (tumble) motion in cylinder, an isotropic and homogeneous turbulence structure is assumed. This assumption is a reasonable description of the small scale motion that affects flame propagation. Since at a highly diluted condition, the flame in engine falls within the turbulent combustion category of “distributed reaction”. Entrainment of the unburned mixture into the enflamed region is assumed to be the dominant effect of turbulence on the combustion process (see next section). The other assumptions used are:

- It is assumed that the average flame front expands spherically away from the spark kernel
- Blowby and crevice flow are neglected. The actual peak pressures are thus slightly higher.

5.3 Combustion model

5.3.1 Eddy burning model

The combustion model is the eddy burning model, which was initially formulated by Blizzard and Keck[30] and is extended to encompass the “distributed reaction” regime[31,32]. The original model is based on the assumption that turbulent flames in spark ignition engines can be modeled as thin wrinkled multiply connected locally laminar flames and simulates the development of the flame as a turbulent entrainment process followed by a burn-up process in a region behind the flame front. The concept could be extended to the flame zone in a spark ignition engine with a highly diluted charge; then the combustion could be categorized as the “thickened wrinkled laminar flamelet” (or distributed reaction) regime rather than in the wrinkled laminar flamelet regime as the experimental evidence attests[33]. The model still applies, but with a much longer burn-out time governed by the substantially lower laminar flame speed of the local charge. The local mixture dilution ratio is empirically modeled by a stratification function (see Sec. 5.3.4).

Burning rate equations with a further modification are modeled [31, 32] as:

$$\dot{m}_b = \rho_u A_f S_L I_o + \frac{m_e - m_b}{\tau_b} \quad (5-1)$$

$$\dot{m}_e = \rho_u A_f \left(u' \left(1 - \exp\left(-\frac{t}{\tau_b}\right) \right) \left(1 - \exp\left(-\frac{r_f}{L}\right) \right) I_o^{\frac{1}{2}} + S_L I_o \right) \quad (5-2)$$

where

m_b	mass burned
m_e	mass entrained into the flame front
ρ_u	density of the unburned mixture
A_f	flame front area
S_L	laminar flame speed
τ_b	characteristic time to burn an eddy of size λ
λ	Taylor micro scale
u'	turbulence intensity
m_e	mass entrained into the flame front
r_f	flame radius
L	macro scale (integral length scale) of turbulence
I_o	strain rate factor

The first term in Eq. (5.1) represents the laminar propagation forward of the approximately spherical front of the thick turbulent flame or the burning of the entrained mass at laminar flame speed; the second term represents the burning of mixture already entrained within this flame front or the burning of the pockets of unburned mixture in the burned region.

In Eq. (5.2), the equation governing entrained mass incorporates contributions to the entrainment rate from the burning speed normal to a local flame front gas and the distortion of that flame front due to turbulent velocity fluctuations with the mixture. The first correction term of the first term in Eq.(5.2) is the time dependent integral time scale for small turbulence present, which means that the flame sheet initially is spherical and laminar like. The second one is the

size dependent integral length scale to take account the influence of flame curvature, which means that early flame growth should not be significantly affected by the turbulence until the kernel achieves a radius on the order of that of a turbulent eddy [34].

Since the eddies are assumed to be burned up by laminar flame propagation, the characteristic time to burn an eddy of size λ is:

$$\tau_b = C_\tau \frac{\lambda}{S_L}, C_\tau \text{ is model constant.}$$

For isotropic and homogeneous turbulence, the Taylor micro scale is defined as:

$$\lambda = \left(15L \frac{\nu}{u'} \right)^{1/2} \quad (5.3)$$

where,

ν viscosity of unburned mixture

5.3.2 Laminar flame speed

The laminar flame speed is calculated from an empirical correlation of Metghalchi and Keck [35]. This is modified in order to account for mixture dilution effect. The correction is a function of burned gas fraction and is based on the data by Rhodes[28] from experiments with constant volume combustion of Indolene-air mixture.

$$\frac{S_L}{S_{L\infty}} = \left(\frac{T_u}{T_\infty} \right)^\alpha \left(\frac{P}{P_\infty} \right)^\beta F_c \quad (5.4)$$

$$F_c = C_1 (1 - 2.06f^{0.773}) + C_2 (1 - 4.1f + 4.7f^2) \quad (5.5)$$

where,

T_u unburned gas temperature (K)

P cylinder pressure (bar)

T_∞, P_∞ reference conditions 298 K and 1 bar

$S_{L\infty}$ laminar flame speed at the reference conditions

α, β constants for propane

f residual gas mole fraction

C_1, C_2 model constants

For propane, these constants can be represented by

$$\alpha = 2.18 - 0.8(\phi - 1)$$

$$\beta = -0.16 + 0.22(\phi - 1)$$

$$S_{L\infty} = 34.2 - 138.7(\phi - 1.08)^2$$

where ϕ is equivalence ratio.

A combination of generally used correlation is used. The first term of Eq. (5.5) is valid with engine internal residual fraction f up to 0.3 and the second term is up to 0.44. This new model extends f up to 0.55. Figure 5.1 shows the comparison between this model and previous models[28,36]. As shown in Fig. 5.1, there is uncertainty in value extrapolated over 0.3 of dilution mass fraction that was not available in test data.

5.3.3 Modeling of strain rate factor I_0

Laminar flame theory shows that the flame response can be affected by stretch, preferential diffusion, and flame curvature. For nonunity Lewis number, defined as the ratio of thermal diffusivity to the mass diffusivity of the mixed reactant, the differential diffusion of heat and species results in a strong sensitivity of the local flame structure to strain rate.

Researches of strain rate effects on combustion illustrated that when Lewis > 1 , lean or dilution mixture, an increase in strain rate results in a decrease in the rate of consumption of reactant, resulting less flame surface area and slower turbulent flame speed [37]. Since engine was operated with a highly diluted mixture, where the Lewis number plays an important role in flame behavior, the consideration of flame response to strain was incorporated into combustion model.

5.3.3.1 Model I: general approach

The concept of flame stretch was used to explain and quantify the various phenomena associated with flame stabilization. There are two types of strain on laminar flames in SI engines [34,38]. Geometric strain is described by the surface increase normalized to its surface.

$$K_g = \frac{1}{A} \left(\frac{dA}{dt} \right) \quad (5.6)$$

A generalized expression is

$$\frac{1}{A} \left(\frac{dA}{dt} \right) = \nabla \cdot v + (v \cdot n)(\nabla \cdot n) \quad (5.7)$$

which is derived by using the invariant formulation[39]. The first term is the stretch due to the non uniform tangential velocity field and the second term represents the effect of curvature of the propagating flame.

In turbulent flow field, turbulence strain is defined as the ratio of turbulence intensity to the Taylor micro scale.

$$K_t = \frac{u'}{\lambda} \quad (5.8)$$

The effective strain rate K is the sum of geometric strain and the turbulence strain.

$$K = K_g + K_t = \frac{1}{A} \left(\frac{dA}{dt} \right) + \frac{u'}{\lambda} \quad (5.9)$$

The expressions of the various flame responses for a wrinkled flame in a non uniform flow field are given by [40]:

$$\begin{aligned} \frac{S_L}{S_L^o} &= 1 - \delta_L \nabla \cdot n + \left(\frac{1}{Le} - 1 \right) \left(\frac{T_{act}}{2T_{ad}} \right) K_a \\ \frac{S_f}{S_f^o} &= 1 - \frac{K_a}{Le} + \left(\frac{1}{Le} - 1 \right) \left(\frac{T_{act}}{2T_{ad}} \right) K_a \end{aligned} \quad (5.10)$$

where

$$K_a = \left(\frac{\delta_L^o}{S_L^o} \right) K \quad \text{Karlovitz number}$$

$$\delta_L^o = \frac{D_T^o}{S_L^o} = \frac{\alpha}{S_L^o} \quad \text{laminar flame thickness}$$

$$Le = \frac{D_T^o}{D_m^o} = \frac{\alpha}{D_m^o} \quad \text{Lewis number}$$

$$\nabla \cdot n = \frac{2}{r_f} \quad \text{for source at the center and } r_f \text{ is the flame radius}$$

$S_f = \frac{dr_f}{dt}$	Burning speed
$T_{act} = \frac{E_a}{R}$	Activation temperature
T_{ad}	Adiabatic flame temperature
E_a	Chemical reaction activation energy
R	Universal gas constant
°	the adiabatic, unstretched planar flame state.

These expressions show that the flame response is affected by the stretch ($K \neq 0$) and preferential diffusion ($Le \neq 1$), and flame curvature ($\nabla \cdot n \neq 0$). Therefore a formulation for the change of the laminar flame speed with respect to the strain rate and the Lewis number is described as:

$$I_o = \frac{S_L}{S_{L_o}} = 1 - 2 \frac{\delta_L}{r_f} + \left(\frac{1}{Le} - 1 \right) \cdot \left(\frac{T_{act}}{2T_{ad}} \right) K_a \quad (5.11)$$

Karlovitz number K_a is the ratio of a chemical time scale to a hydrodynamic time scale.

$$K_a = \left(\frac{\delta_L}{S_L} \right) K = \left(\frac{\delta_L}{S_L} \right) \left(\frac{1}{A} \left(\frac{dA}{dt} \right) + \frac{u'}{\lambda} \right) \quad (5.12)$$

Expressions for K are complex for general flame geometry and velocity fields. But for an unconstrained spherical laminar flame propagating at constant pressure away from an ignition source with negligible motion of the burned gas, the initial development of a spherical flame can be illustrated as

$$\frac{1}{A} \left(\frac{dA}{dt} \right) = \frac{2}{r_f} \left(\frac{dr_f}{dt} \right) = \frac{2}{r_f} \left(\frac{\rho_u}{\rho_b} S_L \right) \quad (5.13)$$

which is based on the assumption that

$$\frac{dr_f}{dt} \approx \frac{\rho_u}{\rho_b} S_L \text{ when } \frac{\delta_L}{r_f} \ll 1$$

After further rearrangement, the stretch factor I_o is described as

$$I_o = 1 - 2 \frac{\delta_L}{r_f} + \left(\frac{1}{Le} - 1 \right) \left(\frac{T_{act}}{2T_{ad}} \right) \left(\left(\frac{\delta_L}{S_l} \right) \left(\frac{u'^3}{15Lv} \right)^{1/2} + 2 \frac{\delta_L}{r_f} \left(\frac{\rho_u}{\rho_b} \right) \right) \quad (5.14)$$

In this model approach, the turbulence strain effect is too high at high dilution ratio and different order of magnitude compared with the geometric strain. The simple sum of two strains might not be a good approach. Laminar flame speed is getting smaller with the increase of dilution mass fraction, which makes Karlovitz number bigger when the magnitude of turbulent strain is too big. In this case the combustion environment in cylinder changes from the flame sheet model applicable region to the boundary region between distributed reaction and flame sheet reaction largely due to the low values of laminar flame speed. Whether the flame structure under these conditions is significantly different is not known[2].

In a turbulent flow the fluctuating nonuniform local velocities impose aerodynamic stretching on the highly-convoluted flame surfaces. Thus the results of stretched laminar flames can be applied to certain situations involving turbulent premixed flames. The minimum requirement for such an application is that the flamelet satisfies the Klimov-Williams criterion, which basically states that the laminar flame thickness must be smaller than the Kolmogorov microscale [37]. When the turbulent Karlovitz number (ratio of laminar flame time to Kolmogorov time) is greater than unity, the flame stretch is strong and the smallest eddies can enter into the flame structure since Kolmogorov length scale is less than laminar flame thickness, thereby broadening the flame structure. These eddies produce the largest straining rates and may lead to local extinction of some inner reaction zone, but nothing definite is known about this interaction at present[41].

5.3.3.2 Model II: eddy burning approach

In a highly diluted mixture, which is located at the boundary region between distributed reaction and laminar flamelet reaction, additional approximation is needed in order to reduce the excessive turbulent stretch effect and incorporate the stretch effect especially in terms of preferential diffusion and curvature.

For spherical flame, the following relation can be derived from a conventional definition.

$$\frac{1}{A} \left(\frac{dA}{dt} \right) = \frac{2}{r_f} \left(\frac{dr_f}{dt} \right), \quad \frac{dr_f}{dt} = \frac{dm_b}{dt} \left(\frac{1}{4\pi\rho_b r_f^2} \right) \quad (5.15)$$

From entrain combustion model and eddy burning characteristic time,

$$\frac{dm_b}{dt} = \rho_u \cdot 4\pi r_f^2 \cdot S_L + \frac{m_e - m_b}{\tau_b} \quad (5.16)$$

$$m_e - m_b = \rho_u \cdot \frac{4\pi}{3} \cdot (r_e^3 - r_f^3) \quad (5.17)$$

Therefore, the stretch factor can be described as follows:

$$K = \frac{1}{A} \left(\frac{dA}{dt} \right) = \frac{2}{r_f} \left(\frac{dr_f}{dt} \right) = \frac{2}{r_f} \cdot \frac{\rho_u}{\rho_b} \cdot S_L \cdot \left(1 + \frac{r_f}{3\lambda} \cdot \left(\left(\frac{r_e}{r_f} \right)^3 - 1 \right) \right) \quad (5.18)$$

In this formulation, the planar flame approximation is not needed. Furthermore, since turbulence eddy effect is included in the flame stretch formulation, additional turbulence strain effect is not considered.

$$K_a = \left(\frac{\delta_L}{S_L} \right) K = \left(\frac{\delta_L}{S_L} \right) \cdot \frac{1}{A} \left(\frac{dA}{dt} \right) = \left(\frac{\delta_L}{S_L} \right) \cdot \frac{2}{r_f} \cdot \frac{\rho_u}{\rho_b} \cdot S_L \cdot \left(1 + \frac{r_f}{3\lambda} \cdot \left(\left(\frac{r_e}{r_f} \right)^3 - 1 \right) \right) \quad (5.19)$$

However there was a serious oscillation in the stretch factor of Model II due to the oscillation in the ratio of entrained radius to flame radius, which was largely caused by the flame area interaction. The oscillation could be the limitation of the combustion geometry or that of eddy entrained model.

5.3.3.3 Model III: general approach without turbulence effect

Effects of flame stretch can best be observed when r_f is small with stable ignition. Experimental results of the flame speed of the positively-stretched outwardly-propagating flame for propane/air mixtures showed that there is clear preferential diffusion effect and the stretch effect is strongest when the flame kernel is small and decreases at the flame propagates outward [37].

When the flame kernel is small, where laminar flame speed dominates and strong flame stretch effect is expected, the incorporation of stretch effect into combustion model is essential to be able to explain the flame behavior especially for the mixture with large Lewis number even though the stretch model itself could not be used for a fully developed flame area with turbulent flame speed.

Next approach for stretch factor calculation is to incorporate the flame stretch effect during initial flame development, which is based on two assumptions.

- The first assumption is that the density in the preheat region is the arithmetic average of burned gas density and unburned one.
- The second one is that the time derivative of laminar flame thickness is zero, which means that laminar flame thickness is relatively constant compared with other parameters.

Since the assumption, $\frac{\delta_L}{r_f} \ll 1$, is not required, this formulation could be applied to initial flame formation stage, where that assumption is weak.

$$K = \frac{1}{A} \left(\frac{dA}{dt} \right) = \frac{2}{r_f} \cdot \frac{\rho_u}{\rho_b} \cdot S_L \cdot \left(\frac{\left(1 + \frac{\delta_L}{r_f} \right)^2}{1 + \frac{\rho_u}{\rho_b} \left(\left(1 + \frac{\delta_L}{r_f} \right)^2 + \left(\frac{\rho_u}{\rho_b} + 1 \right) \left(\frac{\delta_L}{r_f} \right) \right)} \right) \quad (5.20)$$

In this formulation, the assumption that the thickness of the flame reaction zone is negligible is not required.

From the overall mass conservation, the rate of change of mass in the burned, preheat, and unburned zones should be equal to the rate of dispersion of mass in the unburned region:

$$\rho_b \frac{d}{dt} \left(\frac{4}{3} \pi r_f^3 \right) + \frac{1}{2} (\rho_u + \rho_b) \frac{d}{dt} (4 \pi r_f^2 \delta_L) = -4 \pi (r_f + \delta_L) \rho_u u_u \quad (5.21)$$

$$\begin{aligned} S_L = u_{rel} &= \dot{r}_f - u_u \\ &= \left(\frac{\rho_b + (\rho_u + \rho_b) \left(\frac{\delta_L}{r_f} \right)}{\left(1 + \frac{\delta_L}{r_f} \right)^2 \cdot \rho_u} \right) \cdot \dot{r}_f + \frac{\rho_u + \rho_b}{2 \left(1 + \frac{\delta_L}{r_f} \right)^2 \cdot \rho_u} \cdot \dot{\delta}_L \end{aligned} \quad (5.22)$$

If $\dot{\delta}_L \equiv 0$, then

$$\dot{r}_f = \frac{\rho_u}{\rho_b} \cdot S_L \cdot \left(\frac{\left(1 + \frac{\delta_L}{r_f} \right)^2}{1 + \frac{\rho_u}{\rho_b} \left(\left(1 + \frac{\delta_L}{r_f} \right)^2 + \left(\frac{\rho_u}{\rho_b} + 1 \right) \cdot \left(\frac{\delta_L}{r_f} \right) \right)} \right) \quad (5.23)$$

Therefore.

$$K_u = \left(\frac{\delta_L}{S_L} \right) K = \left(\frac{\delta_L}{S_L} \right) \cdot \frac{2}{r_f} \cdot \frac{\rho_u}{\rho_b} \cdot S_L \cdot \left(\frac{\left(1 + \frac{\delta_L}{r_f} \right)^2}{1 + \frac{\rho_u}{\rho_b} \left(\left(1 + \frac{\delta_L}{r_f} \right)^2 + \left(\frac{\rho_u}{\rho_b} + 1 \right) \left(\frac{\delta_L}{r_f} \right) \right)} \right) \quad (5.24)$$

As mentioned before, there is no consideration for turbulent effect on stretch. However, this formulation can be used to include the stretch effect on laminar flame speed.

Coefficient of mass diffusion is calculated based on the relationship by [42]

$$D_m = D_o \frac{P_o}{P} \left(\frac{T}{T_o} \right)^{1.81} \quad (5.25)$$

where, $D_o = 0.09621$ (cm/s): mass diffusivity of propane/N₂ at $T_o = 273$ K, $P_o = 1$ atm

Since the nitrogen concentration in all mixtures considered here is very high as compared with the concentrations of other species, the binary diffusion coefficient of the deficient reactants is used as diffusion coefficients.

General relation for laminar flame thickness is used.

$$\delta_L = \frac{D_T}{S_L} = \frac{\alpha}{S_L}$$

If $Le=Pr=Sc=1$ is true, the relation becomes

$$\delta_L = \frac{\nu}{S_L}$$

5.3.4 Inert gas stratification and mixing model

The mixing model of inert gas in the cylinder, including internal residual and external EGR, was developed. In engines, mixture is not quiescent. As discussed in Sec 4.2.1, EGR gas supplied through the supplementary pipe was mixed during compression stroke and the mixing level at spark time was quite high. Ideally the mixture around spark plug was supposed to be combustible with fuel and air and the other region was filled with inert gas. Since it is not easy to define the stratified region with the limited access to the combustion chamber, the mixing status in terms of a stratification function was incorporated into the combustion model. Introducing the inert gas stratification function as an additional variable in the engine cycle analysis brings about another dimension because it could take many forms at a given inert gas fraction. To simplify, the shape of function and the width of the inert gas variation was considered.

Various stratification functions studied in the analysis are shown in Figure 5.2. It is assumed that the mixture dilution ratio in the burned zone is a function of a progressive variable which is chosen to be the burn gas fraction. Eq. 5.25 indicates the detail of the functions in Fig. 5.2.

$$\begin{aligned}
f_{linear} &= (f_{final} - f_{initial}) \cdot x_b + f_{initial} \\
f_{sinusoidal} &= (f_{final} - f_{initial}) \cdot \sin(\pi(x_b - 0.5)) + f_{initial} \\
f_{step} &= \begin{cases} f_{initial} & x_b < 0.5 \\ f_{overall} & x_b = 0.5 \\ f_{final} & x_b > 0.5 \end{cases}, \quad f_{overall} = \frac{f_{initial} + f_{final}}{2}
\end{aligned} \tag{5.25}$$

For example, by maintaining an overall inert gas mass fraction equal to 36 %, we can have the linear stratification of width 30 %/ 42%, 33 %/ 39%, etc., where the first number corresponds to the mass fraction at $x_b = 0$ and the second number, to the mass fraction at $x_b = 1$.

5.4 Turbulence model

The turbulence model consists of a zero-dimensional energy cascade, which was developed by Mansouri et al. [43]. Mean flow kinetic energy is supplied to the cylinder through the inlet valve and converted to turbulent kinetic energy through a turbulent dissipation process.

The followings are equations for the mean and turbulent kinetic energy.

$$K = \frac{1}{2} m U^2, \quad k = \frac{3}{2} m u'^2 \tag{5.26}$$

The rate of change of the mean kinetic energy K and the turbulent kinetic energy k is described by

$$\frac{dK}{dt} = \frac{1}{2} \dot{m}_i V_i^2 - P - K \frac{\dot{m}_e}{m} \tag{5.27}$$

$$\frac{dk}{dt} = P - m\varepsilon - k \frac{\dot{m}'_e}{m} + A \tag{5.28}$$

$$\varepsilon = \frac{u'^3}{l} = \frac{(2k/3m)^{3/2}}{l} \tag{5.29}$$

$$P = \mu_r \left(\frac{\partial U}{\partial y} \right)^2 = 0.3307 C_\beta \left(\frac{K}{L} \right) \left(\frac{k}{m} \right)^{1/2} \tag{5.30}$$

$$A = 3 m u' \frac{du'}{dt} = \frac{2}{3} k \frac{\dot{\rho}}{\rho} \tag{5.31}$$

where,

m	mass in the cylinder
\dot{m}_i	mass flow rate into the cylinder
\dot{m}_e	mass flow rate out of the cylinder
V_i	velocity into the cylinder
P	rate of turbulence kinetic energy production
ε	rate of viscous dissipation per unit mass
A	rate of turbulence amplification due to rapid distortion
l	characteristic size of large-scale eddies
L	geometric length scale
C_β	adjustable constant

The macro scales of turbulence consist of the characteristic size of large-scale eddies and the geometric length scale, which is assumed to be given by $l = L = \frac{V}{\pi B^2/4}$, which is subject to the restriction that $L \leq \frac{V}{\pi B^2/4}$ during induction, compression and exhaust stroke.

After ignition the macro scale is assumed to be governed by the conservation of angular momentum of eddies,

$$l = l_o \left(\frac{\rho_{uo}}{\rho_u} \right)^{1/3} \quad (5.32)$$

where the subscript u stands for unburned mass and the subscript o for the value at the time of ignition. Another macro scale was defined to incorporate the squish effect on turbulence generation,

$$l_{sq} = \frac{V - V_c}{\pi B^2/4} + t \quad (5.33)$$

where,

V_c	cylinder volume at TDC
-------	------------------------

t cylinder head gasket thickness

Therefore the rate of turbulent kinetic energy production consists of two terms during combustion.

$$P = 0.3307 C_{\beta} \left(\frac{K}{l} \right) \left(\frac{k}{m} \right)^{1/2} \frac{A_{bore} - A_{squish}}{A_{bore}} + 0.3307 C_{\beta} \left(\frac{K}{l_{sq}} \right) \left(\frac{k}{m} \right)^{1/2} \frac{A_{squish}}{A_{bore}} \quad (5.34)$$

The modeling of tumble and tumble-generated turbulence with quasi-dimensional has been difficult because there are no adequate techniques to quantify the mean flow field as well as turbulence flow field.

The tumble generated turbulence is interpreted through shear stress. Large shear stress exists near the cylinder wall around TDC due to the breakdown of the tumble vortex and there is the energy transfer of the tumble rotational energy to turbulent kinetic energy. Since the shear stress

is proportional to $\frac{U}{h/2}$, the turbulence generation was modeled as:

$$P = C_{\mu_t} \left(\frac{\partial U}{\partial y} \right)^2 = C_{\mu_t} \left(\frac{U}{h} \right)^2 \quad (5.35)$$

Due to the lack of experimental data, the turbulence model validation was qualitative; burn rate data was used for the indirect turbulence model validation.

5.5 Heat transfer model

Heat loss to combustion chamber in SI engines is mainly due to convection. In quasi-dimensional model, the heat transfer rate in each zone is generally determined by using:

$$\dot{Q}_w = hA(T_g - T_w) \quad (5.36)$$

where

h convective heat transfer coefficient

A	surface area of cylinder head, piston, cylinder liner
T_g	mean temperature of the gas
T_w	wall temperature of each area

During combustion, the heat transfer rate in unburned and burned zone is determined separately.

The convective heat transfer coefficient, h , is calculated from a Nusselt - Reynolds number correlation.

$$N_u = \alpha R_e^d \quad (5.37)$$

where

$$N_u = \frac{hL}{\kappa} \quad \text{Nusselt number}$$

$$R_e = \frac{VL}{\nu} \quad \text{Reynolds number}$$

L characteristic length scale (macroscale of turbulence)

κ thermal conductivity

ν kinematic viscosity

α, d constants

The effective velocity

$$V = \left(U^2 + u^2 + (V_p/2)^2 \right)^{1/2} \quad (5.38)$$

was used to obtain the heat transfer coefficient, where U is the mean flow velocity, V_p is instantaneous piston speed[29]. This heat transfer model was found to yield over prediction of heat transfer rate due to the high velocity of Eq.(5.8). Therefore Woschni's correlation was used to calculate the convective heat transfer coefficient h .

Woschni's correlation [24] is summarized as:

$$h = 3.26B(m)^{-0.2} P(kpa)^{0.8} T(K)^{-0.55} w(m/s)^{0.8} \quad (5.39)$$

The average velocity w was expressed as follows:

$$w = C_1 \bar{S}_p + C_2 \frac{V_d T_r}{p_r V_r} (p - p_m) \quad (5.40)$$

where B is the cylinder bore, \bar{S}_p is the mean piston speed, V_d is the displaced volume, p is the instantaneous cylinder pressure, p_r , V_r , T_r are the working-fluid pressure, volume, and temperature at intake valve closing and p_m is the motored cylinder pressure at the same crank angle as p .

For the gas exchange period: $C_1 = 6.18$, $C_2 = 0$

For the compression period: $C_1 = 2.28$ $C_2 = 0$

For the combustion and expansion period: $C_1 = 2.28$ $C_2 = 0.00324$

Woschni's correlation represents spatially averaged combustion chamber heat fluxes. However during combustion, where substantial temperature nonuniformities exist between burned gases and unburned gases, zone averaged approach is expected to be more accurate than global models. The heat transfer to the combustion chamber surfaces in contact with the unburned and burned gas zones is given by:

$$\dot{Q}_u = h_{c,u} A_{u,w} (T_u - T_w), \quad \dot{Q}_b = h_{c,b} A_{b,w} (T_b - T_w) \quad (5.41)$$

respectively. Since h_c depends on local gas properties and velocities, $h_{c,u}$ and $h_{c,b}$ are not necessarily the same.

5.6 NOx formation model

Analysis of NOx formation mechanism has been done to see the burned gas temperature effect with the fully mixed model and unmixed model of burned gas.

5.6.1 Models for burned gas temperature for NO calculation

- 1) A fully mixed model

The model assumes that the burned gas region is homogeneously mixed, and the temperature for NO calculation is based on the averaged adiabatic core temperature of the burned gas,

$$\bar{T}_b = \bar{T}_{b,ac} \quad (5.42)$$

where $\bar{T}_{b,ac}$ is the adiabatic core temperature which is based on the total sensible enthalpy of the burned gas.

2) An unmixed model

This model is based on the assumption that no mixing occurs between gas elements that burn at different times, and each burned gas element is isentropically compressed and expanded according to the cylinder pressure after combustion.

In order to specify the temperature of each element of charge, the following supplemental relationships are employed. The mean burned gas temperature \bar{T}_b , is calculated by using enthalpy balance in the cycle simulation program.

Since $\bar{T}_b = \frac{1}{x_b} \sum_i^n T_{bi} x_{bi}$, the temperature T_{bi} of the mass element which just burns may be calculated from \bar{T}_b by

$$T_{bi} = \frac{\bar{T}_b m_b - \sum_{j=1}^{i-1} T_{bj} m_b(j)}{m_b(i)}, \quad m_b = \sum_{j=1}^i m_b(j) \quad (5.43)$$

where the index i indicates the sequence of burning of the mass elements.

The temperature of the burned gas element after combustion is given by

$$\frac{T_{bi}(x'_b, x_b)}{T_{bi}(x'_b)} = \left[\frac{P(x_b)}{P(x'_b)} \right]^{\frac{(\gamma_b(m_b(i))-1)}{\gamma_b(m_b(i))}} \quad (5.44)$$

where $T_{bi}(x'_b, x_b)$ is the temperature of the element (i) when the pressure is $P(x_b)$. The index x'_b denotes the burning time of element i , which the temperature is $T_{bi}(x'_b)$.

In the boundary layer region, the burned gas temperature is compensated by

$$T_{bl} = \frac{T_b + T_{wb}}{2} \quad (5.45)$$

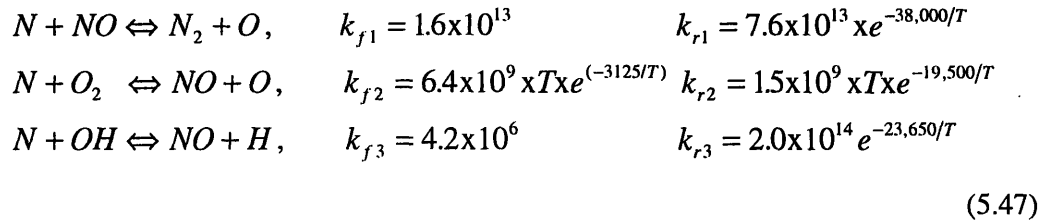
where T_{wb} is the weighted mean of the wall temperature in the burned zone.

When the unmixed model applies only to the adiabatic core region, the temperature of subdivision can be calculated based on the following equation.

$$T_{bi,ac} = \frac{\bar{T}_{b,ac} m_{ac} - \sum_j^{i-1} T_{bj} m_b(j)}{m_b(i)} \quad (5.46)$$

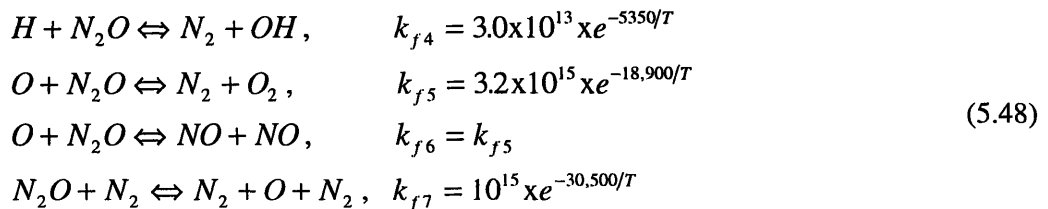
5.6.2 NO kinetics

1) The extended Zeldovich mechanism



, where T is in °K and the forward and reverse reaction rate constants are cm³/mole.s. The rate constants are based on the Table in the book[2]. Except for rich mixture at a low temperature where prompt NO may be important, most of the NO formation will occur via the extended Zeldovich mechanism.

2) The N₂O mechanism for lower temperatures and excess air



where the rate constants are given in $\text{cm}^3/\text{mole}\cdot\text{s}$. These are based on the theory developed by Lavoie et al[44] with some modification by P.C. Baruah.

Using the principal reactions governing the formation of NO and steady state approximation for [N], the following expression is obtained.

$$\frac{d\{NO\}_{ac}}{dt} = 2 \frac{M_{NO}}{\rho_a} (1 - \alpha^2) \left[\frac{R_1}{1 + \alpha[R_1/(R_2 + R_3)]} + \frac{R_6}{1 + [R_6/(R_4 + R_5 + R_6)]} \right] - \frac{\dot{m}_{bl}}{m_a} \{NO\}_{ac} \quad (5.49)$$

where $R_1 = k_{f1}[N]_e[NO]_e$ etc., $\alpha = [NO]/[NO]_e$, $[]_e$ denotes the equilibrium concentration.

The NO formation at boundary is assumed like the following equation.

$$\frac{d}{dt} \{NO\}_{bl} = \frac{\dot{m}_{bl}}{m_{bl}} \{NO\}_{ac} \quad (5.50)$$

$$[NO]_{avg} = \frac{[NO]_{ac} \frac{V_{adia}}{T_{adia}} + [NO]_{bl} \frac{V_{bl}}{T_{bl}}}{\frac{V_{adia}}{T_{adia}} + \frac{V_{bl}}{T_{bl}} + \frac{V_{unburned}}{T_{unburned}}} \quad (5.51)$$

Once the NO chemistry has frozen during the early part of expansion stroke, the integration over all elements will give the final exhaust NO concentration. Thus, if $\{NO\}$ is the local mass fraction on NO, then the average exhaust NO mass fraction is given by

$$\{NO\} = \frac{\sum_{i=1}^n \{NO(i)\} m_b(i)}{m_b} \quad (5.52)$$

where $\{NO(i)\}$ is the final frozen NO mass fraction in the element of charge which burned when the mass burned was $m_b(i)$.

5.7 Results and discussion

Since the model describes the mixing and combustion processes in terms of parameters related to the charge turbulence, these parameters need to be calibrated with respect to the current engine application. In this section, the calibration process is first described. Then the model is exercised to study the sensitivity of the engine behavior as a function of the various subprocesses.

5.7.1 Model calibration

Most of the simulation work was carried out at one EGR operation condition. Lean burn condition was briefly introduced in order to assess the system operation in that condition.

The followings are important parameters to be calibrated to match experimental results:

- C_β : The coupling constant that connects the mean kinetic energy to turbulent kinetic energy; see equation (5.30). This factor should be unique to each engine design and engine operation condition.
- C_τ : The scaling factor for the eddy burning time; $\tau_b = C_\tau \frac{\lambda}{S_L}$; reducing C_τ has the same effect as making small Taylor length scale or increasing laminar burning speed.
- *Flame stretch factor* I_o : which is based on mathematical interpretation of flame structure. There is still open question whether turbulent flame will really follow the simplified mathematical model. However during flame initiation stage, it is generally recognized that burning is controlled by the laminar burning speed with the negligible turbulence effect.
- *Assumption on initial burn fraction* x_b : This factor has a significant effect on initial burn duration. When the spark ignition model is not included, the simulation should start based on the assumption that flame has grown to a certain diameter. This is not critical in stoichiometric operation, but it is required for highly diluted mixture.

5.7.2 Combustion in the EGR dilution

Simulation was calibrated to match the experiments largely in IMEP, peak pressure and combustion phasing. Two kinds could be tried in calibration. One is based on the assumption that flow field conditions are the same between stratification and homogeneous strategy even with the different EGR supply method. The other is that each case has its own calibration condition. Since adjusting model constants for each condition seems too arbitrary even though supplementary gas could change flow field in the cylinder, a single calibration was applied to both homogeneous and stratified mixture. The control of turbulence generation was calibrated with C_β in Eq. 5.30. the calibration coefficient of rate of the turbulence kinetic energy production and the eddy burning time was calibrated with C_τ .

The effect of flame stretch factor

The parameters related to the flame stretch factor are shown in Figure 5.3, where the conditions for calculation are homogeneous mixture: 30 % EGR ratio, 45 BTDC spark timing and stoichiometric operation. Figure 5.3a illustrates a significant magnitude difference in Karlovitz No between geometric strain and turbulent strain model. As noted in section 5.3.3.1, this difference is largely due to the low value of laminar flame speed. Since the turbulent Karlovitz No is greater than unity, the engine operating conditions are found to be in the boundary regime of the flame sheet model. The flame curvature effect is shown in Fig 5.3b. This factor should be considered when the flame model based on the spherical flame propagation assumption is used. The non dimensional numbers shown in Fig. 5.3c indicate that the preferential diffusion effects are needed to be considered. Since the propane has large Lewis number at a highly diluted mixture[45], this result supports the need to include Lewis number effect on the flame stretch. Figure 5.3d is the calculation result of the flame stretch factor, which shows that the flame stretch factor has a strong effect on early flame development phase.

Figure 5.4 shows the flame stretch effect on engine performance. The calculation was carried out with and without the stretch factor. Even though the stretch factor has strong effect on the flame development phase, its effect propagates throughout the whole combustion period. Since the simulation has shown the fast burn characteristic in both cases, as addressed before, the flame stretch effect to reduce the burning speed is needed.

The effect of initial flame growth

At the condition of the dilution limit, the initial flame size, which is induced by ignition has a significant influence on combustion. Strong spark energy is able to extend the lean/dilution limit of combustion. In simulation, this effect can be incorporated into the initial condition of the mass fraction burned. Therefore the relative magnitude of contribution to combustion between stratified strategy and high spark energy can be assessed by the sensitivity analysis. The physical meaning for the variation of initial mass fraction burned $x_{b,ini}$ can be interpreted as a sparking condition.

Figure 5.5 shows the effect of the initial mass fraction burned on combustion. In homogeneous mixture, the initial mass fraction burned had a significant effect on combustion. However the initial size of the stratified mixture combustion highly contributed to the flame propagation until around 0.2%. This result showed that at large dilution ratio the initial flame formation was hard. Therefore a slight favorable mixture around spark plug could improve the combustion stability. Since there is a linear relationship between $x_{b,ini}$ and the initial flame radius, the flame radius can be used for criterion of setting initial condition. One research on the initial flame size showed that the flame radius after ignition was about 1 mm at a highly diluted condition[34]. In this simulation, the initial mass fraction burned was assumed as 0.25%, which is equivalent to about 1mm flame radius.

The effect of charge mixing and stratification

The effect of mixing during combustion on combustion properties was examined by adopting a mixing function. When the flame grows during the initial phase within the combustion chamber, the stratification effect on combustion would be significant. The stratification of the inert gas near the spark plug or the location of unburned air/fuel mixture near it will contribute to accelerate the flame development by enhancing the laminar flame speed. Even though the complete stratification had been achieved during induction and compression, it is expected that the mixing between inert gas and fresh mixture would occur due to the expansion of the burned gas.

Figure 5.6a shows the comparison of IMEP vs. initial EGR fraction with the difference of mixing function at same calibration condition between homogeneous and stratified mixture: $C_\beta = 0.45$ and $C_\tau = 1$. As the EGR fraction of the initial burning mixture gets smaller with the constant overall residual fraction, the fast burn could be accomplished. Since the spark timing was

maintained at fixed value, the fast burn did not contribute to IMEP increase. The less EGR fraction during the flame development phase, the step mixing function, reduced the $\theta_{0-10\%}$ and $\theta_{0-50\%}$, but it increased the flame propagation angle $\theta_{10-90\%}$, precisely $\theta_{50-90\%}$ as shown in Fig 5.6. The longer duration of $\theta_{10-90\%}$ reduced IMEP even with the fast burn characteristic during flame development phase. Since the experiment result shown in Fig 4.23 indicated that the faster the flame development angle is, the shorter is the flame propagation duration, the increase of $\theta_{10-90\%}$ might not be the real situation in engine. The mixing effect on combustion parameters versus crank angle is compared in Figure 5.7. The slow burn of step mixing model after 50 % mass fraction burned is reflected on the less pressure and mass fraction in Fig 5.7a and b.

The linear mixing model was used for further investigation on the mixing during combustion. The comparison with the experiment results illustrated that the mixing profile of models during combustion did not make a big difference on engine performance parameters up to the level where calculation results match experimental results.

Figure 5.8 and 5.9 show the detail comparison of engine performance for the homogeneous mixture and the stratified mixture respectively. Experimental results are typical 10 cycles of each condition and calculation results are from the linear mixing model. As shown in Fig 5.8, there are significant cyclic variations in the experiment results in the homogeneous mixture. The simulation indicates faster burning during the flame propagation phase than the experiment. The fast burning characteristic in simulation is also shown in Fig 5.9 for the case of stratified mixture.

The variation of IMEP around 30 % EGR ratio has a stiffer slope in case of homogeneous mixture than that of stratified mixture, which is shown in Figure 5.10. Therefore a small perturbation of EGR gas could aggravate IMEP fluctuation, which illustrates that with the stratified strategy the combustion stability was improved in addition to the increase of IMEP. The result showed that at high dilution ratio the laminar flame speed had a dominant effect on the flame propagation because the effect of volume expansion after TDC on the decrease of the pressure and unburned gas temperature is relatively high as shown in Fig 5.10e and f. This may explain that the cyclic variation of IMEP in homogeneous mixture is due to the variation in the amount of dilution gas.

The effect of turbulence

Since the turbulence intensity level was not measured in this work, it is not sure that the performance improvement of the stratified-EGR operation is with the help of turbulence or stratification itself.

The simulation was done to examine the effect of the variation of turbulence level as an independent variable on the system performance. If the turbulence intensity level during combustion is adjusted to match IMEP of the homogeneous operation to that of the stratification strategy at 30 %, the performance improvement of the stratification strategy can be assumed to be from the turbulence intensity increase rather than the stratification effect. The turbulence level was arbitrarily increased to 10 % higher than that of the homogeneous mixture during the combustion period. Figure 5.11 shows that the trend of variation of IMEP around 30 % EGR follows that of the stratified strategy. When the dilution fraction is less than 30 %, the increase of turbulence promotes flame propagation. However at high dilution ratio the turbulence effect is not much because the laminar flame speed is the dominant factor in this range as shown in Fig 5.11e. Comparing with the experimental result shown in Fig 4.23 c and d, the variation of IMEP as a function of the flame development angle shows the similar trend. Since the supply of external EGR was maintained at the constant level, the fluctuation of the amount of dilution gas was due to the cyclic variation of the internal residual gas. These characteristics are clearly shown in Figure 4.21 g and h, in which the engine was operated with more EGR fraction.

5.7.3 Lean burn

Excess air in lean burn condition acts as inert gas too. Since oxygen does help combustion, even with the same level of dilution ratio between air dilution and N_2 dilution, there are significant differences in the combustion performances as illustrated in Figure 4.26 . The main factors that make the performance of the stratified lean operation better than that of the stratified EGR operation was addressed. The simulation methods are the same, which is described in section 5.6.1.2.

The effect of the charge stratification is shown in Figure 5.12. In this calculation, $C_\beta = 0.375$ and $C_\tau = 0.9$ were used as a calibration condition for both mixtures. A relatively big discrepancy resulted in the homogeneous mixture. A possible explanation is that the turbulence flow field is not same between the homogeneous mixture and the stratified mixture because the discrepancy is largely due to the flame propagation angle, which is strongly affected by the turbulence effect. The trend in the combustion phasing is similar to the EGR combustion shown in Fig.5.6.

5.7.4 System performance on engine NOx emissions

This work has emphasized on the engine operation at the stoichiometric air fuel condition in order to use three way catalytic converter and to use a significant amount of EGR gas to reduce the pumping loss.

In this section, the effect of this strategy on engine NOx emission was discussed. The optimum mixture distribution near the spark plug was intended to improve combustion, but it would have an adverse effect on NOx formation. Therefore, it is needed to assess the effect of the mixture stratification on NOx formation.

In this simulation, two kinds of strategies were addressed. One is the stratification of mixture composition of unburned gas and the other is to take account of the stratification of burned gas, which is described in Sec.5.6.

The stratification of EGR in unburned mixture and the temperature layer of burned gas

Even though the engine was operated in the stoichiometric condition, the level of NOx formation is relatively small with the high dilution. However if each burned gas element is isentropically compressed and expanded without mixing, it will enhance NOx formation due to the element with the high temperature. Figure 5.13 illustrates the effect of stratification of the unburned gas mixture and the burned gas temperature on NOx formation. Since the spark timing was maintained at the constant value, the fast burning with the help of the stratification of EGR gas increased the peak pressure as shown in Fig. 5.6b, which formed a significant amount of NOx; more than 3 times at about 0.33 the initial EGR stratification. This is an indication of NOx fluctuation mainly caused by the mixture non-uniformity burned or unburned.

The stratification of excess air in unburned mixture and the temperature layer of burned gas

Figure 5.14 shows the NOx formation in lean burn condition. The order of magnitude in NOx level is 10 times that of EGR burn even at the lower load condition. The NOx formation trend shows the exponential growth with the stratification, which means that a small fluctuation in the non-uniformity of in-cylinder gas could cause a significant variation of NOx formation.

5.7.5 System performance prediction at different engine speed

In order to predict the engine performance operating in the stratified-EGR mode at the different engine speed, a calculation was carried out at 1500 rpm, MBT spark timing and stoichiometric condition. Since the stratification of about 10 % of residual gas was expected with

the current system, the engine performance was compared at the same brake mean effective pressure(BMEP) between 30 % external EGR condition with 10% stratification effect and base condition without EGR

Figure 5.15 shows the comparison of the combustion performance at the 695 kpa BMEP. The slow burn due to the high EGR ratio caused higher compression work as shown in the figure and reduced IMEP.

Figure 5.16 illustrates the performance comparison at low and high load conditions. As expected, a significant improvement in pumping loss and cooling loss was resulted. At low load, the effectiveness of stratification strategy is diminished due to the higher internal residual gas. Around 1 % improvement in brake specific fuel consumption and brake thermal efficiency is shown at low load, but over 5 % improvement was resulted at high load as shown in Fig. 5.16a and b. In the NO_x formation, about 100 times difference is shown in Fig. 5.16e.

CHAPTER 6 Summary and conclusions

A spark ignition engine operating in a stratified-EGR mode was developed to use a substantial amount of EGR to improve the fuel economy of spark ignition engines under part load. The fuel economy gain was achieved mainly by reducing the pumping loss with EGR and by improving heat loss. Stable combustion at high level of EGR was achieved by charge stratification, so that the fresh mixture and the burned gas from EGR are essential in different regions of the cylinder. The research has been largely focused on the understanding of the mixing progress between the air/fuel mixture and the dilution gas, and its effect on combustion at low load and low speed condition.

In order to study the means of supplying the stratified EGR gas, of maintaining the stratification in the cylinder, and of obtaining fast burn by increasing the tumble motion in the cylinder, a new transparent engine test facility was developed and experiments were performed to demonstrate the concept of the spark ignition engine operating in a stratified_EGR mode. Laser diagnostics including PLIF technique and Mie scattering technique were applied to observe the in-cylinder flow motion and mixing process during intake and compression. The engine was also operated at firing condition to assess the engine performance operating in a stratified-EGR mode. Cylinder pressure measurements were used to gain information about the combustion process.

A new combustion model incorporating a mixing function and the flame stretch factor was developed to examine the flame propagation properties. Simulations under highly diluted mixture were carried out to investigate the effect of charge mixing and stratification in unburned mixture and turbulence. In addition to the engine performance prediction, NO_x emission calculation was also investigated by incorporating a layer model in the burned gas.

The contributions and conclusions of this research are described as follows:

1. The feasibility of the stratified-EGR concept in a spark ignition engine was demonstrated in a single cylinder engine.

2. A transparent engine was developed to examine the level of in-cylinder flow control. Flow visualizations(Mie scattering and PLIF) were applied to observe the fluid motion and mixing progress in the cylinder.
3. Acetone was effective as a fluorescent tracer for the PLIF experiments. Single laser shot and averaged images of 2D-acetone distribution illustrated the instantaneous qualitative measure of cycle-by-cycle variation of fuel distribution and the progress of turbulent mixing.
4. Comparisons of PLIF and Mie scattering images at the similar field of view and crank angle revealed the relationship between the large scale motion and the mixing process. There were less cycle by cycle variations in the large scale tumble motion introduced during the intake stroke than the small eddies distribution during the compression stroke.
5. The stratification between air/fuel mixture and EGR gas was relatively well established during the intake stroke. There was, however, a significant mixing in the later part of the compression stroke. This process may be explained by that large scale tumble motion was introduced into the cylinder during the intake stroke, and that the organized motion broke into small eddies during the compression stroke and hence resulted in the substantial mixing.
6. Injection of the supplementary gas before intake valves open did not make a notable difference in combustion characteristics at low dilution ratio; however injection during valve-open and minimizing the mixing between the supplementary gas and the fresh mixture improved the combustion at high dilution ratio.
7. Performance comparison between the engine operating with the homogeneous mixture and with the stratified mixture illustrated that the stratified mode greatly improved fuel consumption and provided the stable combustion at over 30 % EGR. The combustion variability was significantly improved up to 40 %, where the amount of internal residual gas has a dominant effect on the laminar flame speed.
8. The observed trend on the burning process could be reproduced reasonably well in an engine simulation model by incorporating a mixing function and a flame stretch factor. Linear mixing assumption can relatively well predict the trend of engine performance compared

with the test data. Simulation underpredicted the flame development angles and overpredicted the flame propagation angle, and the model with flame stretch factor improved the model prediction.

9. In highly diluted mixture, the stratification in unburned mixture had a bigger effect on the combustion stability than the turbulence. Turbulence effect, however, was stronger in low dilution mixture.

10. A model using layering of burn gas and stratification of dilution gas in the unburned mixture is developed to evaluate NO_x formation. The results indicate that the overall NO_x production is very sensitive to the mixture distribution.

11. The implementation of the stratified-EGR concept engine for prototype engine development is recommended. The major components to be developed include the EGR distribution system, charge motion control, and the appropriate engine management for the optimum operation.

References

1. Gomez, A.J. and Reinke, P.E., "Lean burn: A Review of Incentives, Methods, and Tradeoffs", SAE Paper 880291, 1988.
2. Heywood, J.B., "Internal Combustion Engine Fundamentals", McGraw-Hill Book Co., New York, 1988.
3. Nakamura, N., Baika, T. and Shibata, Y., "Multipoint Spark Ignition for Lean Combustion", SAE Paper 852092, 1985.
4. Oblander, K., Abthhoff, J. and Fricker, L., "From Engine Testbench to Vehicle - an Approach to Lean Burn by Dual Ignition", I Mech E 1979, C97/79, p. 19-24.
5. Nakajima, Y., Sugihara, K. and Takagi, Y., "Lean mixture or EGR - which is better for fuel economy and NOx reduction ?", I Mech E 1979, C94/79, p.81-86.
6. Nakanishi, K., Igushi, S., Okano, H., Okumura, T. and Furuno, S., "Development of a New Intake System for a 4-valve Lean Burn Engine", C389/243, I Mech E 1992, p.25-31.
7. Horie, K., Nishizawa, K., Ogawa, T., Akazaki, S. and Miura, K., "The Development of a High Fuel Economy and High Performance Four-Valve Lean Burn Engine", SAE Paper 920455 1992.
8. Kuwahara, K., Watanabe, T., Takemura, J., Omori, S., Kume, T. and Ando, H., "Optimization of In-Cylinder Flow and Mixing for a Center-Spark Four Valve Engine Employing the Concept of Barrel-Stratification", SAE Paper 940986, 1994.
9. Nakajima, Y., Sugihara, K., Takagi, Y. and Muranake, S., "Effects of Exhaust Gas Recirculation on Fuel Consumption", Proc Instn Mech Engrs Vol. 195, I Mech E 1981.
10. Heywood, J.B. and Watts, P.A., "Parametric Studies of Fuel Consumption and NOx Emissions of Dilute Spark Ignition Engine Operation using a Cycle Simulation", Instn Mech Engrs Conference on Fuel economy and emissions of lean burn engines, Paper C98/79, 1979.
11. Groves, W. N. and Bjorkhaug, M., "Stratified Exhaust Gas Recirculation in a SI Engine", SAE Paper 860318, 1986.
12. Stokes, J., Lake, T.H., Christle, M.J. and Denbratt, I., "Improving the NOx/Fuel Economy Trade-off Gasoline Engines with the CCVS Combustion System", SAE Paper 940482, 1994.
13. Lake, T.H., Stokes, J., Pendlebury, K.J. and Denbratt, I., "Development Experience of a Multi-Cylinder CCVS Engine", SAE Paper 950165, 1995.
14. Bates, S. C., "A Transparent Engine for Flow and Combustion Visualization Studies", SAE Paper 880520, 1988.

15. Lozano, A., Yip, B. and Hanson, R.K., "Acetone: a tracer for concentration measurements in gaseous flows by planar laser-induced fluorescence", *Experiments in Fluids*, Vol.13, p.369-376, 1992.
16. Hansen, D.A. and Lee, E.K.C., "Radiative and nonradiative transitions in the first excited singlet state of symmetrical methyl-substituted acetones", *The Journal of Chemical Physics*, Vol. 62, No. 1, p.183-189, 1975.
17. Wolff, D., Beushausen, V., Schluter, H., Andresen, P., Hentschel, W., Manz, P. and Arndt, S., "Quantitative 2D-Mixture Fraction Imaging Inside an Internal Combustion Engine using Acetone-Fluorescence", *International Symposium COMODIA 94*, p.445-451, 1994.
18. Holder, D. W. And North, R. J., "Schlieren Methods", *Notes on Applied Science No. 31*, National Physical Laboratory, 1963.
19. Richman, R.M. and Reynolds, W. C., "The Development of a Transparent Cylinder Engine for Piston Engine Fluid Mechanics Research", *SAE Paper 840379*, 1984.
20. Fujikawa, T., Ozasa, T. and Kozuka K., "Development of Transparent Cylinder Engines for Schlieren Observation", *SAE Paper 881632*, 1988.
21. Gatowski, J. A., Balles, E.N., Chun, K.M., Nelson, F.E., Ekchian, J.A., and Heywood, J.B., "Heat Release Analysis of Engine Pressure Data", *SAE Paper 841359*, 1984.
22. Chun, K.M., and Heywood, J.B., "Estimating Heat-release and Mass of Mixture Burned from Spark Ignition Engine Pressure Data", *Combust. Sci. Technology*, Vol.54, pp.133-144, 1987.
23. Sztenderowicz, M.L, and Heywood, J.B., " Cycle to Cycle IMEP Fluctuations in a Stoichiometrically -Fueled SI engine at Low Speed and Load", *SAE Paper 902143*, 1990.
24. Woschni, G., "A Universally Applicable Equation for Instantaneous Heat Transfer Coefficient in the Internal Combustion Engine", *SAE Paper 670931*, *SAE Transactions*, Vol.77, 1967.
25. Fox, J.W., Cheng, W.K. and Heywood, J.B., "A Model for Predicting Residual Gas Fraction in Spark-Ignition Engines", *SAE Paper 931025*, 1993.
26. Hadded, O. and Denbratt, I., "Turbulence Characteristics of Tumbling Air Motion in Four-valve SI Engines and their Correlation with Combustion Parameters", *SAE Paper 910478*, 1991.
27. Ozdor, N., Dulger, M. and Sher, E., "Cyclic variability in Spark Ignition Engines A Literature Survey", *SAE Paper 940987*, 1994.
28. Rhodes, D.B., Keck, J.C., "Laminar Burning Speed Measurements of Indolene-Air-Diluent Mixtures at High Pressures and Temperatures," *SAE Paper 850047*, 1985.

29. Poulos, S.G., "The Effect of Combustion Chamber Geometry on S.I. Engine Combustion Rates- a Modeling Study", S.M. Thesis, Massachusetts Institute of Technology, 1982.
30. Blizard, N.C. and Keck, J.C., "Experimental and Theoretical Investigation of Turbulent Burning Model for Internal Combustion Engines," SAE Paper 740191, 1974.
31. Keck, J.C., Heywood, J.B. and Noske, G., "Early Flame Development and Burning Rates in Spark Ignition Engines and Their Cyclic Variability," SAE Paper 870164, 1987.
32. Dai, W, Davis, G. C., Hall, M.J. and Matthews, R. D., "Diluents and Lean Mixture Combustion Modeling for SI Engines with a Quasi-Dimensional Model", SAE Paper 952382, 1995.
33. Matthews, R. D. and Chin, Y. W., "A Fractal-Based SI Engine Model: Comparisons of Predictions with Experimental Data", SAE Paper 9110079, 1991
34. Herweg, R. and Maly, R.R., "A Fundamental Model for Flame Kernel Formation in S.I. Engines," SAE Paper 922243, 1992.
35. Metghalchi, M. and Keck, J.C., "Laminar Burning velocity of Propane-Air Mixtures at High Temperature and Pressure", *Combustion and Flame*, Vol.38, pp.143-154, 1980.
36. Wahiduzzaman, S., Morel, T. and Sheard, S., "Comparison of Measured and Predicted Combustion Characteristics of a Four-Valve S.I. Engine," SAE Paper 930613, 1993.
37. Law, C.K., "Dynamics of Stretched Flames," 22nd Symposium (International) on Combustion, the Combustion Institute, Pittsburgh, pp. 1381-1402, 1988.
38. Chin, Y.W., Matthews, R.D., Nichols, S.P. and Kiehne, T.M., "Use of Fractal Geometry to Model Turbulent Combustion in SI Engines," *Combustion Science and Technology*, Vol. 86, pp. 1-30, 1992.
39. Chung, S.H. and Law, C.K., "An Invariant Derivation of Flame stretch," *Combustion and Flame*, Vol. 55, pp. 123-125, 1984.
40. Chung, S.H. and Law, C.K., "An Integral Analysis of the Structure and Propagation of Stretched Premixed Flames," *Combustion and Flame*, Vol. 72, pp. 325-336, 1988.
41. Peters, N., "Laminar Flamelet Concepts in Turbulent Combustion", 21st Symposium (International) on Combustion, the Combustion Institute, Pittsburgh, pp. 1231-1250, 1986.
42. Eckert, E.R.G and Drake, R.M., "Analysis of Heat and Mass Transfer", Table B-7, McGraw-Hill Inc., 1972.
43. Mansouri, S.H., Heywood, J.B., Radhakrishnan, K., "Divided-Chamber Diesel Engines, Part 1: A Cycle-Simulation which Predicts Performance and Emissions", SAE Paper 820273, 1982.

44. Lavoie, G.A., Heywood, J.B. and Keck, J. C., "Experimental and Theoretical Study of Nitric Oxide Formation in Internal Combustion Engines", *Combustion Science and Technology*, Vol.1, p. 313-326, 1970.
45. Abdel-gayed, R.G. and Bradley, D., "Criteria for Turbulent Propagation Limits of Premixed Flames", *Combustion and Flame*, Vol. 62, p.61-68, 1985.
46. Kiyota, Y., Akishino, K. and Ando, H., " Concept of Lean Combustion by Barrel Stratification", SAE Paper 920678, 1992.

Table 2.1 Engine geometry and specifications

Contents	Description
• Model:	DAEWOO 1.5 DOHC
• Type:	Four cylinder, iron block and aluminum cylinder head, two intake valves, two exhaust valves, double overhead cams
• Combustion Chamber:	Pentroof, central ignition
• Bore:	81.5 mm
• Stroke:	76.5 mm
• Con rod length:	127.5 mm
• Clearance volume:	46.80 cc
• Displacement:	0.375 liters
• Compression ratio:	9.0
• Valve opening duration	INT: 230° EXH : 230°
• Valve timings:	IVO 35° BTDC (505° CA) IVC 15° ABDC (195° CA) EVO 45° BBDC (315° CA) EVC 5° ATDC (545° CA)
• Valve overlap:	40°
• Valve lift, Max:	INT: 8.5 mm EXH: 8.5 mm

Table 2.2 Tumble adapter design and velocity ratio

	Main flow pipe	EGR flow pipe
• Diameter (mm)	23	5
• Length (mm)	100*	190
• Velocity ratio in order to meet system requirement	1	10

* intake port length

Table 2.3 Data on acetone properties

Properties	data
• Boiling point (°C)	56
• Molecular weight	58.08
• Specific gravity (kg/cm ³)	0.79
• Autoignition temperature (°C)	465
• Absorption wavelength (nm)	225 - 320
• fluorescence quantum efficiency (ϕ_f), %	0.2
• Emission wavelength (nm)	350 - 550
• fluorescence lifetime (τ_f), ns	4 ns
• phosphorescence quantum efficiency (ϕ_p), %	1.8
• phosphorescence emission (nm)	350 - 600
• phosphorescence lifetime (τ_p), μ s	200

Table 2.4 Experimental conditions

	Reference condition	EGR operation	Lean operation
• Engine speed (rpm)	1000 rpm	←	←
• Spark timing (deg, BTDC)	MBT	←	←
• Mixture	Homogeneous	Homog / Stratif	Homog / Stratif
• Air/fuel ratio (Lamda)	1.	1.	1.4-1.6
• EGR ratio (%)	0.	30 - 40	0.
• Load (IMEP, bar)	4 - 6	2.5 - 6	4. - 6.

Table 4.1 Design target, design parameters and test required

Design target	Design parameter	Test
<ul style="list-style-type: none"> High turbulence - increase turbulent flame speed 	Tumble adapter	Firing Mie scattering (motoring)
<ul style="list-style-type: none"> Stratification - increase laminar flame speed 	Symmetric EGR supply	PLIF (motoring)
<ul style="list-style-type: none"> Minimize mixing in the intake port - synchronize with the intake stroke 	Solenoid valve	Firing Pressure wave in the intake port

Table 4.2 System performance requirement of each stroke

Status	Target
<ul style="list-style-type: none"> Before intake stroke 	No mixing in the intake port
<ul style="list-style-type: none"> Intake stroke 	Supply supplementary gas at stratified condition
<ul style="list-style-type: none"> Compression stroke 	Maintain momentum for stratification
<ul style="list-style-type: none"> Expansion stroke 	Control the spark timing

Table 4.3 Test results summary of the tumble adapter performance

	Low tumble	High tumble
<ul style="list-style-type: none"> IMEP (COV of IMEP) bar 	4.26 (2.9%)	4.36 (2.2%)
<ul style="list-style-type: none"> Pmax @ ang (bar @ deg ATDC) 	19.7@21.6	21.8@19.5
<ul style="list-style-type: none"> Peak mass burning rate @ ang (1/deg @ deg ATDC) 	0.032@16.4	0.037@13.2
<ul style="list-style-type: none"> 0 - 2 % (deg) 	27.0	26.2
<ul style="list-style-type: none"> 0 - 10 % (deg) 	34.7	33.5
<ul style="list-style-type: none"> 0 - 50 % (deg) 	50.2	46.9
<ul style="list-style-type: none"> 0 - 90 % (deg) 	66.3	60.8
<ul style="list-style-type: none"> 10 - 90 % (deg) 	31.6	27.3

Table 4.4 Test results summary of the supplementary gas supply timing control

Supply Timing	IMEP (bar)	COV	Pmax (bar)	CA,Pmax (deg)	0 - 10 % (deg)	10 - 90 % (deg)	Dilution ratio
160	5.06	3.67	29.41	16.86	35.17	29.17	21.64
340	5.26	3.53	28.87	17.77	36.33	29.91	21.51
520	5.32	3.75	27.79	18.47	37.1	31.79	20.90
700	5.11	3.81	27.44	18.01	36.86	31.17	21.41

Table 4.5 Engine operation for baseline

Load(IMEP, gross) (bar)	Spark timing (deg, BTDC)	Lamda	HC (ppm C ₁)	P _s (bar)
4.2	30	1.04	1365.7 ± 233.0	5.4
4.1	30	1.03	1310.5 ± 238.0	5.6
4.1	35	1.04	1275.3 ± 220.9	4.8
4.0	35	1.03	1230.0 ± 220.9	4.8

93

Table 4.6 Reference test results for lean burn and EGR test

<i>File</i>	<i>Spark Timing</i>	<i>Fuel mass per cycle (g/cyc)</i>	<i>IMEP, bar (COV)</i>	<i>P_{max} bar (COV)</i>	<i>CA P_{max} deg (COV)</i>	<i>0-10%, deg (COV)</i>	<i>10-90%, deg (COV)</i>
Part_1	30	0.0088	4.29 (1.38)	24.25 (6.99)	16.77 (13.1)	25.61 (6.33)	23.35 (9.84)
Part_2	25	0.012	5.60 (1.14)	29.39 (6.97)	18.63 (12.93)	22.77 7.01	22.47 8.38

Table 4.7 Test results summary of lean burn operation

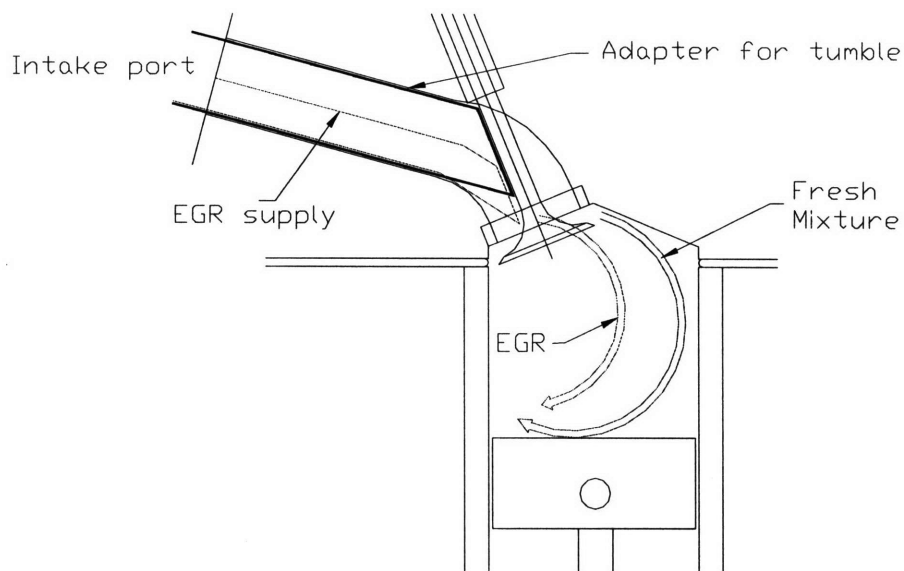
File	Spark Timing	Lamda (COV)	Dilution ratio ¹	IMEP, bar (COV)	P _{max} , bar (COV)	CA P _{max} , deg (COV)	0-10%, deg (COV)	10-90%, deg (COV)
Lean H_ Part	35	1.56 (1.96)	34.5	4.22 (17.04)	18.93 (15.34)	15.66 (31.90)	39.16 (9.90)	54.22 (29.92)
Lean S_ Part	35	1.58 (1.95)	35.3	4.71 (6.00)	23.73 (14.52)	17.85 (13.57)	34.47 (8.43)	36.66 (26.94)
Lean H_ WOT	35	1.45 (1.83)	29.7	5.97 (3.24)	29.40 (13.09)	19.53 (14.22)	33.16 (8.22)	30.36 (16.31)
Lean S_ WOT	35	1.54 (2.32)	33.7	5.86 (3.65)	31.57 (12.66)	17.48 (15.83)	31.98 (8.27)	28.42 (18.26)

Table 4.8 Test results summary of EGR operation

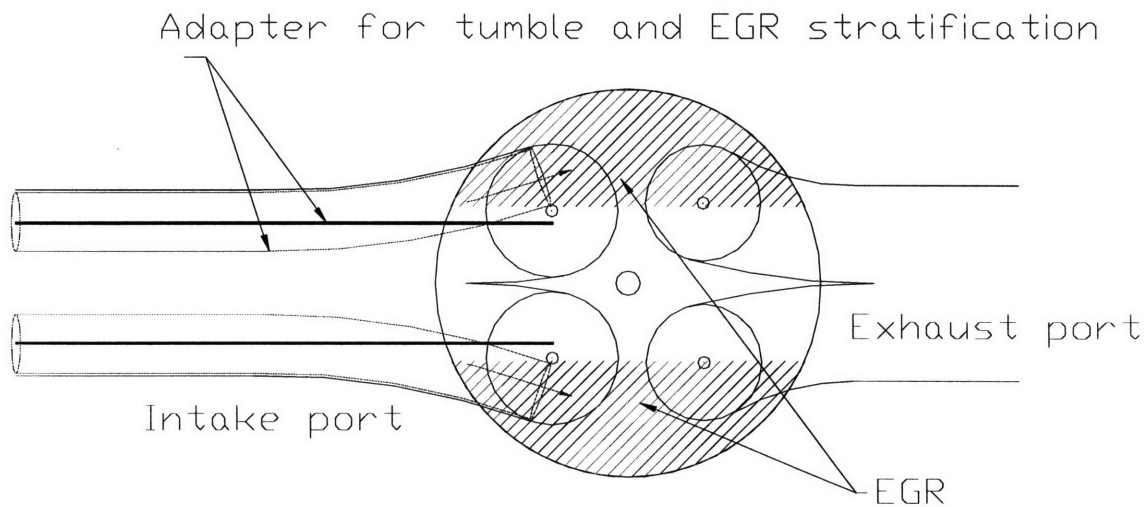
File	Spark Timing, deg	EGR gas ratio, % ²	IMEP, bar (COV)	P _{max} , bar (COV)	CA P _{max} , deg (COV)	0-10%, deg (COV)	10-90%, deg (COV)
EGR H_ Part	50	38.7	2.82 (66.72)	17.84 (18.47)	10.4 (56.47)	55.66 (17.03)	56.2 (26.04)
EGR S_ Part	50	38.0	3.44 (36.59)	19.96 (19.61)	12.81 (33.5)	48.12 (6.56)	45.84 (19.97)
EGR H_ WOT	45	30.4	4.77 (16.20)	22.42 (15.3)	15.41 (24.11)	44.80 (12.99)	51.92 (29.55)
EGR S_ WOT	45	31.5	5.23 (6.06)	26.66 (12.37)	16.86 (12.51)	41.38 (6.74)	37.83 (22.95)

¹ Dilution Ratio = $\frac{m_{air}}{m_{air,s} + m_{fuel} + m_{air}} = \frac{15.67(\lambda - 1)}{15.67\lambda + 1}$ where m_{air} is surplus air mass for lean condition, m_{fuel} is fuel mass, $m_{air,s}$ is air mass for stoichiometric a/f ratio with m_{fuel} , λ is lamda.

² EGR% = $\frac{m_{EGR}}{m_i} \times 100$, where m_{EGR} is the mass of exhaust gas recycles, m_i is the inducted mass per cycle.

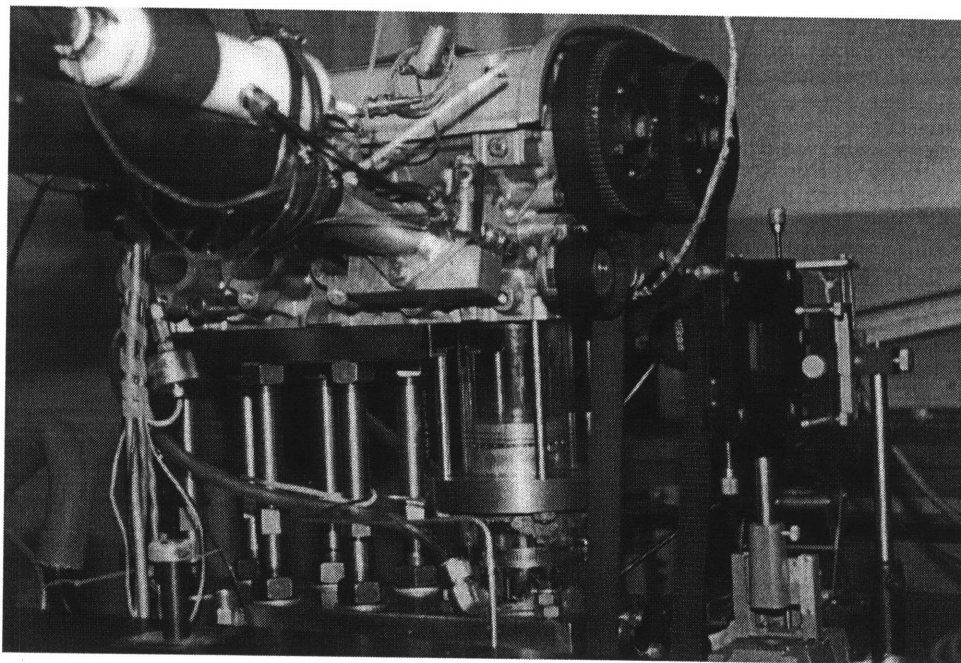


(a) concept of stratified_EGR flow configuration

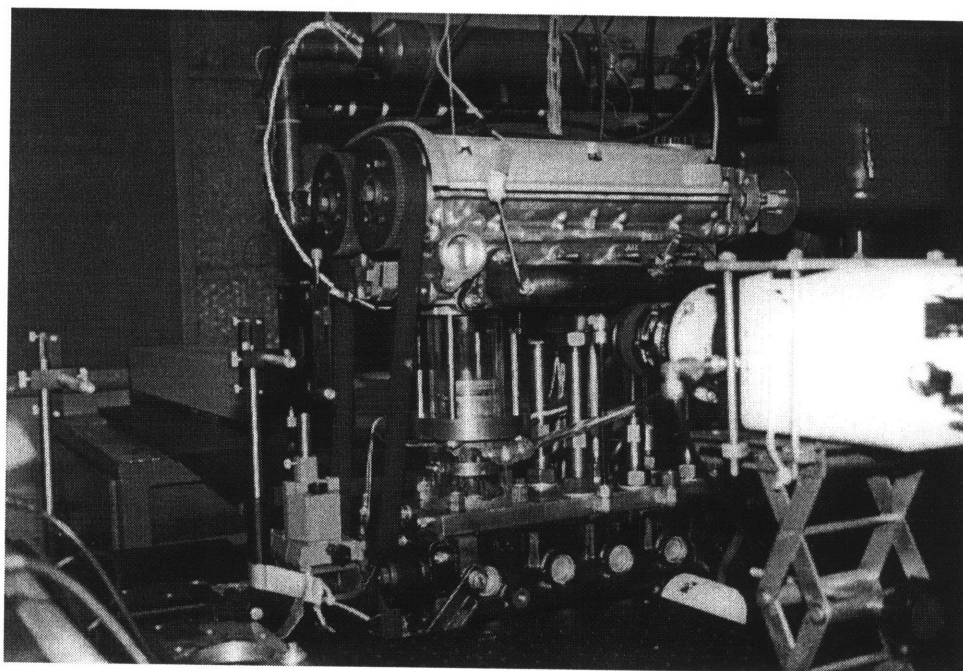


(b) intake system design for stratified_EGR system

Figure 1.1 Engine configuration. (a) concept of stratified_EGR flow configuration, (b) intake system design for stratified_EGR system



(a) Intake side view



(b) Exhaust side view

Figure 2.1 Engine assembly view

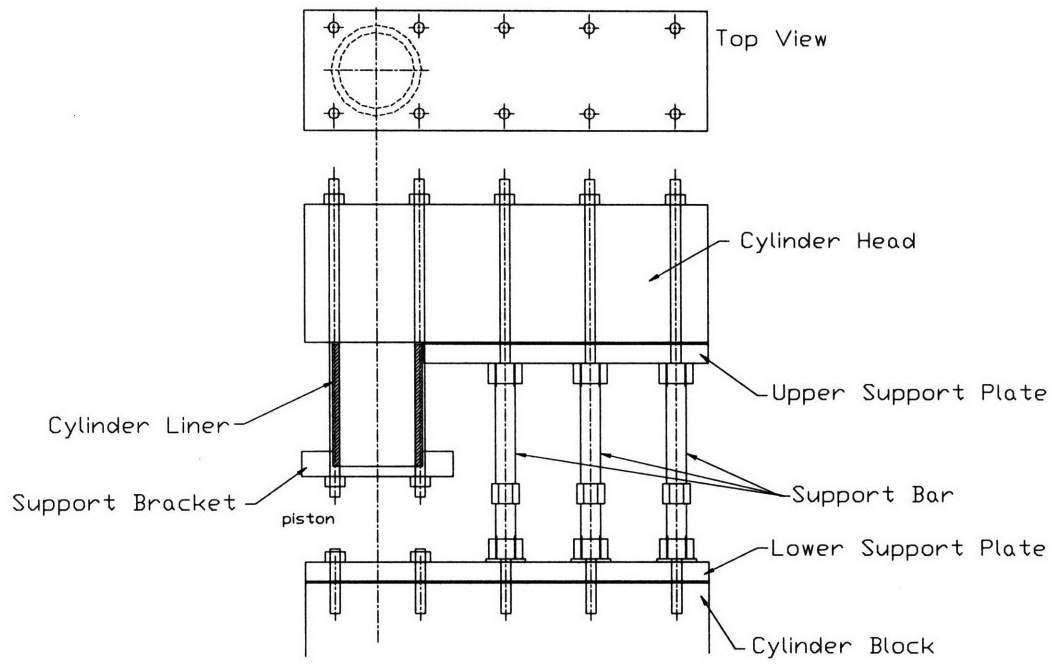


Figure 2.2 Side view of the transparent engine assembly

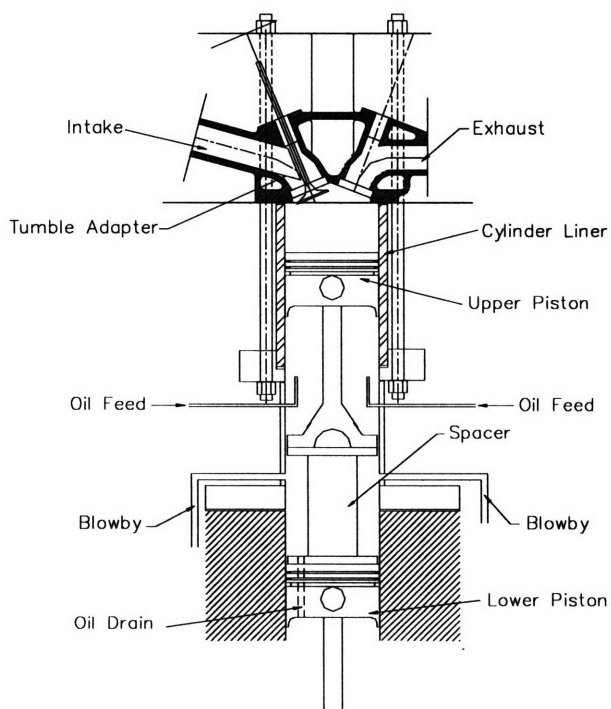


Figure 2.3 Front view of the transparent engine assembly

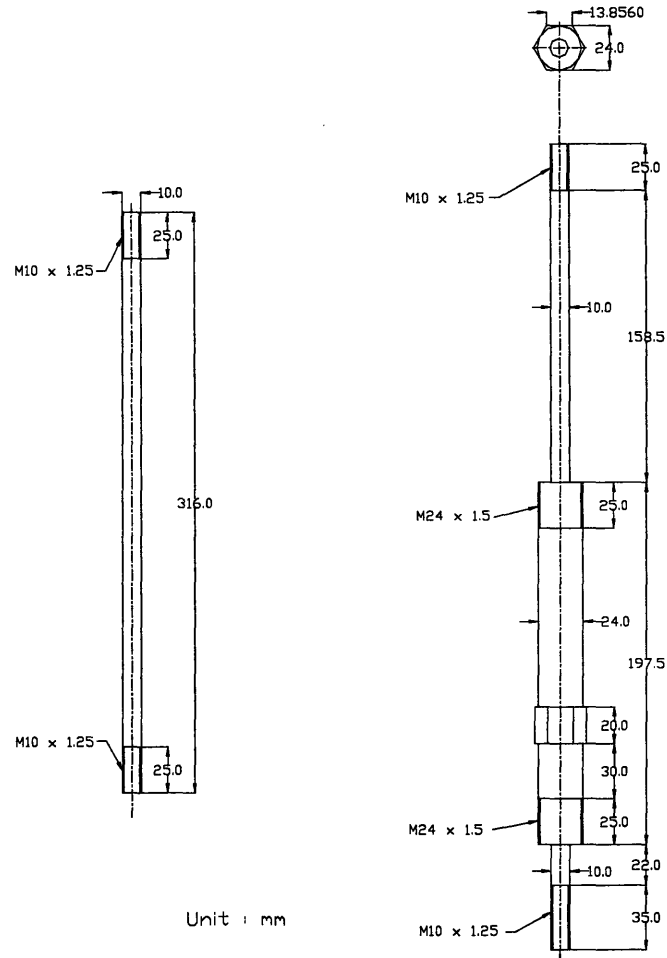
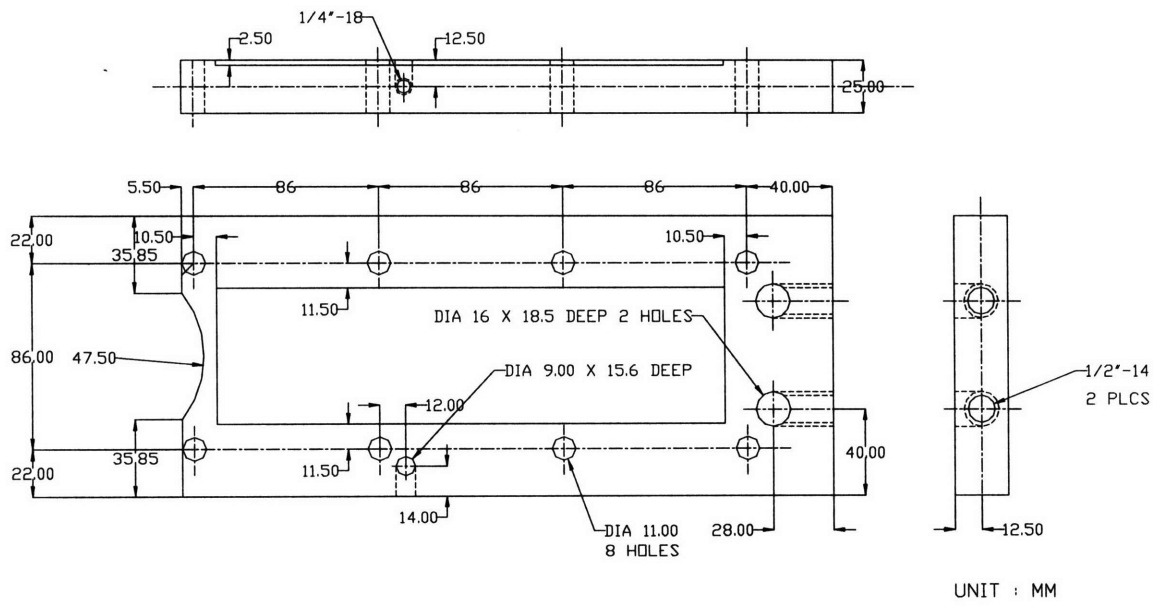
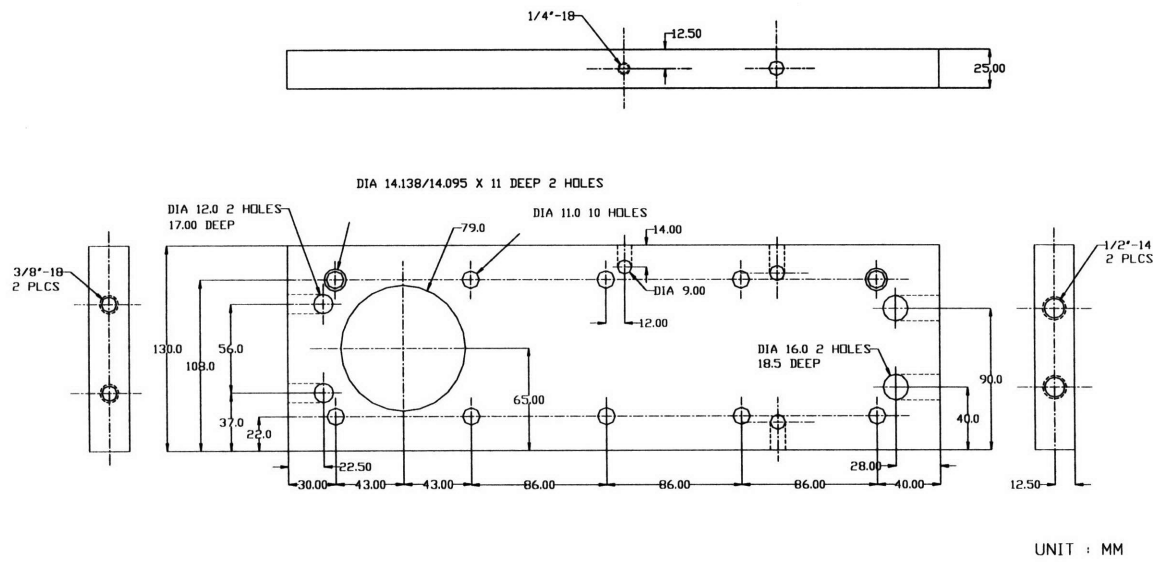


Figure 2.4 Support bar and cylinder mount bolt drawing



(a) Upper plate



(b) Lower plate

Figure 2.5 Support plate drawing

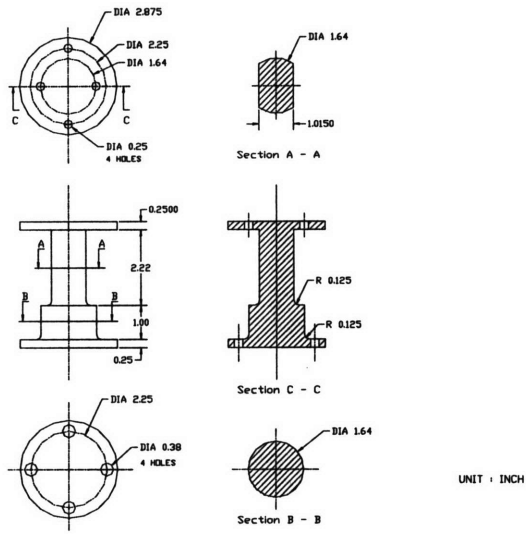


Figure 2.6 Spacer drawing

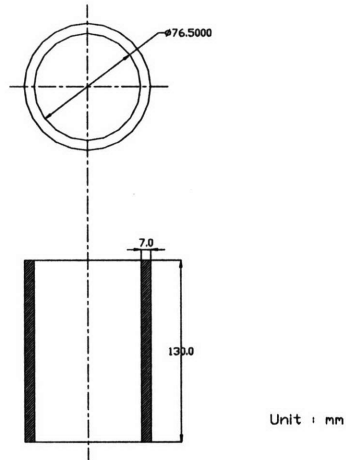


Figure 2.7 Cylinder liner drawing

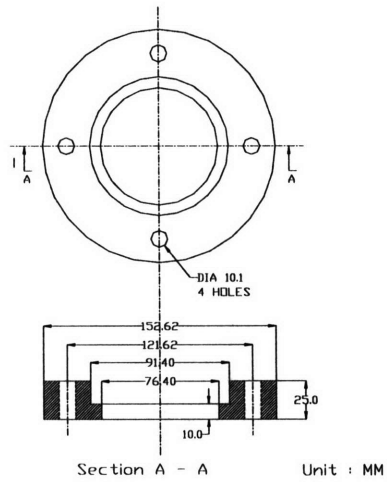


Figure 2.8 Cylinder liner support bracket drawing

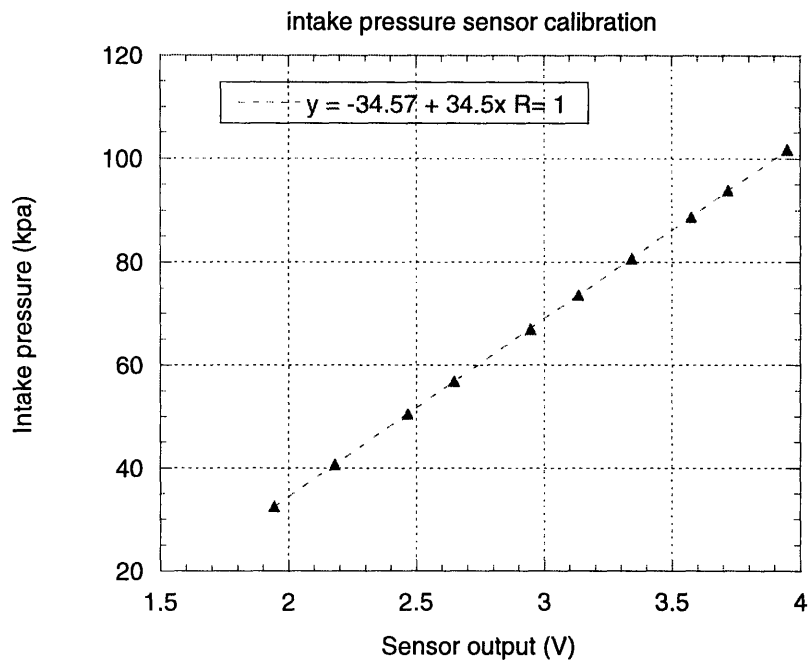


Figure 2.9 Calibration curve of the intake pressure sensor

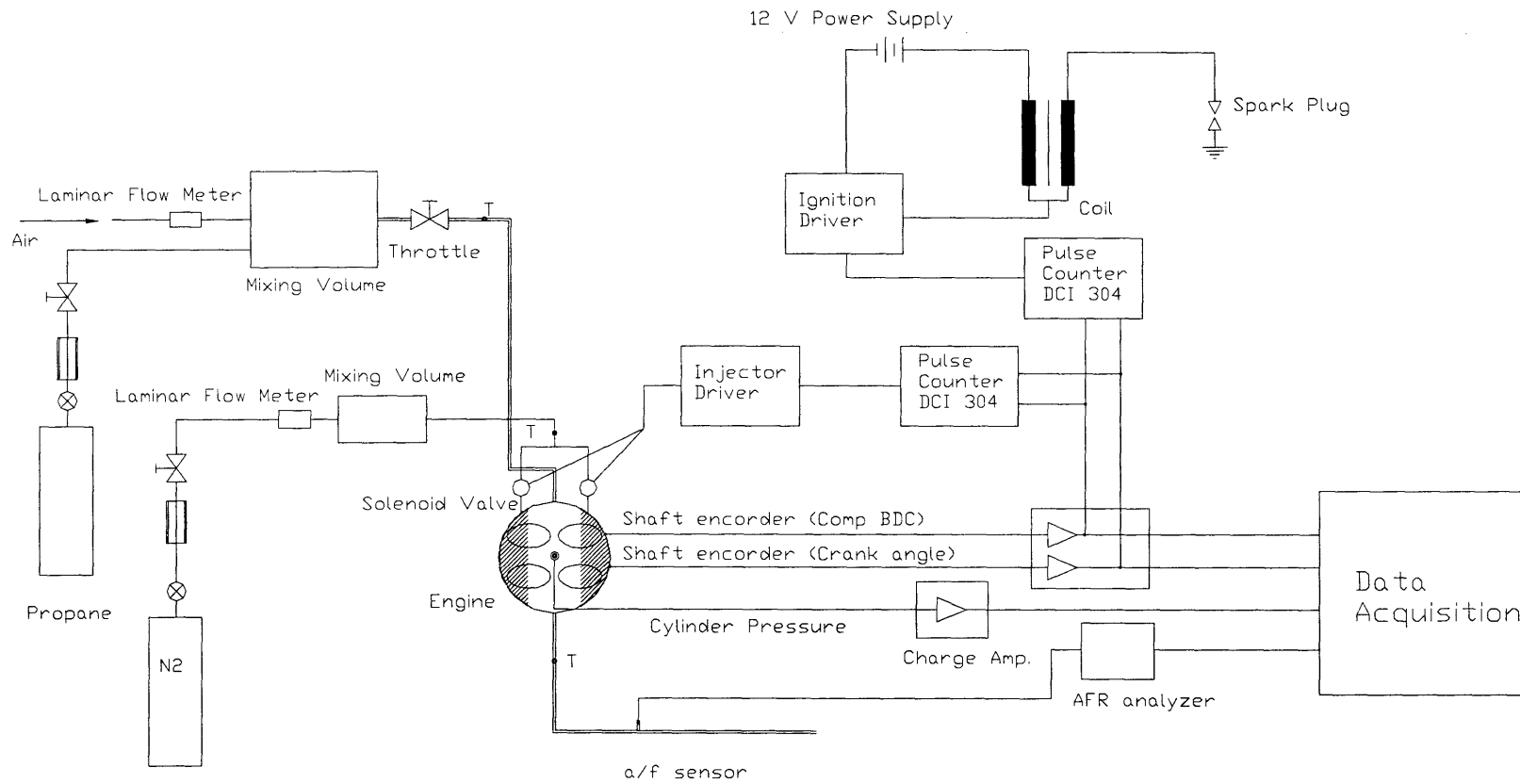
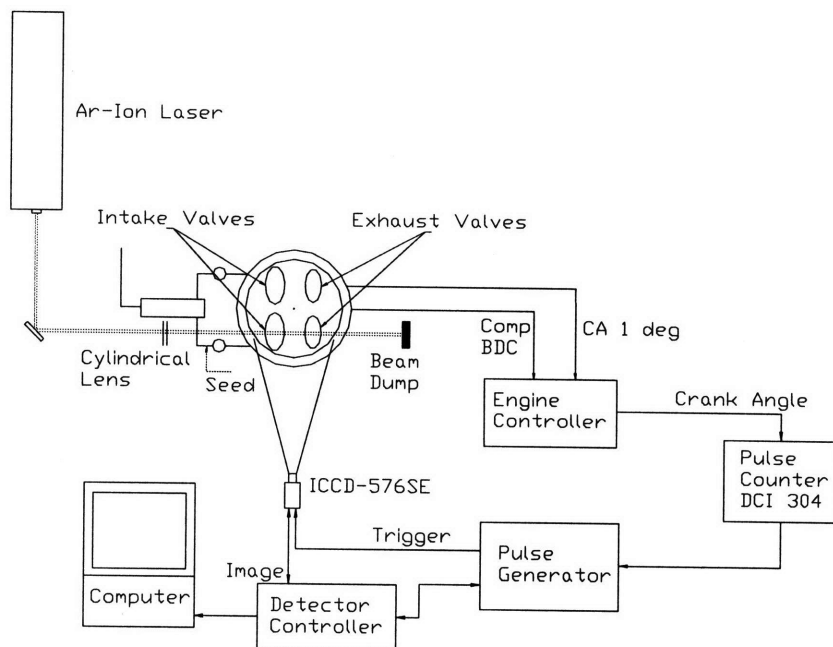
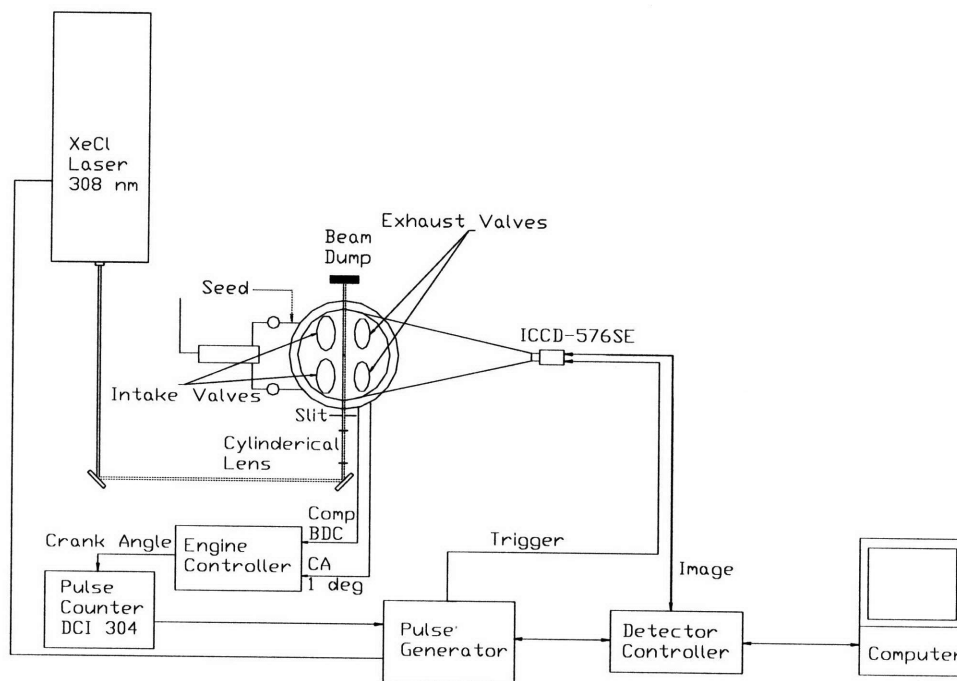


Figure 2.10 Schematic of the experimental set-up.



(a) Mie scattering experiment setup



(b) PLIF experiment setup

Figure 2.11 The schematic of the experimental setup

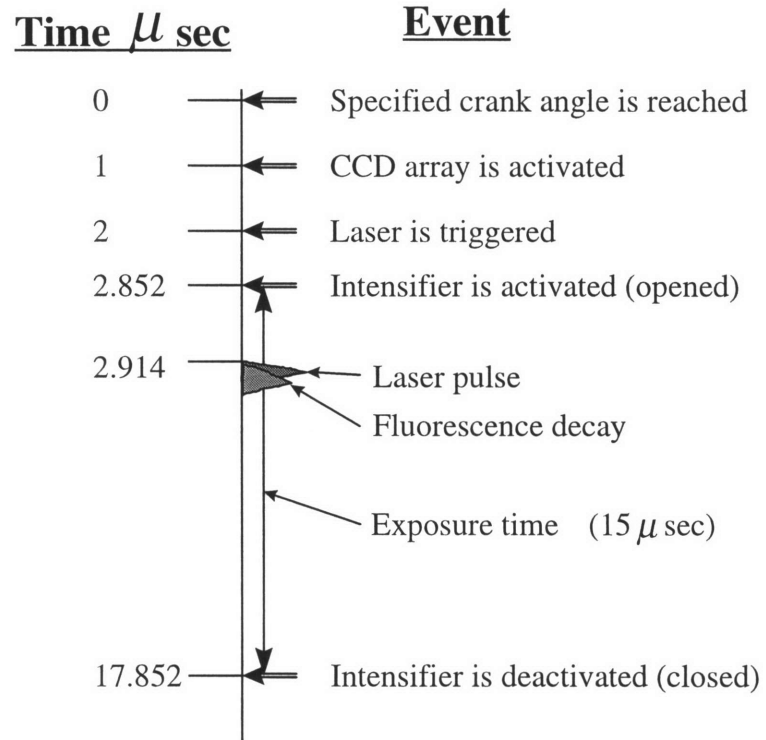


Figure 2.12 The flow chart of laser and camera control timing for PLIF test.

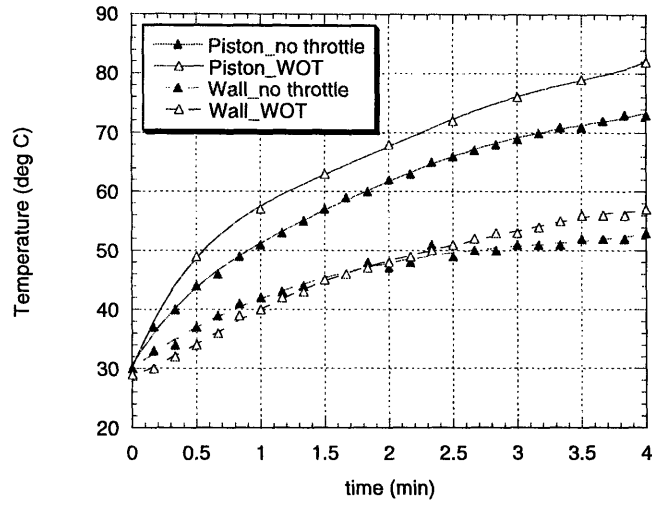


Figure 2.13 Temperature variation on the bottom of the piston and the quartz wall at motoring condition. Comparison between wide open throttle and throttle closed

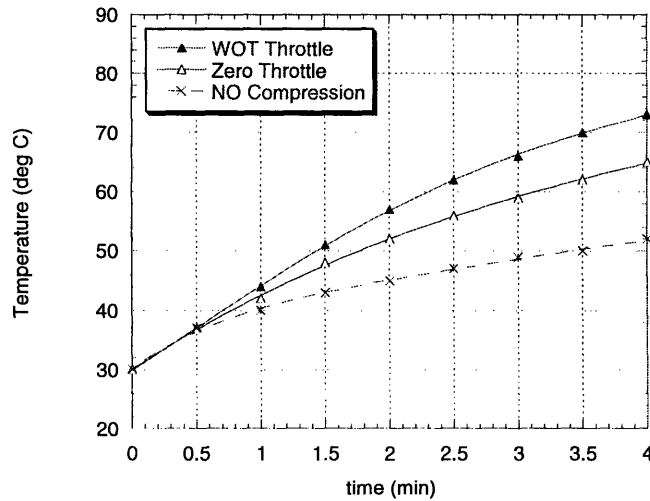
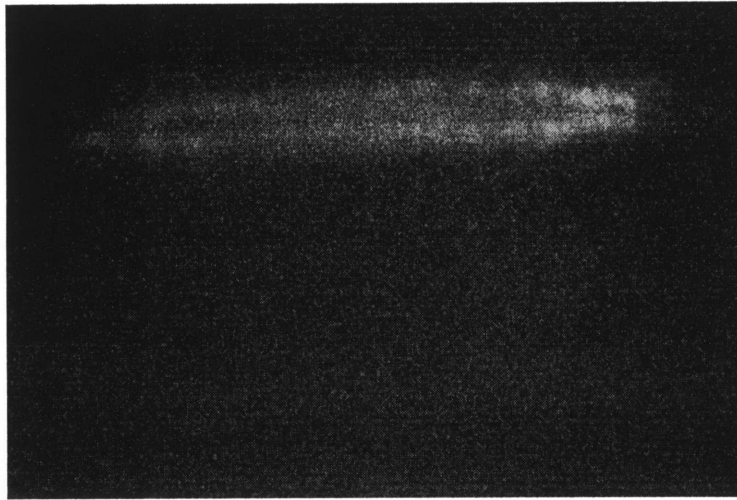
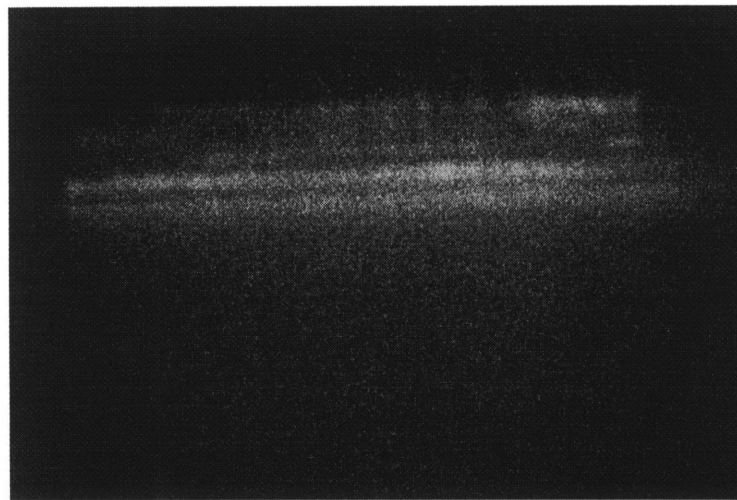


Figure 2.14 Outside wall temperature of the metal cylinder with difference of cylinder pressure. Data for no compression is obtained by removing spark plug.

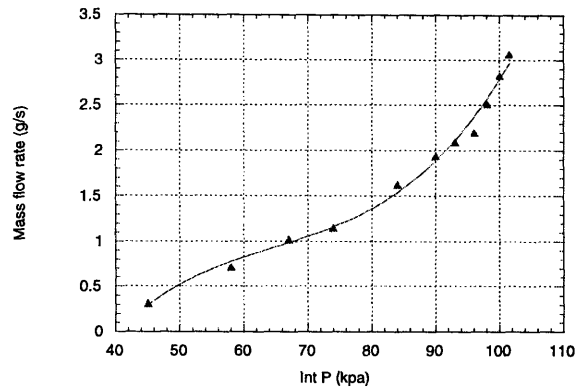


(a) 30 deg ATDC : Expansion Stroke

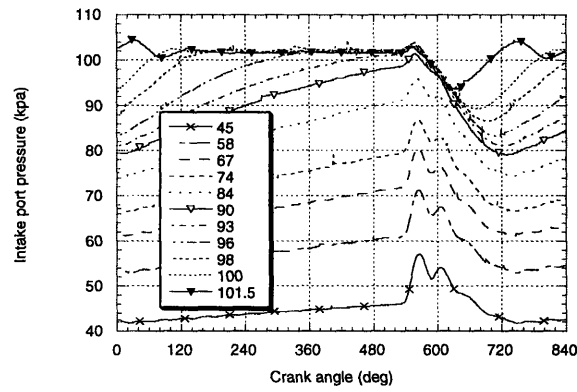


(b) 50 deg ATDC : Expansion Stroke

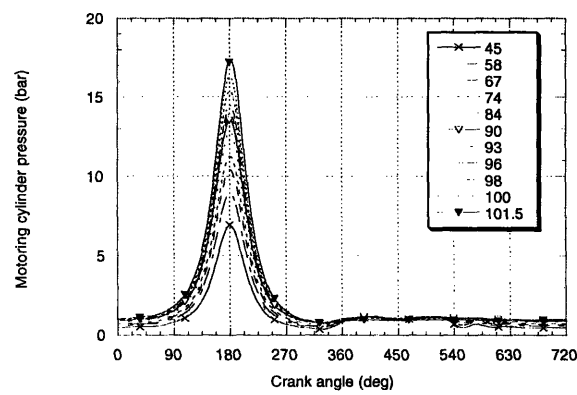
Figure 2.15 Shadowgraph images of combustion. 1000 rpm, $\lambda = 1$, part load



(a)



(b)



(c)

Figure 3.1 Intake mass flow rate and pressure characteristics at motoring condition (a) mass flow rate vs. intake pressure. (b) intake pressure vs. crank angle. (c) cylinder pressure vs. crank angle. 1000 rpm.

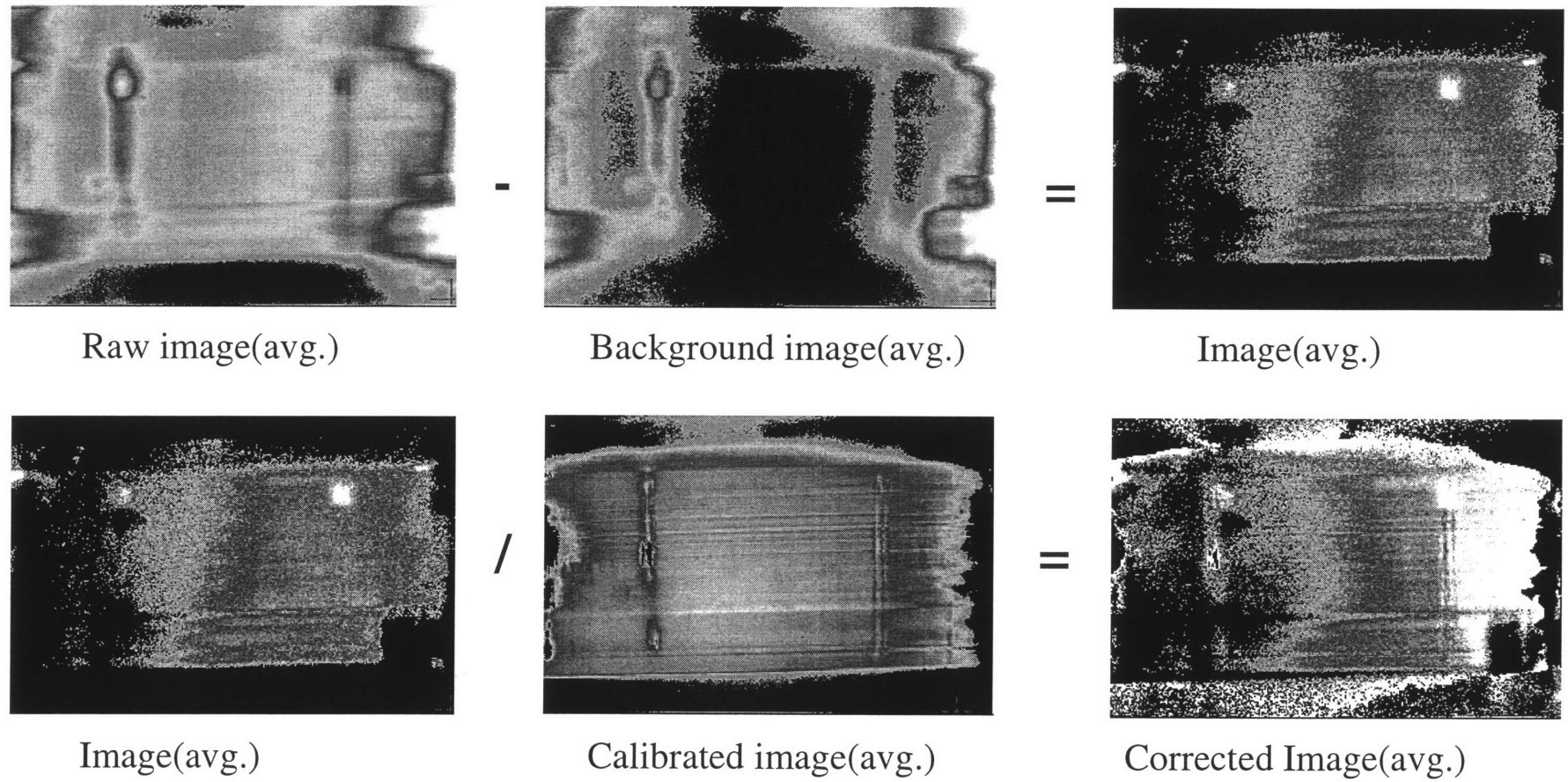


Figure 3.2 Image Correction for background and cylinder wall curvature

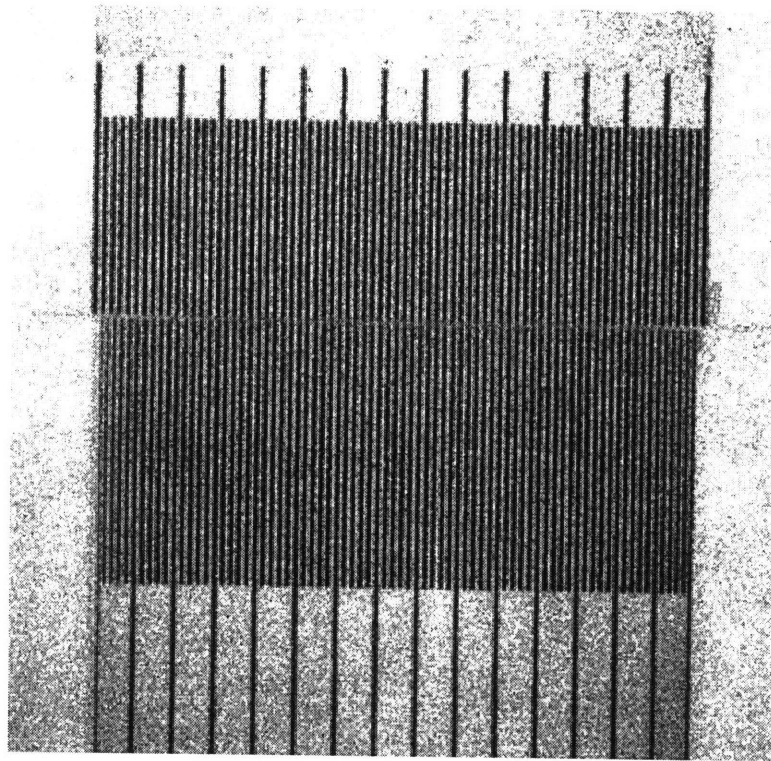
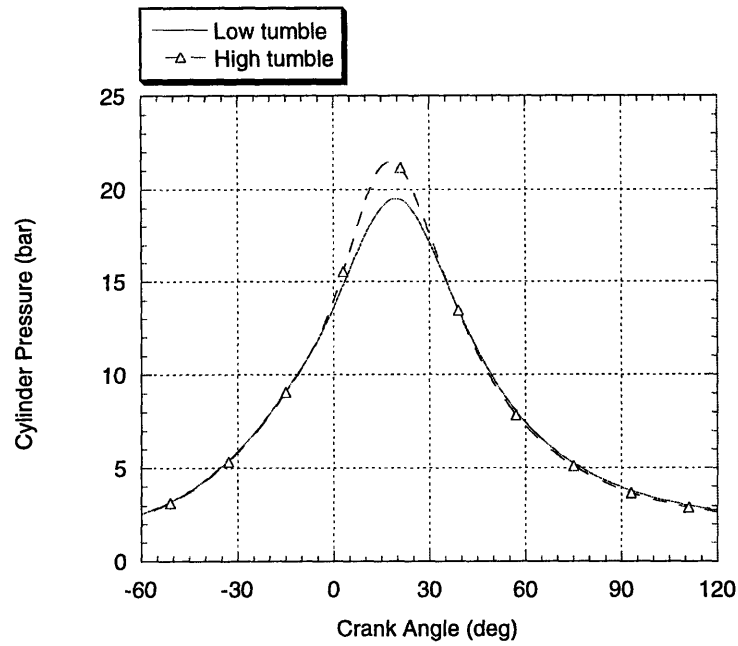
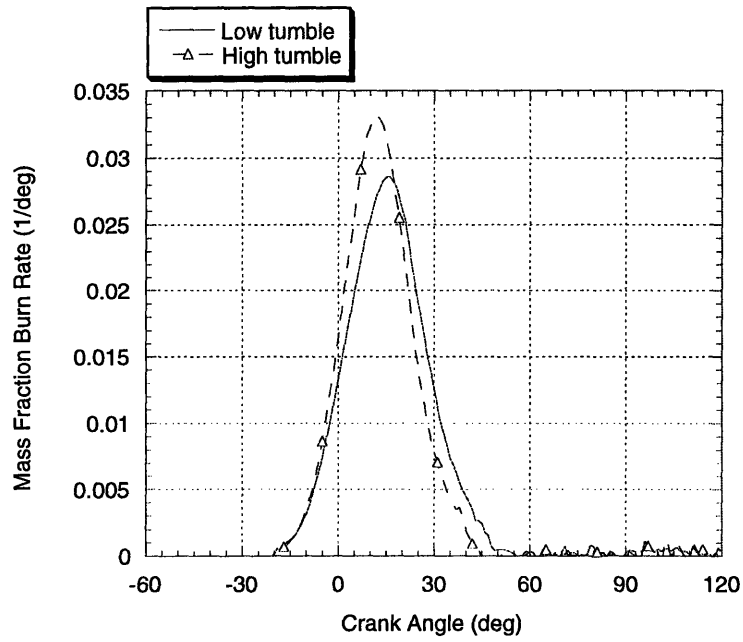


Figure 3.3 Calibration image for cylinder wall contraction. The small scale is 1 mm.

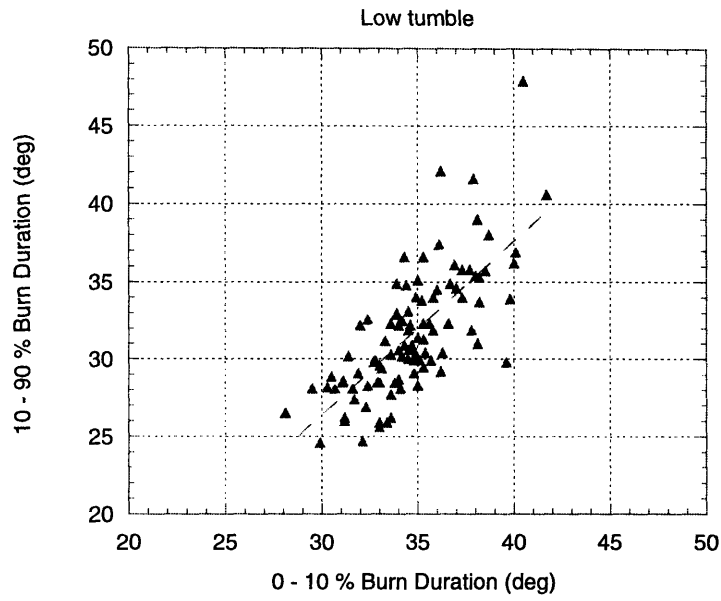


(a)

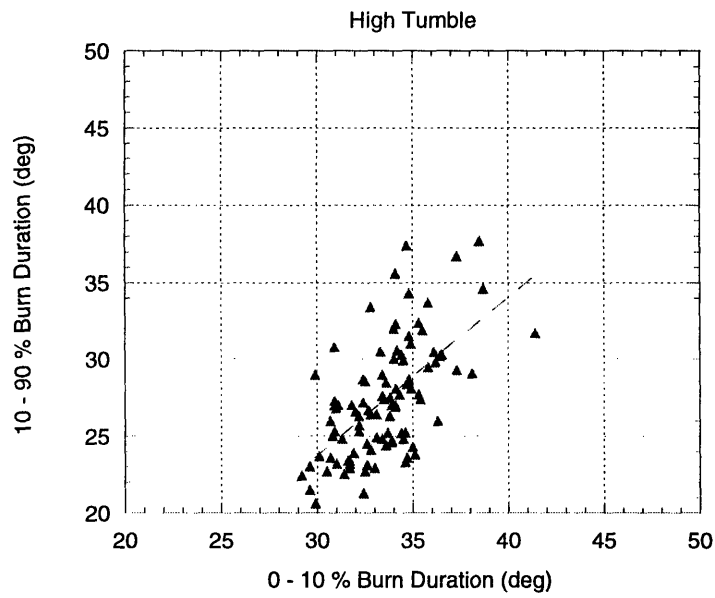


(b)

Figure 4.1 Effect of tumble on combustion. Comparison between production condition and tumble enhancement condition. (a) Cylinder pressure vs. crank angle (b) Mass fraction burn rate vs. crank angle. 1000 rpm, $\lambda=1$, MBT spark timing.

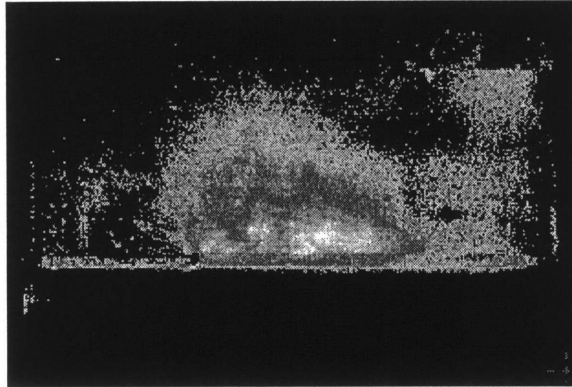


(a)

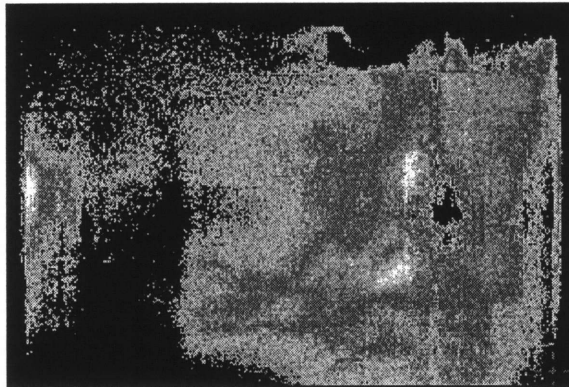


(b)

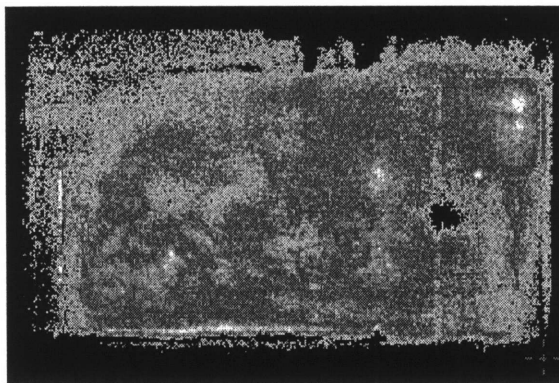
Figure 4.2 Effect of tumble on burn duration. Comparison between production condition and tumble enhancement condition. Burn angle $\theta_{10-90\%}$ vs. burn angle $\theta_{0-10\%}$. 1000 rpm, $\lambda=1$, MBT spark timing.



(a) 70 ATDC intake stroke



(b) 120 BTDC intake stroke



(c) 90 BTDC compression stroke

Figure 4.3 In-cylinder flow motion at motoring. Mie scattering test results. 1000 rpm, WOT

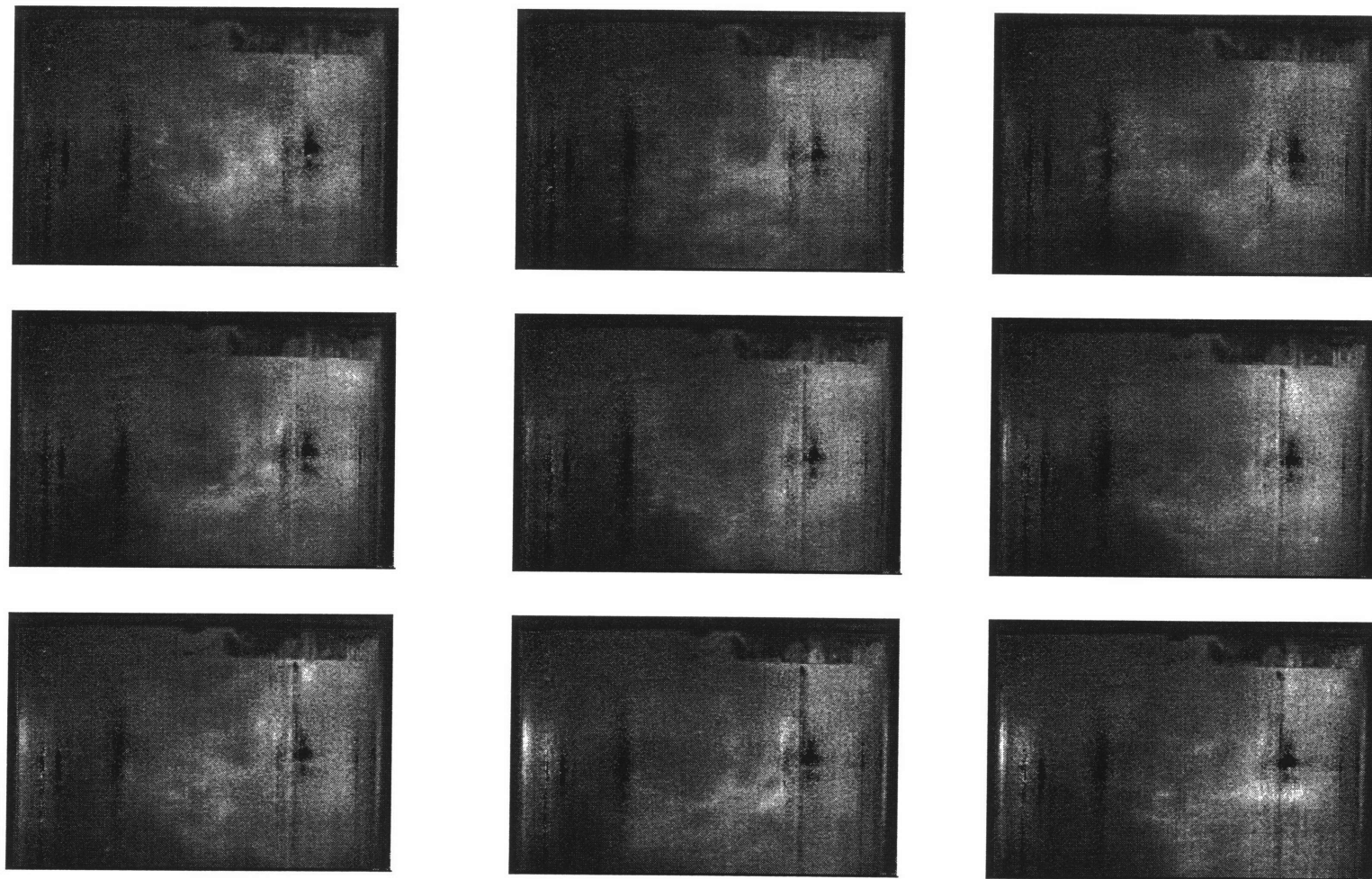


Figure 4.4 The cycle by cycle variation of in-cylinder flow motion during the intake stroke.
1000 rpm , motoring , 120 deg ATDC, WOT

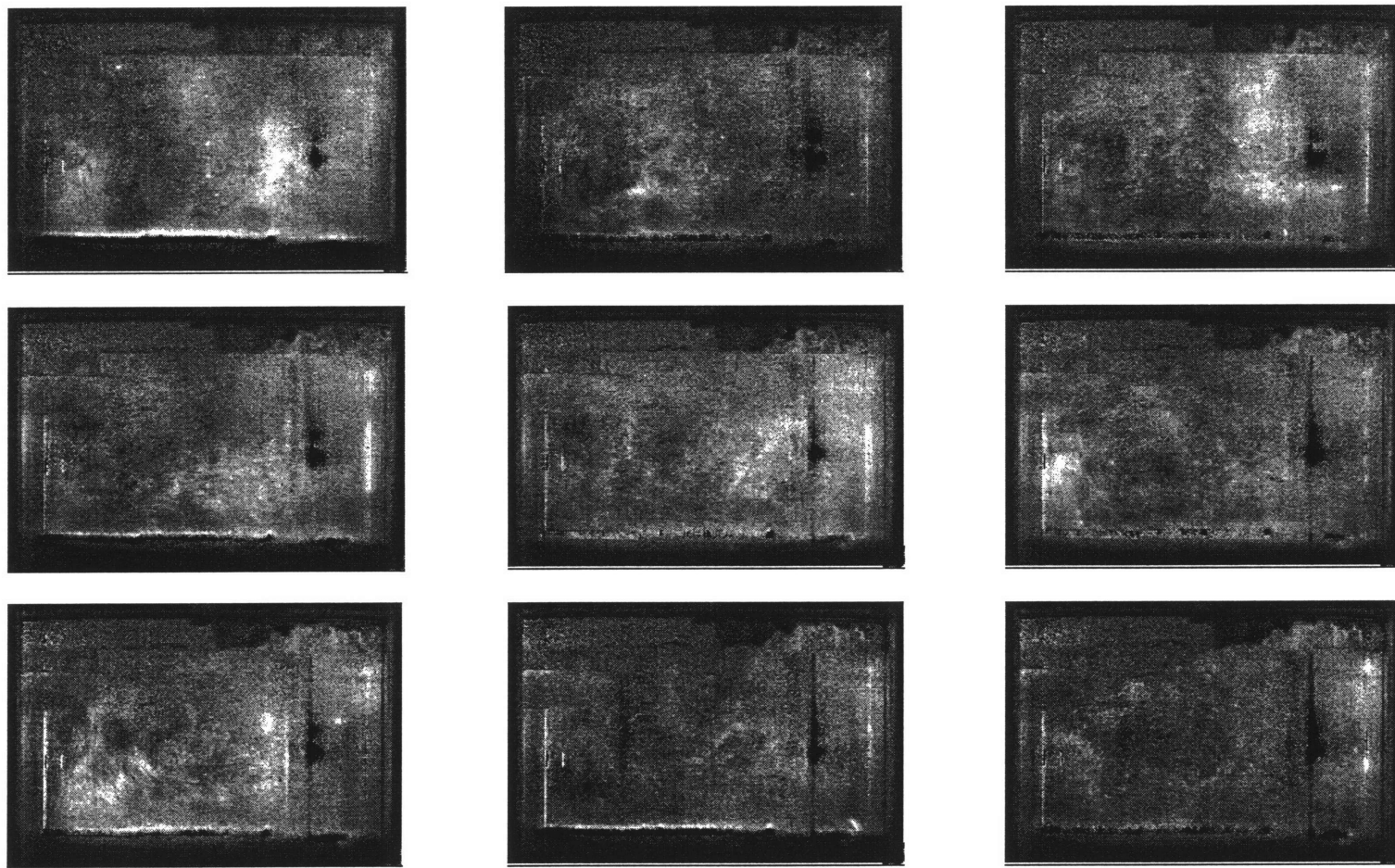


Figure 4.5 The cycle by cycle variation of in-cylinder flow motion during the compression stroke
1000rpm, motoring, 90 deg BTDC, WOT

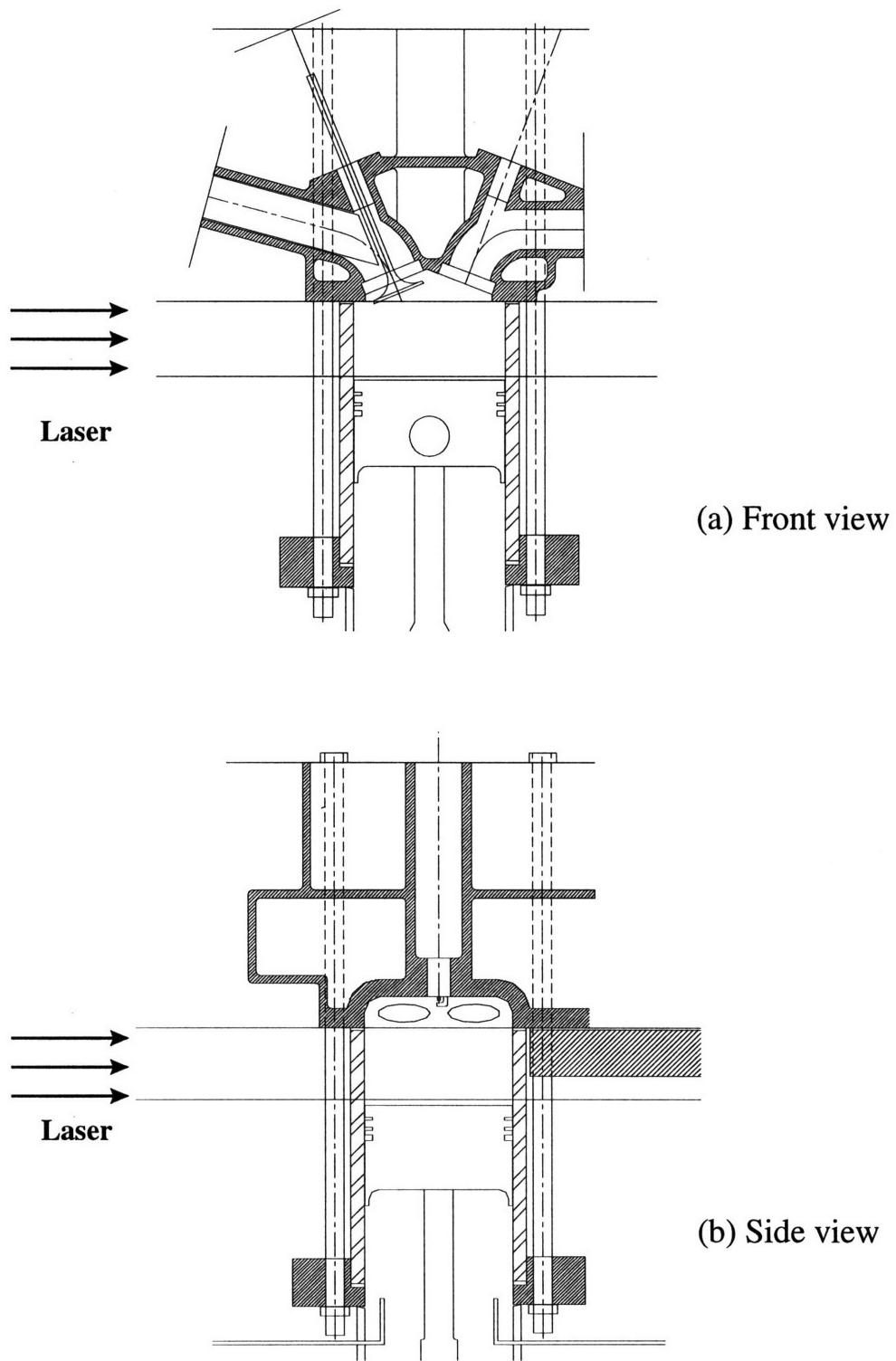
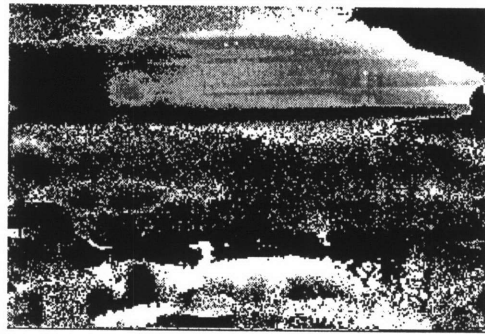
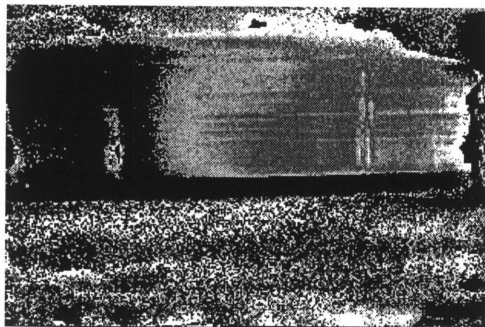


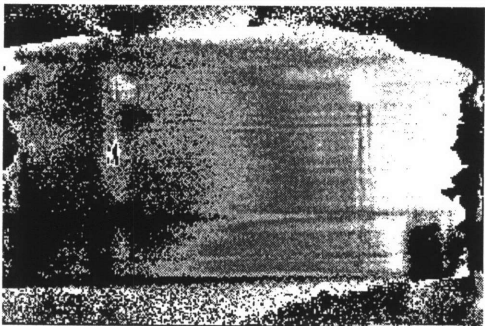
Figure 4.6 Engine front and side view including combustion chamber



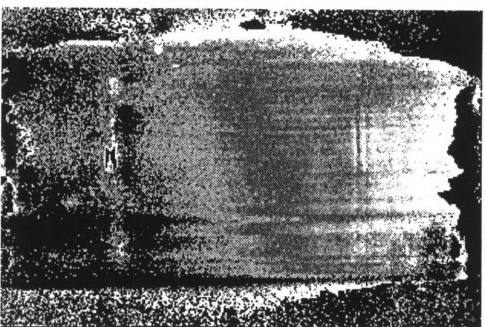
45 ATDC



60 ATDC

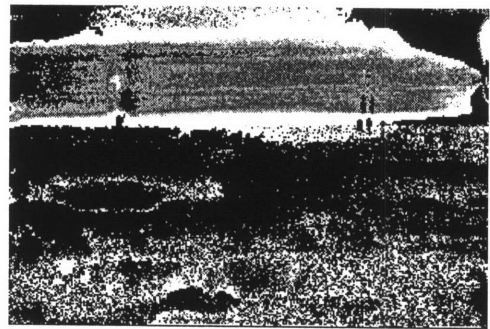


90 ATDC

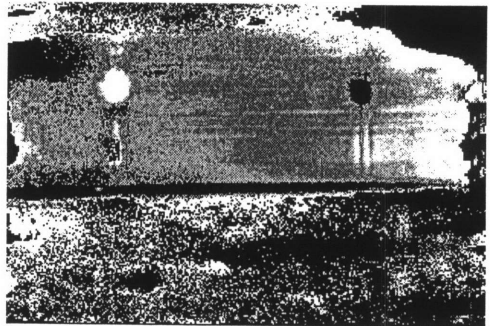


120 ATDC

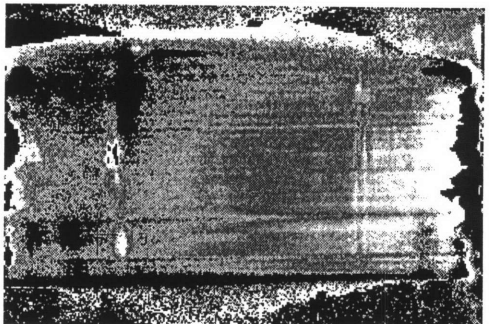
(a) Intake stroke



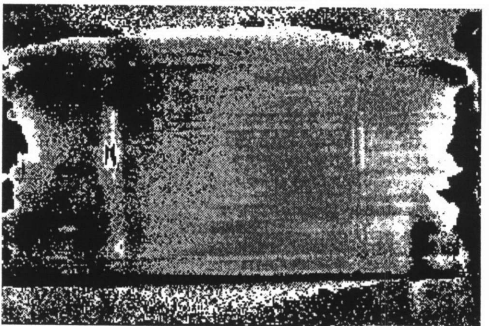
45 BTDC



60 BTDC



90 BTDC



120 BTDC

(b) Compression stroke

Figure 4.7 Images of PLIF to show overall mixing process:
(a) intake stroke (b) compression stroke, 1000 rpm, WOT, motoring

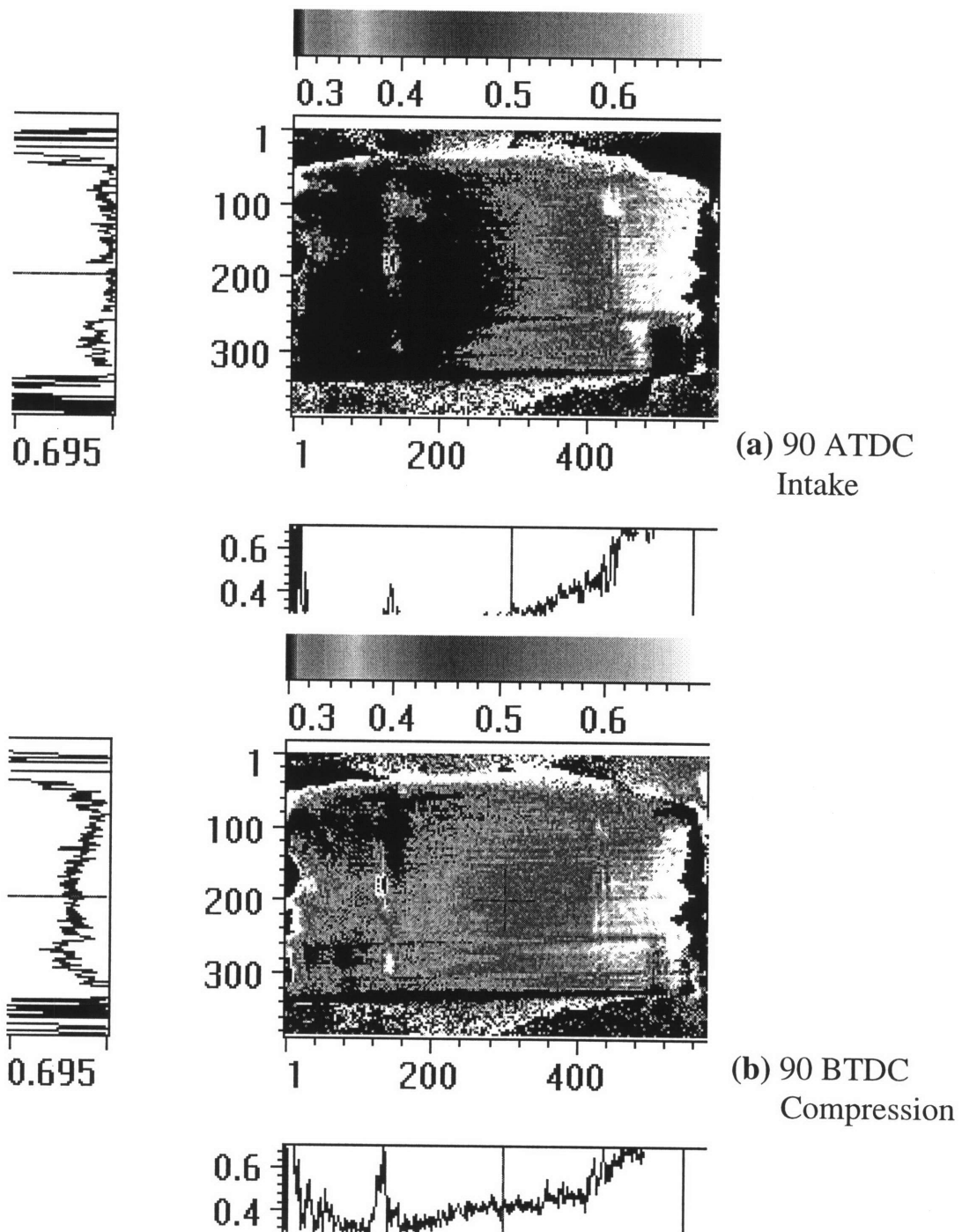


Figure 4.9 Mixing comparison at 90 deg; The distribution of acetone concentration (a) intake stroke, (b) compression stroke

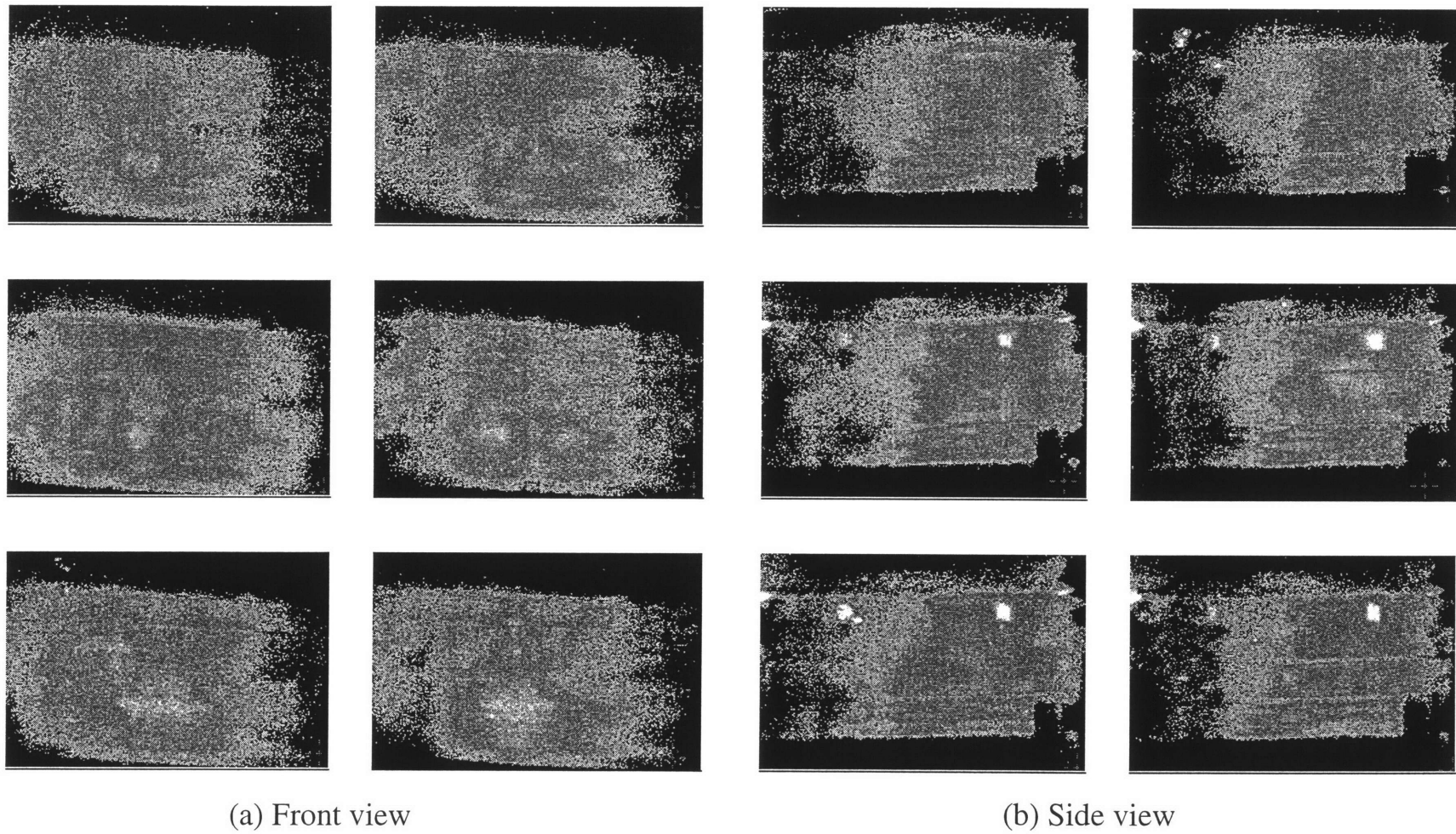


Figure 4.10 Cycle by cycle variation of mixing process during the intake stroke
(a) front view (b) side view, 90 deg ATDC

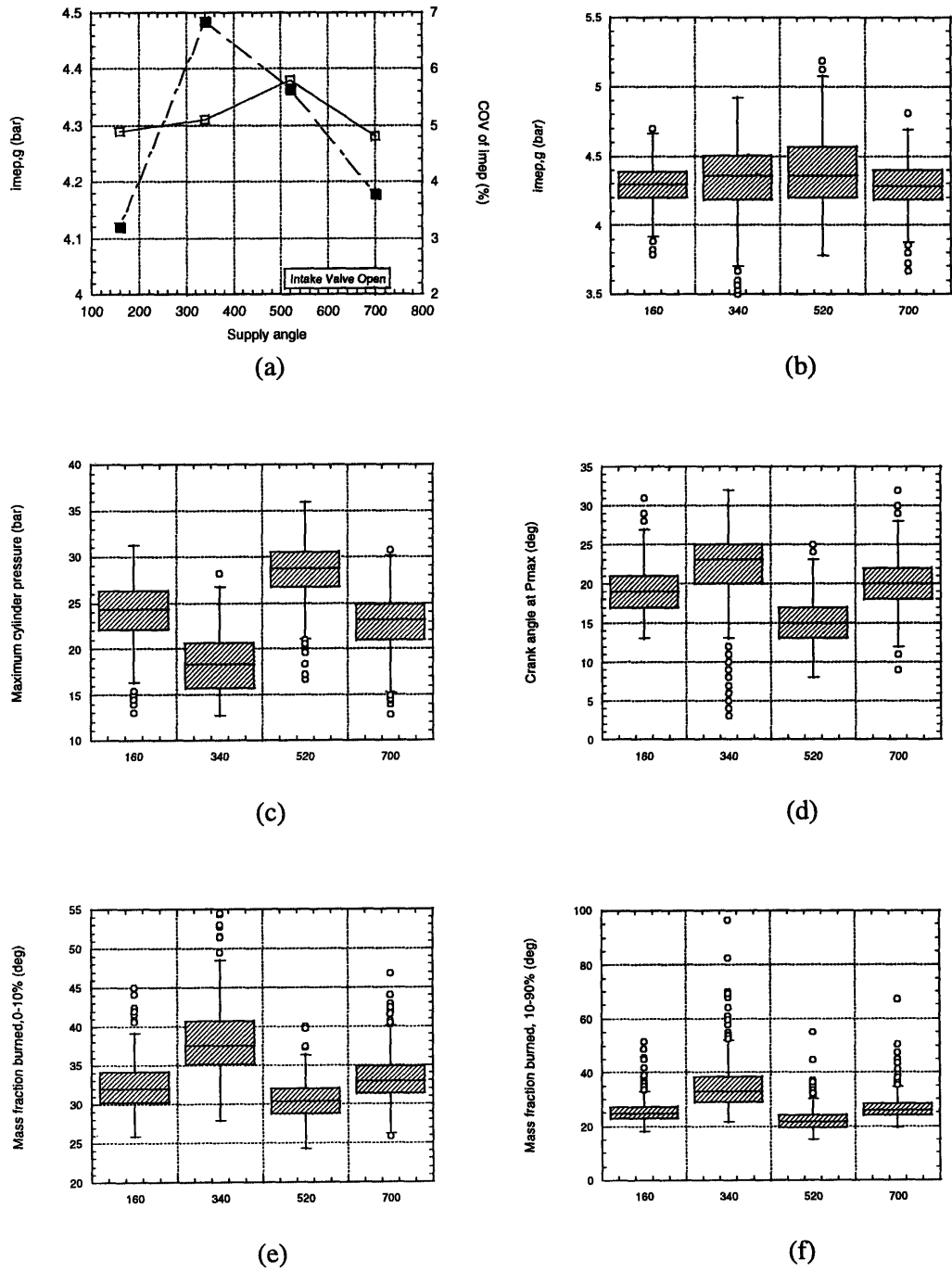
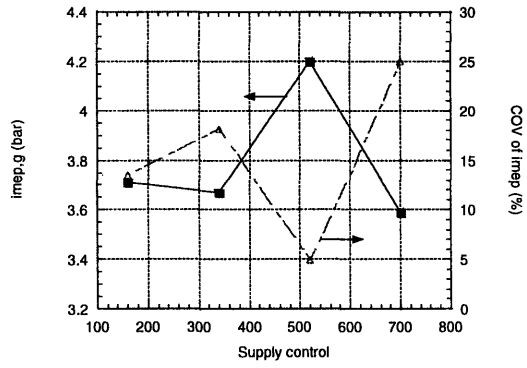
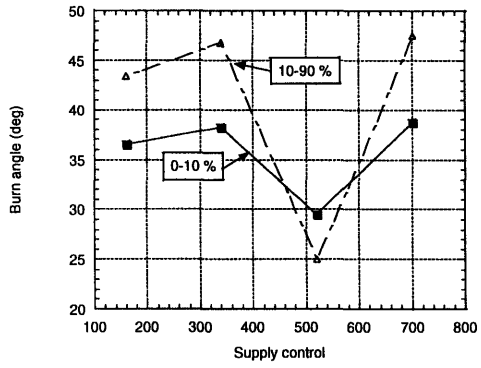


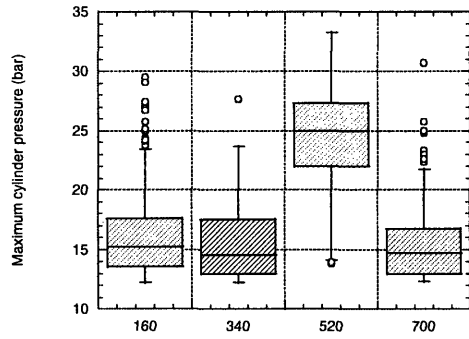
Figure 4.11 The effect of supply timing on combustion performance at lean operation. 1000 rpm, $\lambda=1.4$, spark timing = 35 deg BTDC. Horizontal axis is CA at which injection commences. IVO at 505. (540 deg is TDC intake)



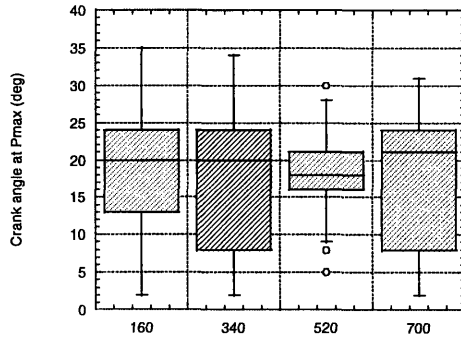
(a)



(b)

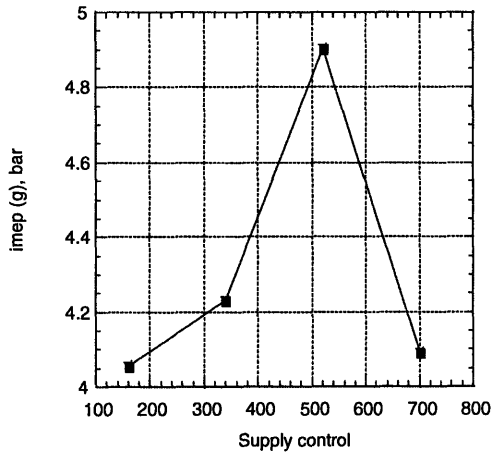


(c)

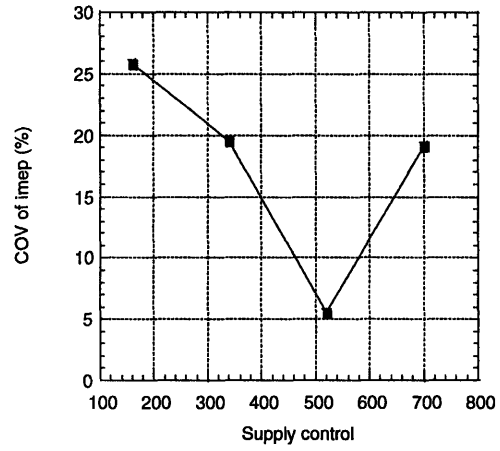


(d)

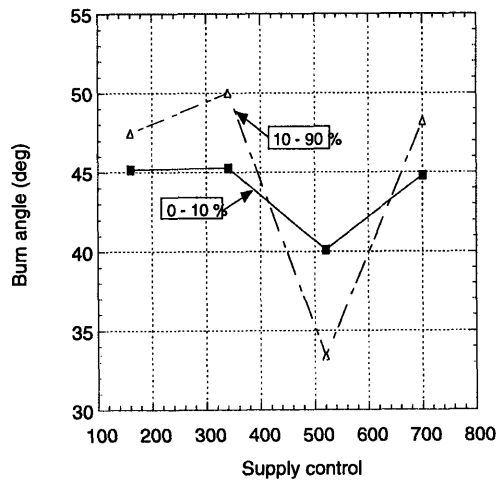
Figure 4.12 The effect of supply timing on combustion performance at lean operation. 1000 rpm, $\lambda = 1.55$, spark timing = 30 deg BTDC



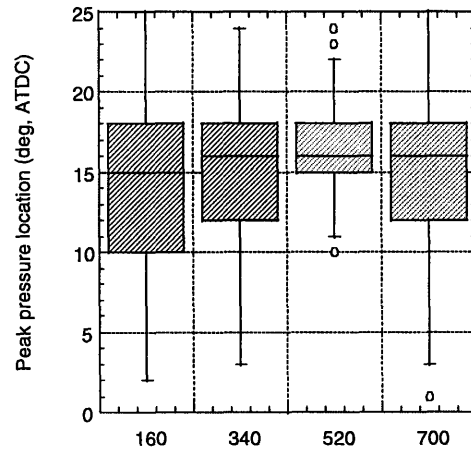
(a)



(b)

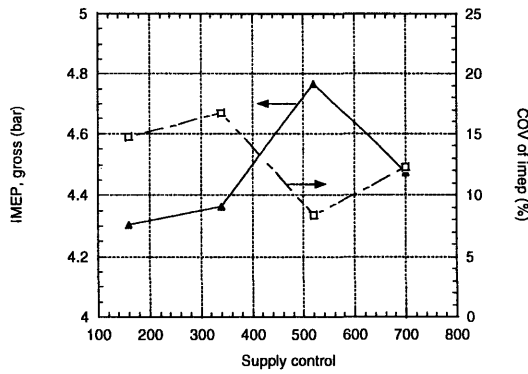


(c)

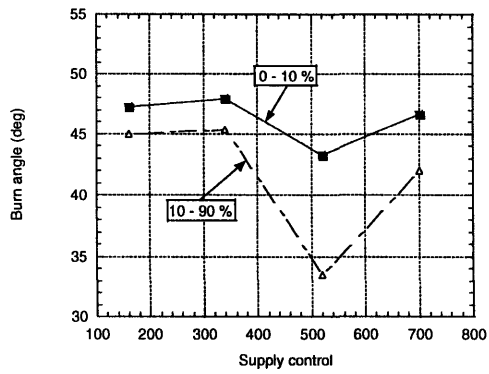


(d)

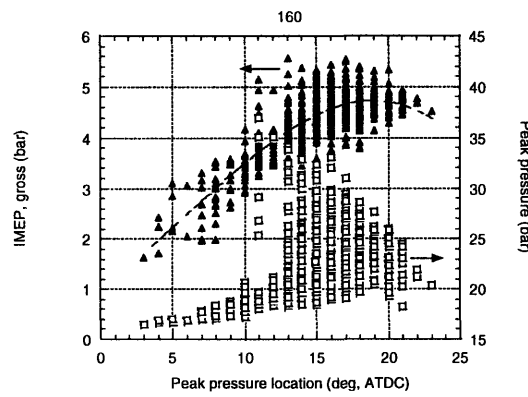
Figure 4.13 The effect of supply timing on combustion performance at EGR operation. 1000 rpm, $\lambda = 1$, EGR ratio = 30 %, spark timing = 45 deg BTDC



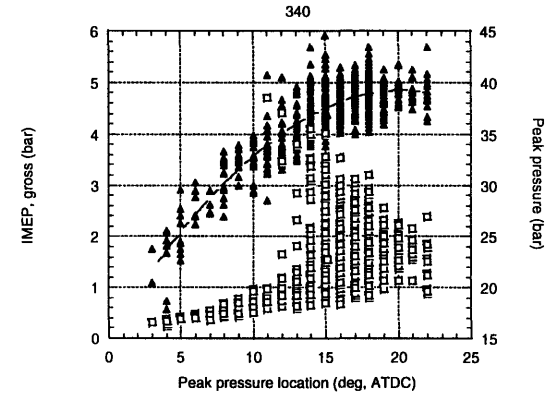
(a)



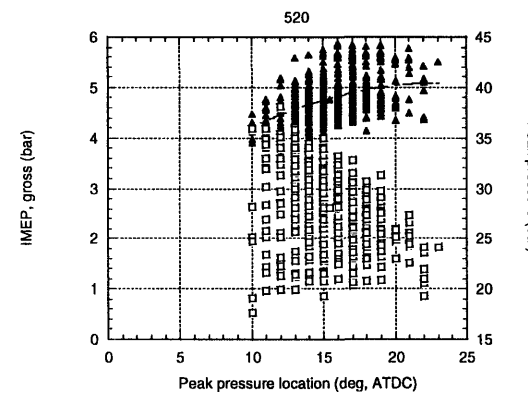
(b)



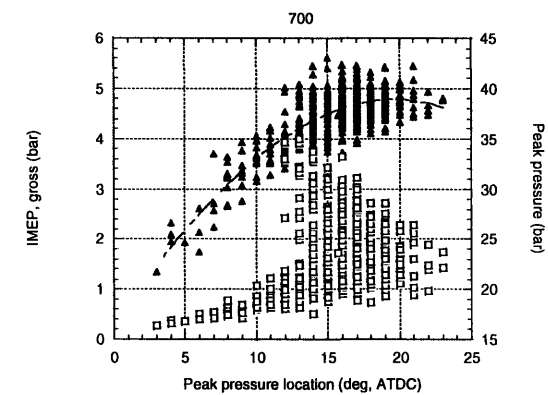
(c)



(d)

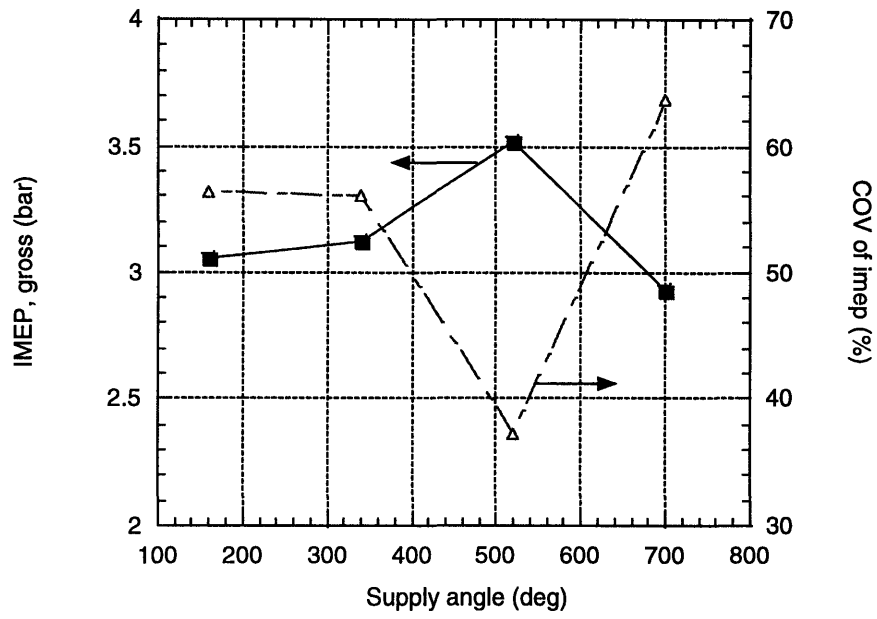


(e)

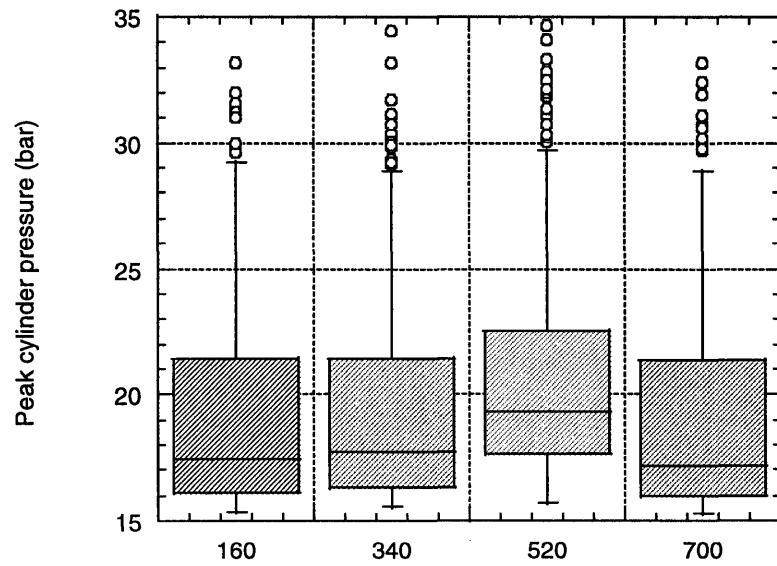


(f)

Figure 4.14 The effect of supply timing on combustion performance at EGR operation. 1000 rpm, $\lambda=1$, EGR ratio=30%, spark timing=50 deg BTDC



(a)



(b)

Figure 4.15 Performance comparison between the supply timing control strategies. (a) IMEP and COV of IMEP vs. supply angle, (b) Pmax vs. supply angle. 1000 rpm, $\lambda=1$, EGR ratio=40 %, spark timing =50 deg BTDC

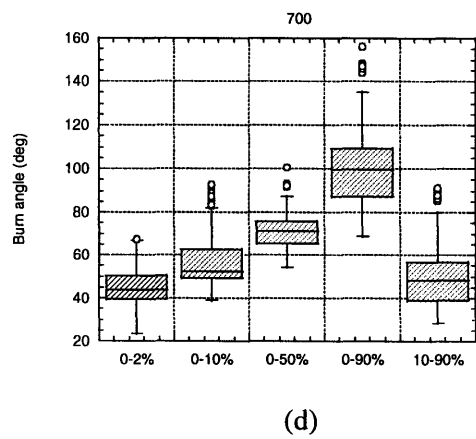
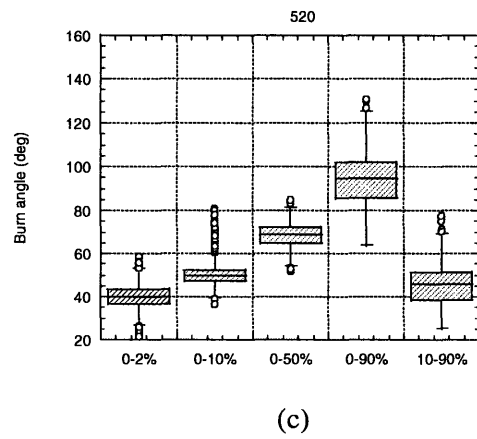
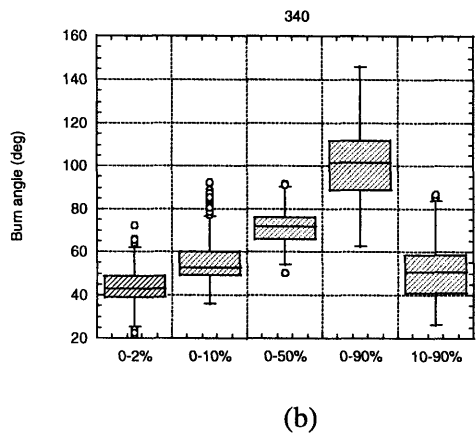
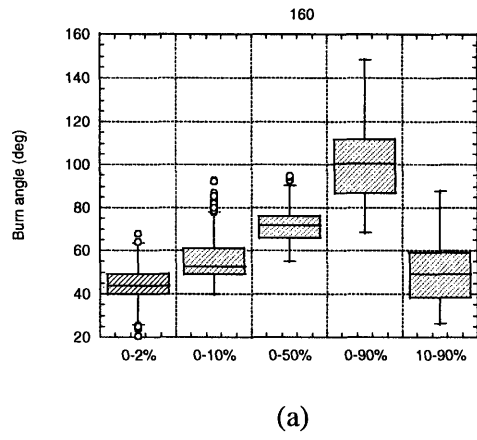
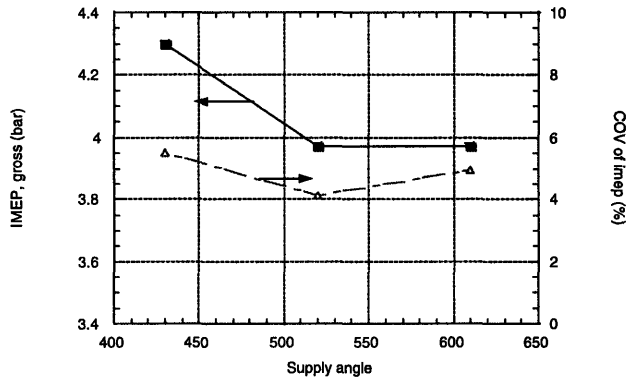
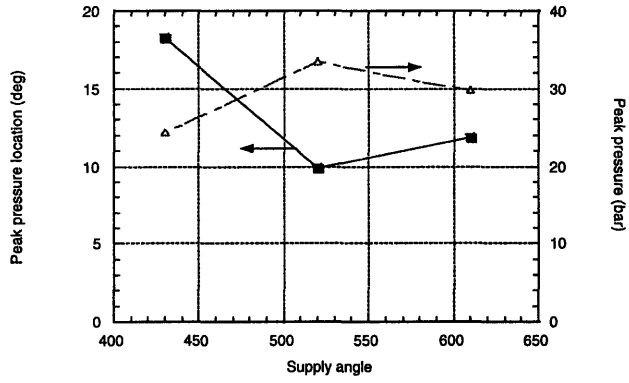


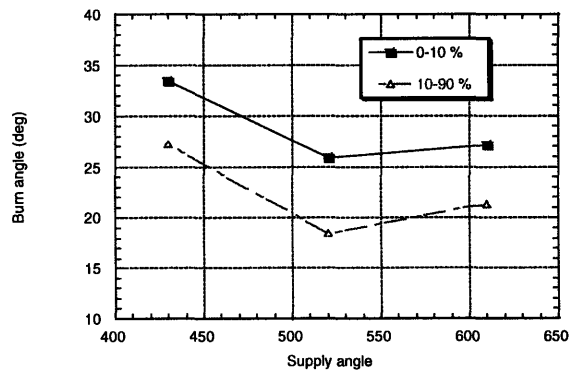
Figure 4.16 Burn angle comparison with the difference of supply time.
 1000 rpm, $\lambda = 1$, EGR ratio = 40 %, spark timing = 50 deg BTDC



(a)



(b)



(c)

Figure 4.17 The effect of supply timing on combustion performance at lean burn condition with the narrow gap of supply angle. 1000 rpm, $\lambda=1.4$, spark timing=35 deg BTDC

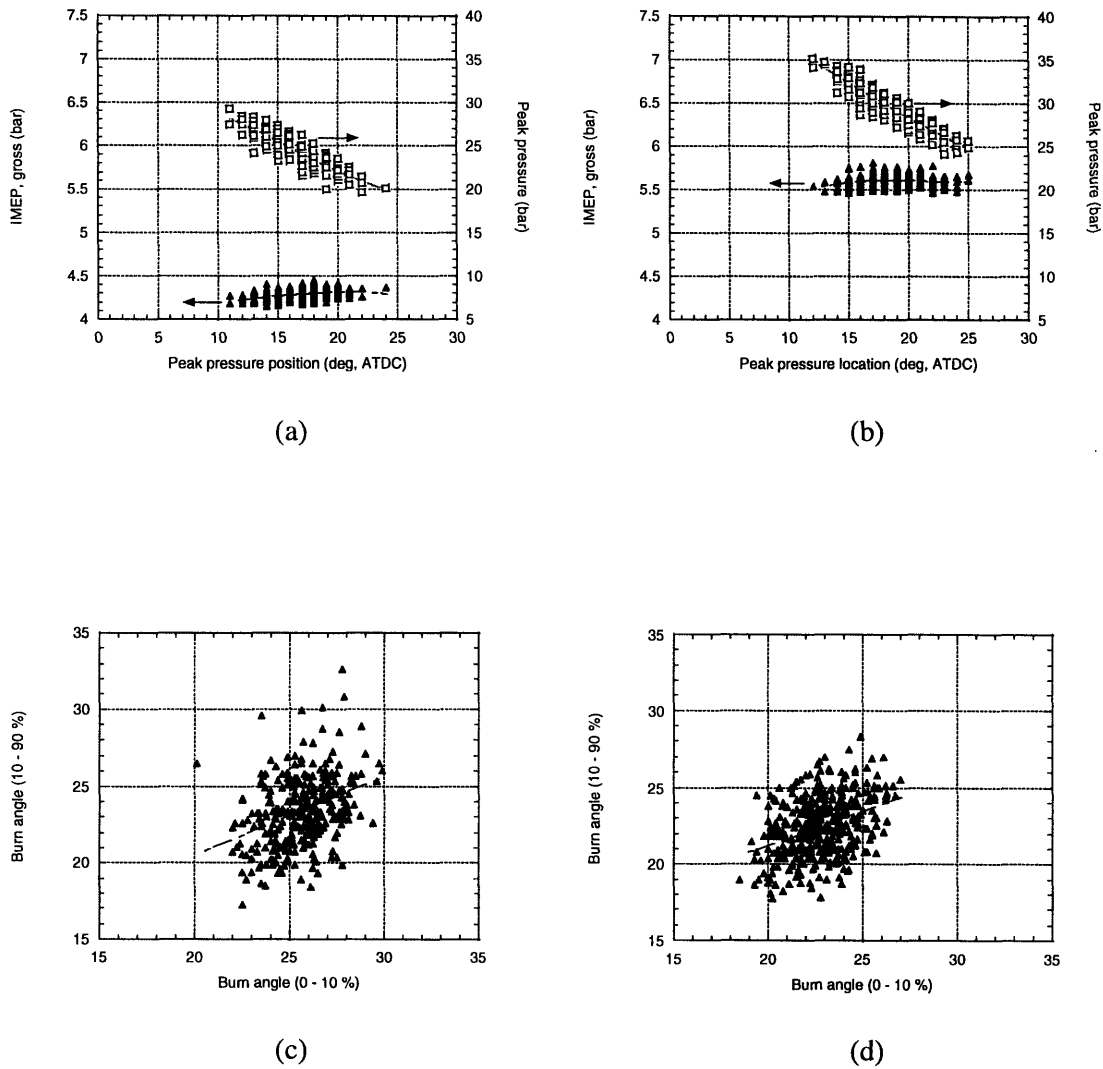


Figure 4.18 The engine performance comparison of reference test
 (a), (c) $\lambda = 1$, spark timing = 30 deg BTDC
 (b), (d) $\lambda = 1$, spark timing = 25 deg BTDC

Homogeneous Mixture

Stratified Mixture

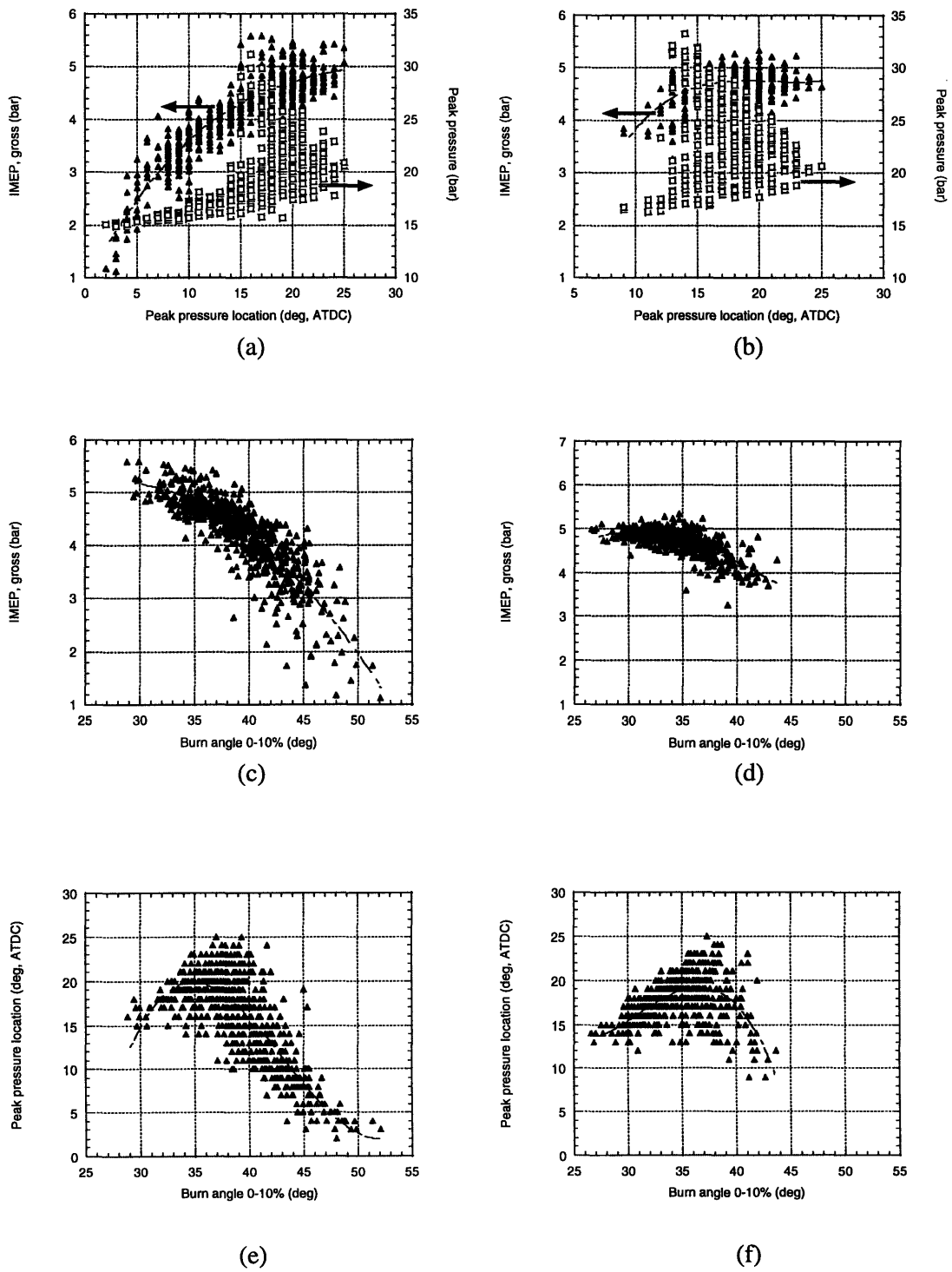
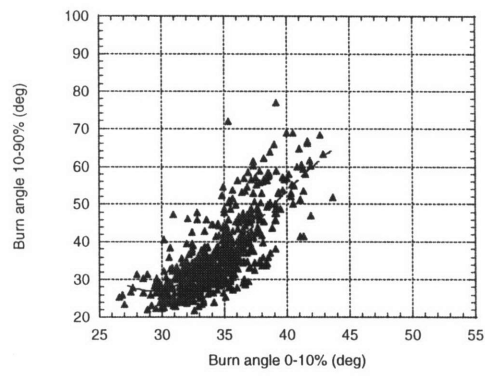
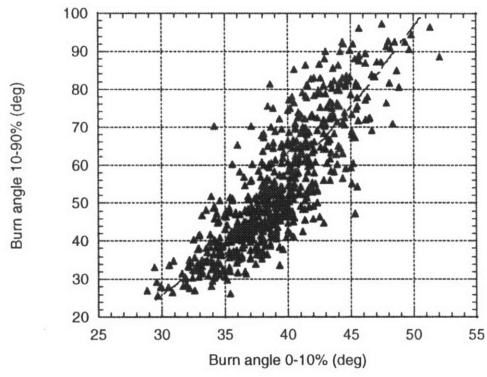


Figure 4.19 Engine performance comparison at lean burn operation.
 1000 rpm, $\lambda=1.55$, spark timing=35 deg BTDC, part throttle

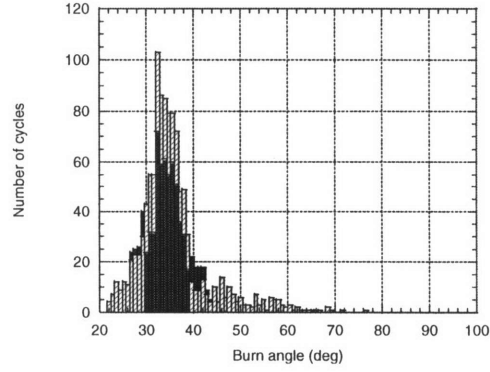
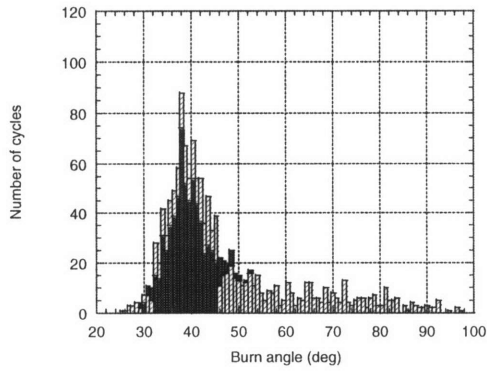
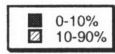
Homogeneous Mixture

Stratified Mixture



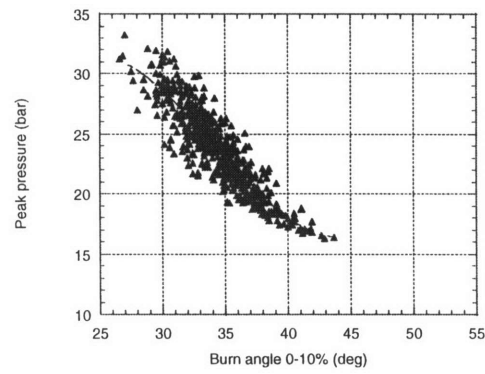
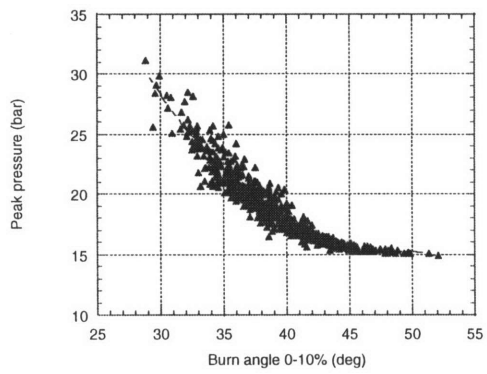
(g)

(h)



(i)

(j)



(k)

(l)

Figure 4.19 Engine performance comparison at lean burn operation. 1000 rpm, $\lambda=1.55$, spark timing=35 deg BTDC, part throttle

Homogeneous mixture

Stratified mixture

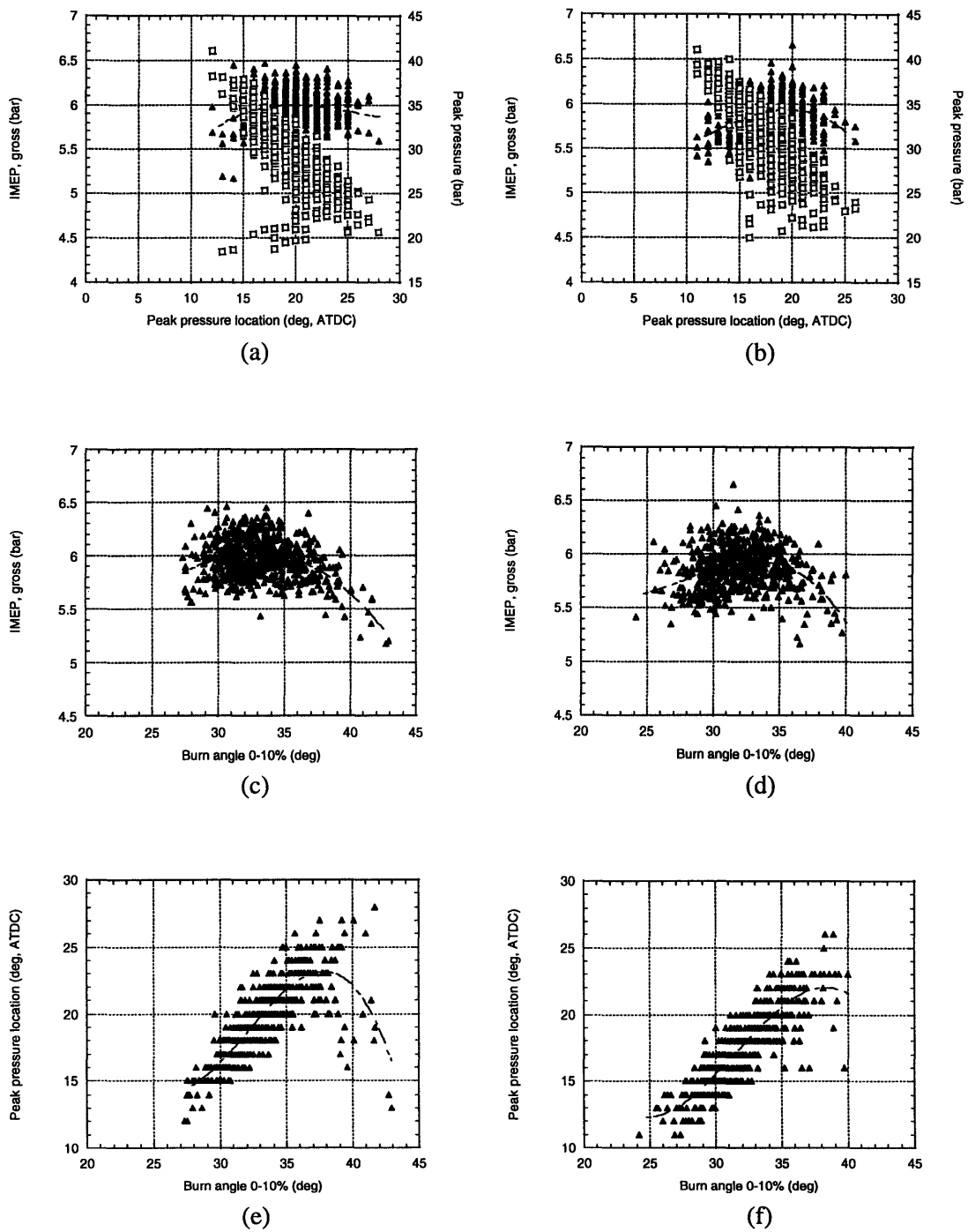


Figure 4.20 Engine performance comparison at lean burn operation.
1000 rpm, $\lambda = 1.5$, spark timing=35 deg BTDC, WOT

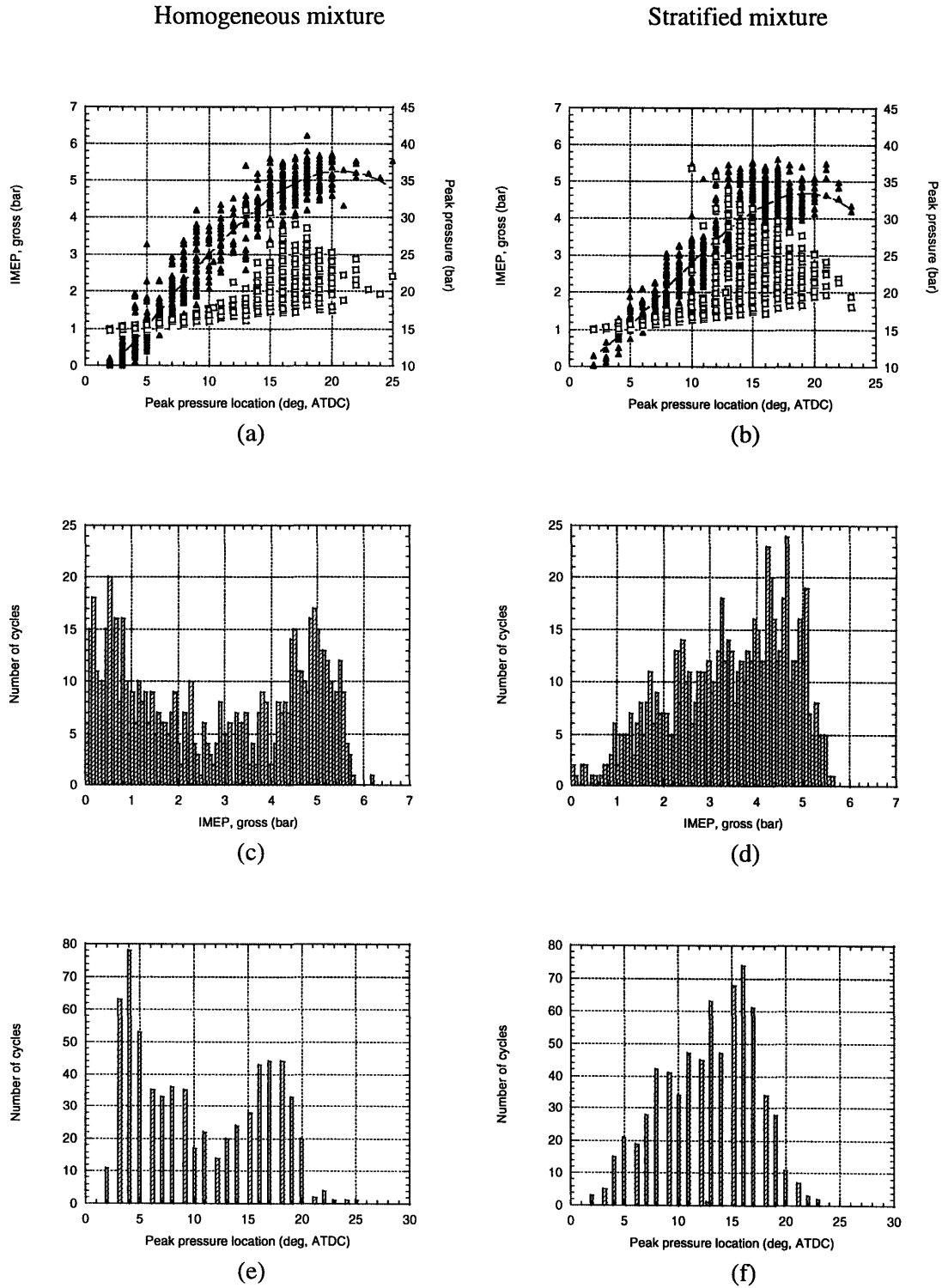


Figure 4.21 Engine performance comparison at EGR operation.
 1000 rpm, $\lambda = 1$, EGR ratio=38 %, spark timing =50 deg BTDC, part throttle

Homogeneous mixture

Stratified mixture

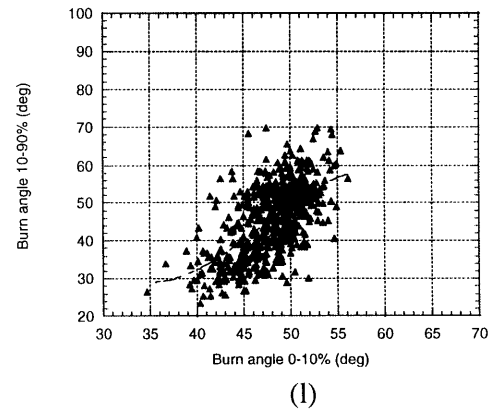
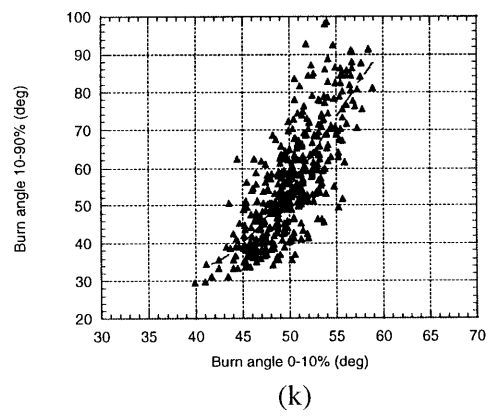
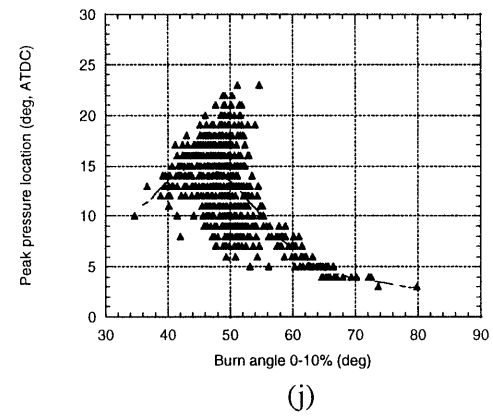
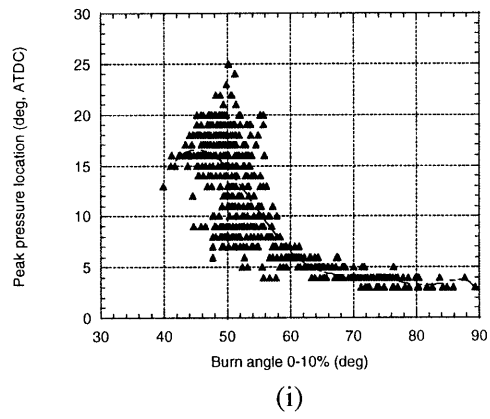
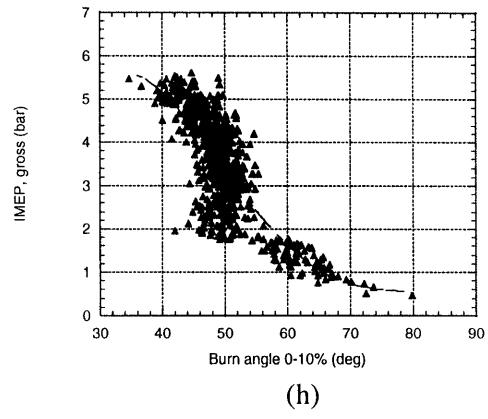
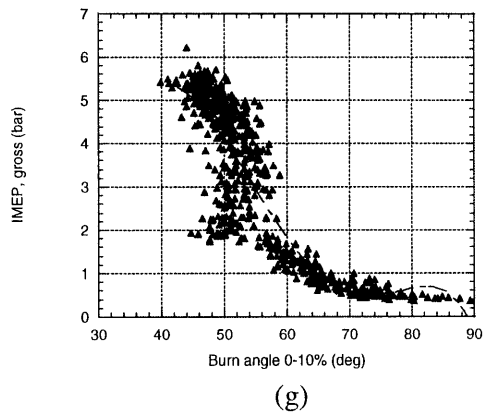
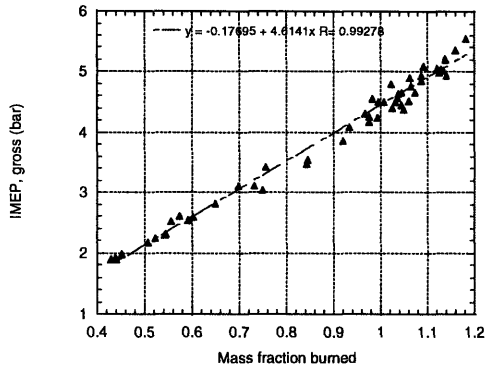


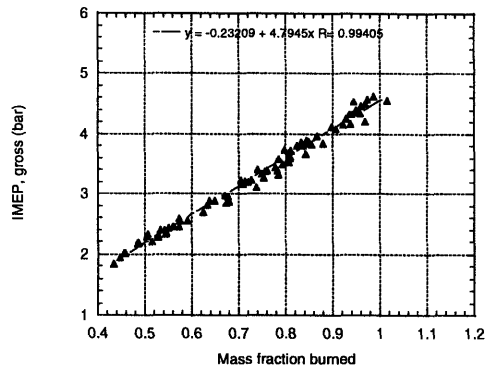
Figure 4.21 Engine performance comparison at EGR operation.
 1000 rpm, $\lambda=1$, EGR ratio=38 %, spark timing=50 deg BTDC, part throttle

Homogeneous mixture

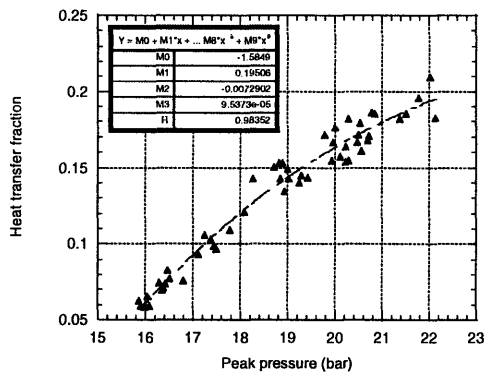
Stratified mixture



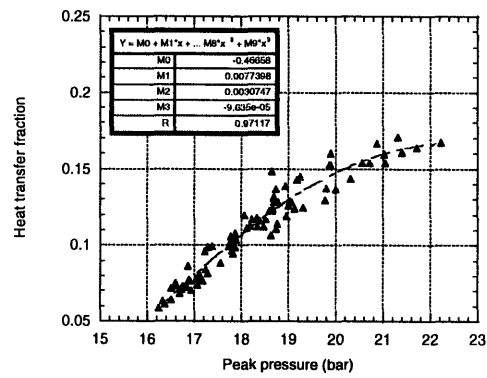
(a)



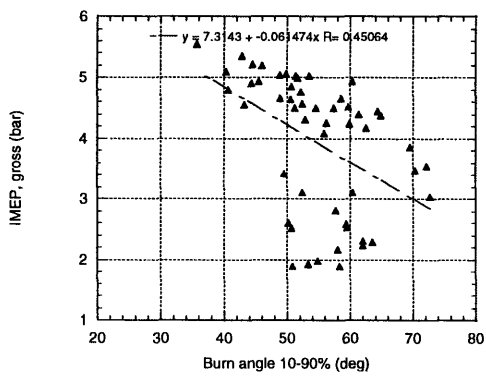
(b)



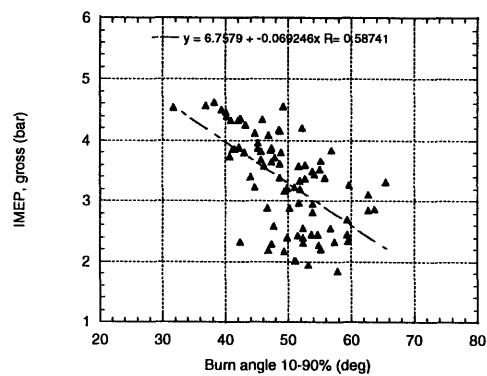
(c)



(d)



(e)



(f)

Figure 4.22 Combustion properties of cycles of the same 50 deg cycles of $\theta_{0-10\%}$.
1000 RPM, $\lambda=1$, EGR ratio=38%, spark timing=50 deg BTDC, part throttle

Homogeneous mixture

Stratified mixture

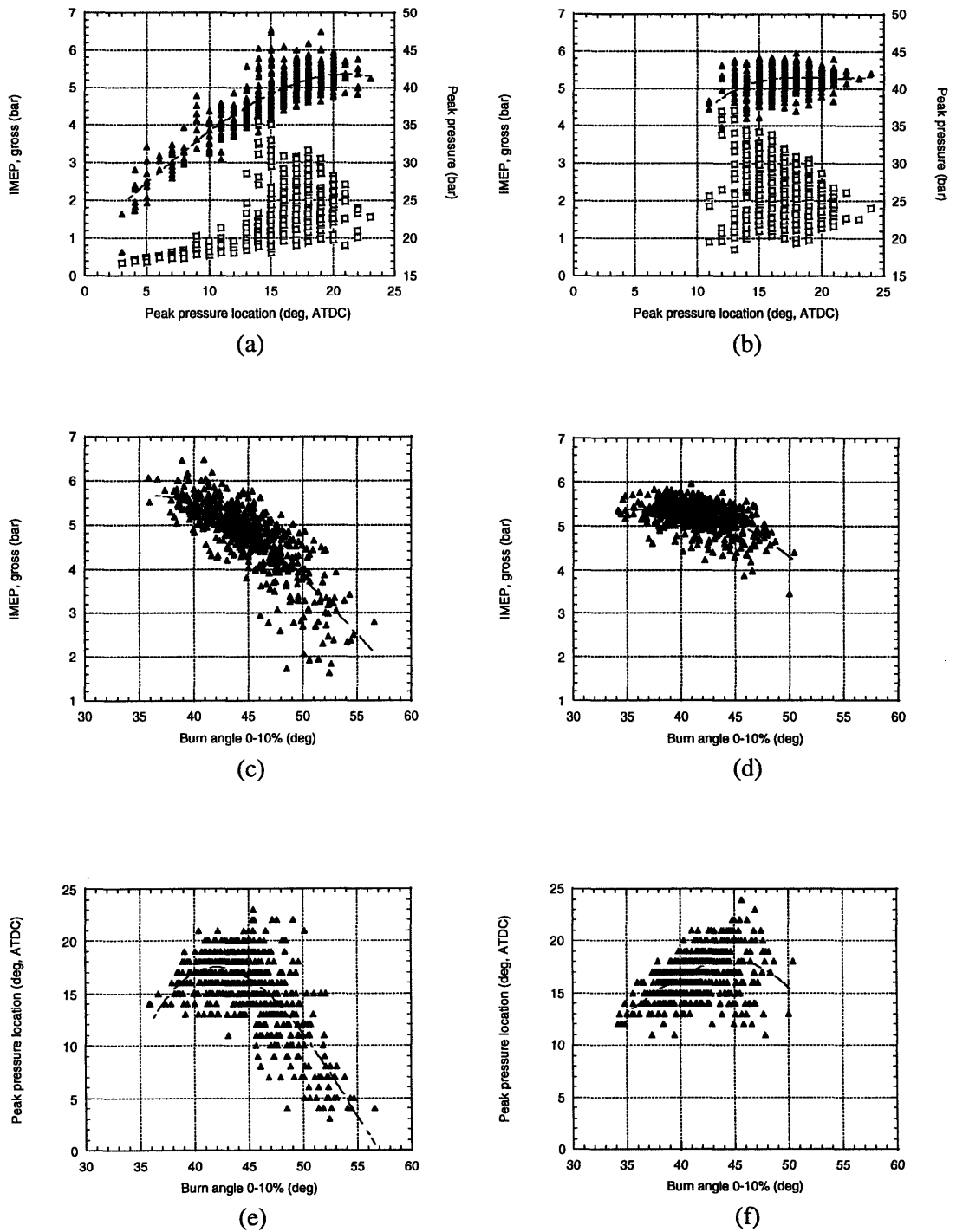
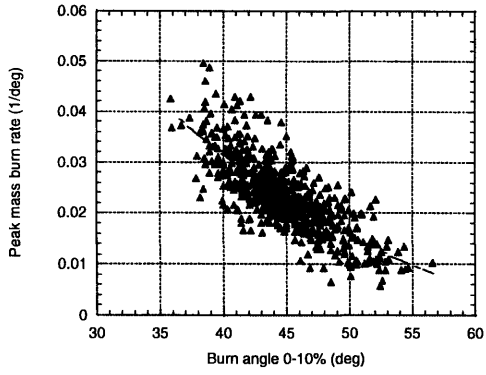


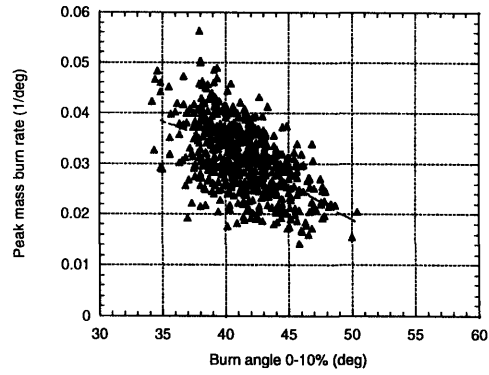
Figure 4.23 Engine performance comparison at EGR operation.
 1000 rpm, $\lambda = 1$, EGR ratio = 31 %, spark timing = 45 deg BTDC, WOT

Homogeneous mixture

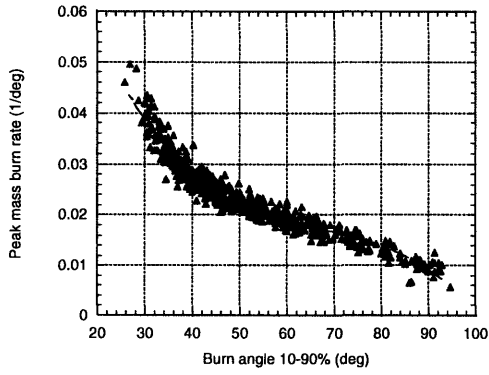
Stratified mixture



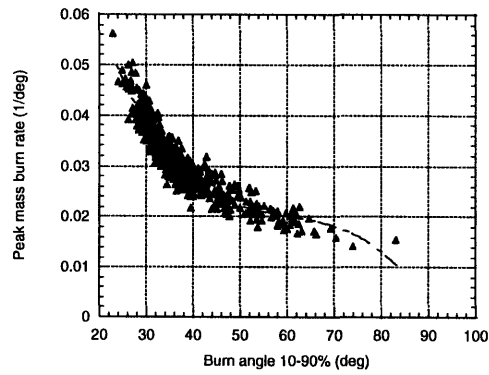
(g)



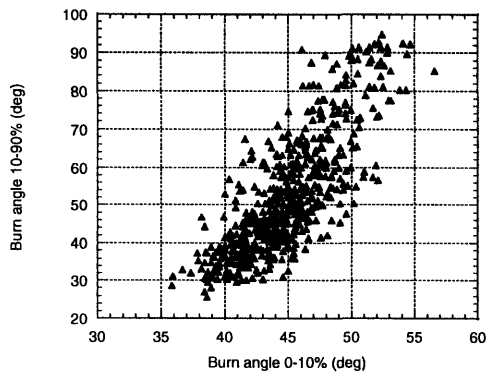
(h)



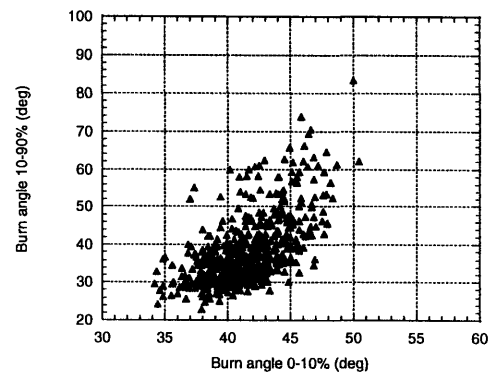
(i)



(j)



(k)

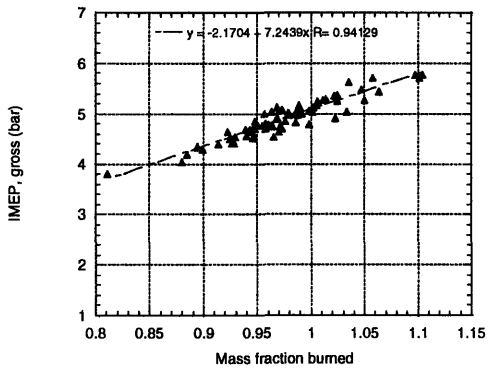


(l)

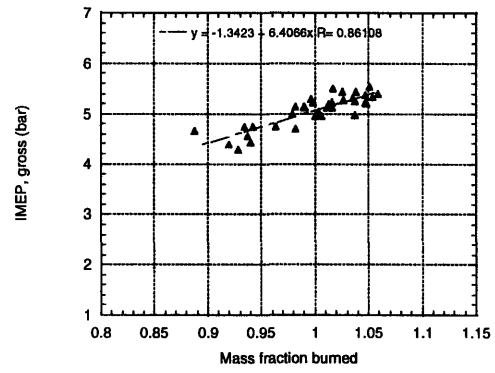
Figure 4.23 Engine performance comparison at EGR operation.
1000 rpm, $\lambda=1$, EGR ratio = 31 %, spark timing = 45 deg BTDC, WOT

Homogeneous mixture

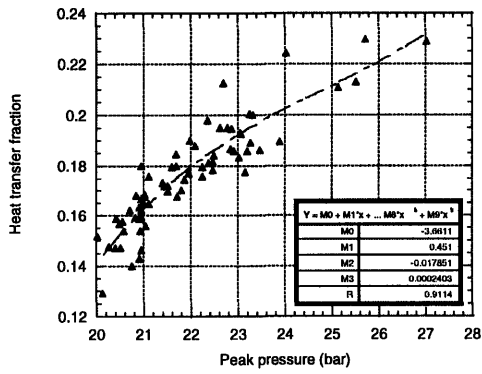
Stratified mixture



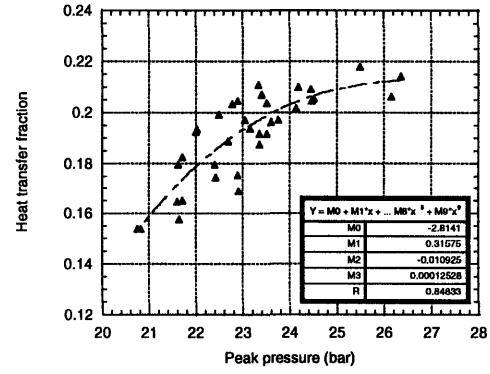
(a)



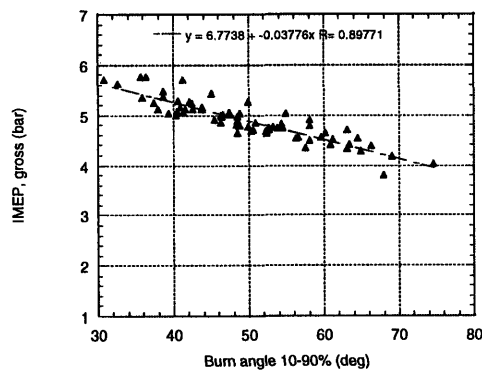
(b)



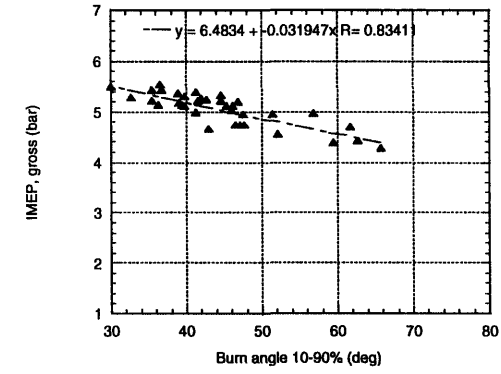
(c)



(d)



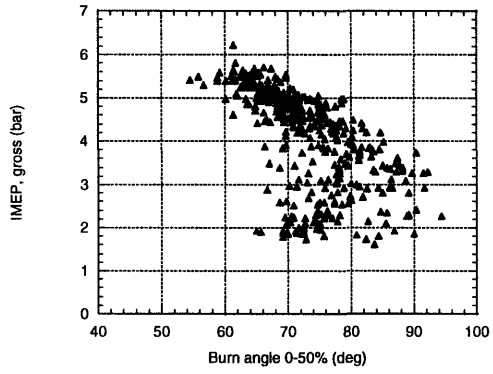
(e)



(f)

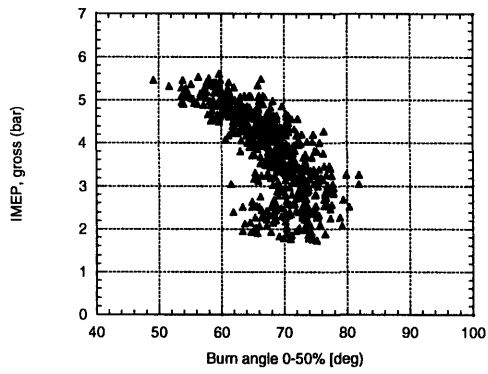
Figure 4.24 Combustion properties of cycles of the same 45 deg of $\theta_{0-10\%}$.
1000 RPM, $\lambda=1$, EGR ratio=31%, spark timing = 45 deg BTDC, WOT

Homogeneous mixture

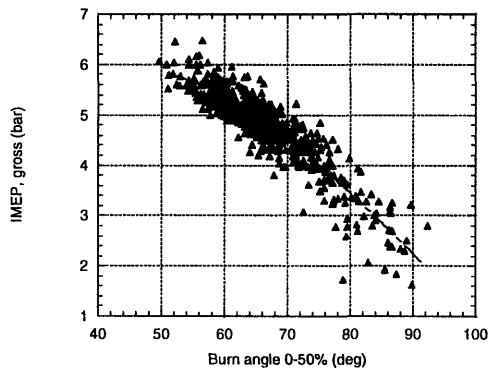


(a)

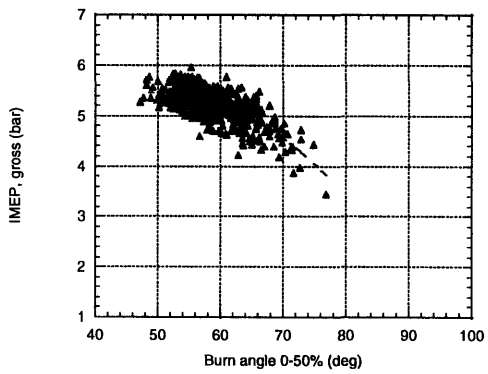
Stratified mixture



(b)

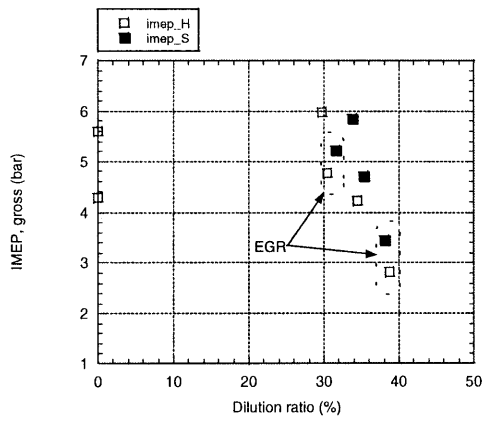


(c)

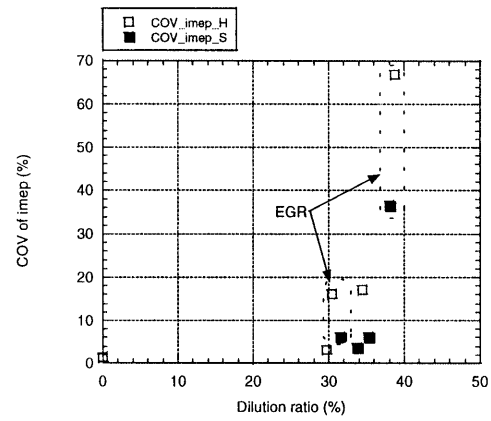


(d)

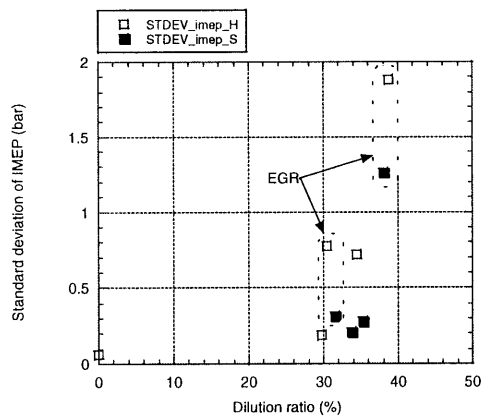
Figure 4.25 The comparison of IMEP as a function of $\theta_{0-50\%}$
1000 rpm, $\lambda=1$, (a), (b) : 38 % EGR ratio, 50 deg BTDC, (c), (d) : 31 % EGR, 45 deg BTDC



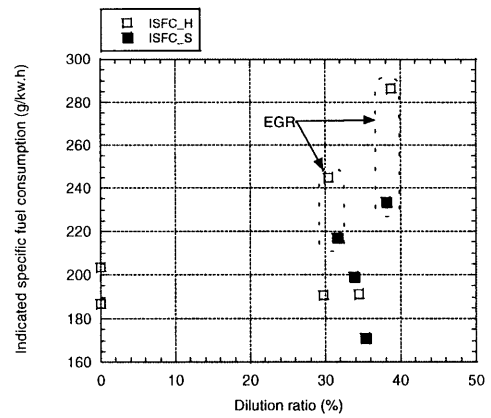
(a)



(b)



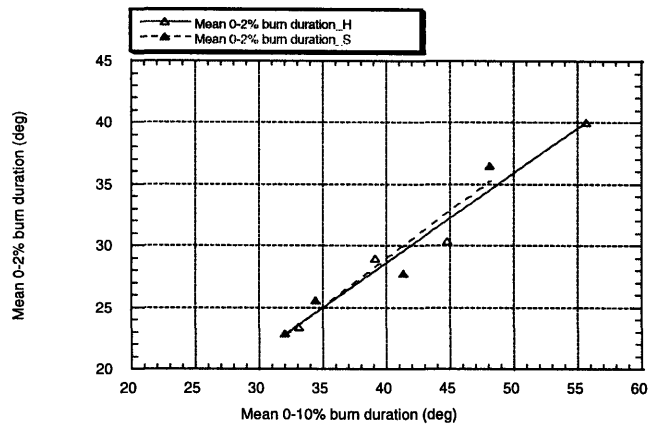
(c)



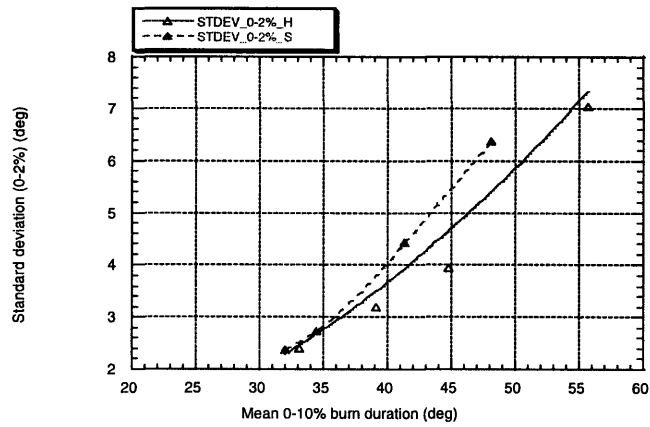
(d)

Figure 4.26 Performance comparison between the homogeneous mixture and the stratified mixture including the lean burn and EGR burn.

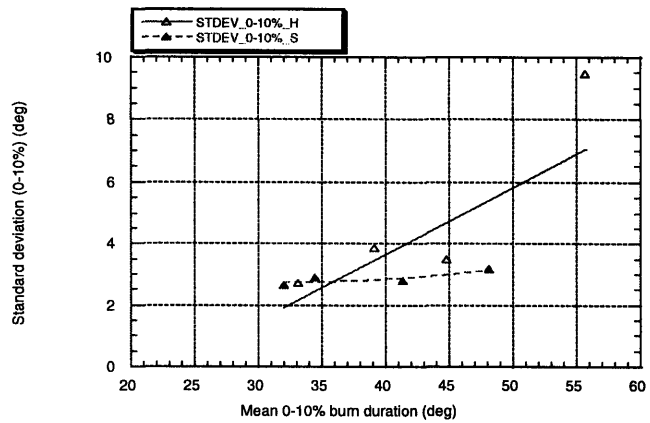
- (a) IMEP vs. dilution ratio
- (b) COV of IMEP vs. dilution ratio
- (c) σ_{imep} vs. dilution ratio
- (d) ISFC vs. dilution ratio



(a)

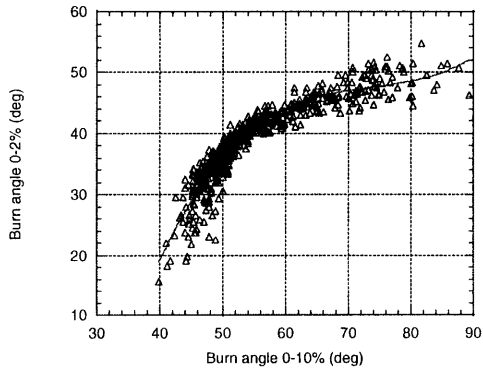


(b)

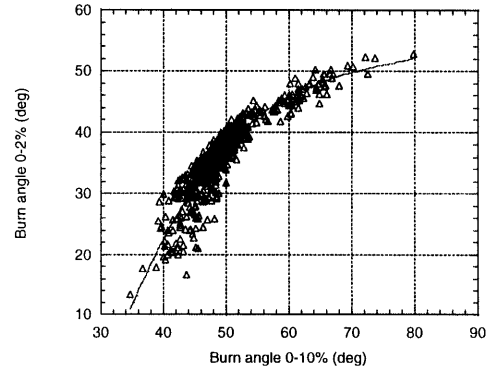


(c)

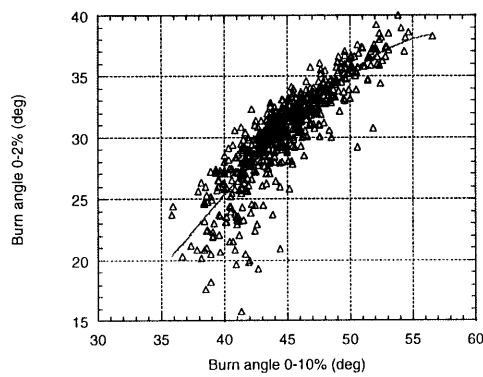
Figure 4.27 Effect of stratification strategy on variations in flame initiation $\theta_{0-2\%}$ and development angle $\theta_{0-10\%}$. Comparison between the homogeneous mixture and the stratified mixture in average value.



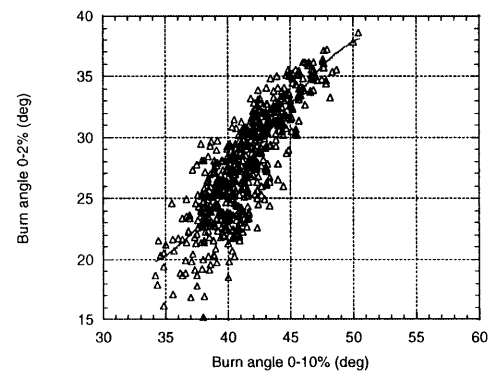
(a) EGR part (homogeneous)



(b) EGR part (stratified)

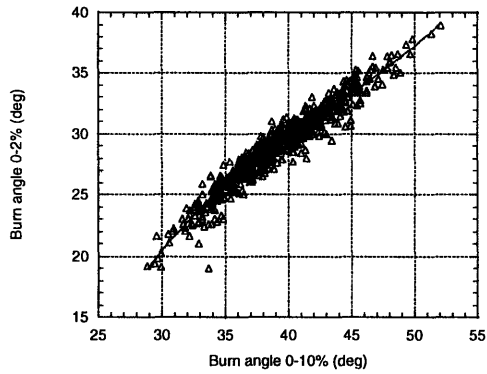


(c) EGR WOT (homogeneous)

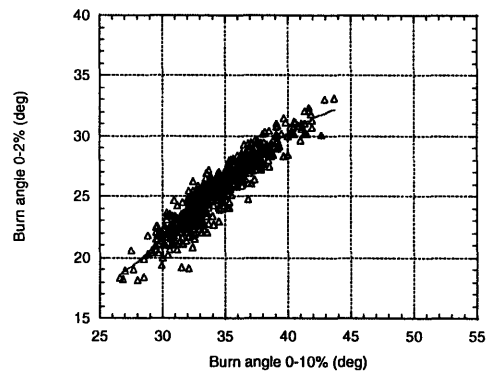


(d) EGR WOT (stratified)

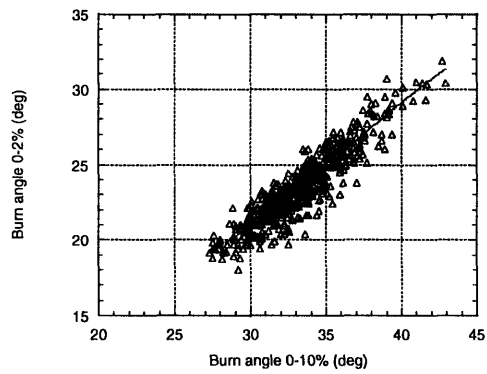
Figure 4.28 Effect of stratification strategy on variations in flame initiation $\theta_{0-2\%}$ and development angle $\theta_{0-10\%}$. Comparison between the homogeneous mixture and the stratified mixture in detail



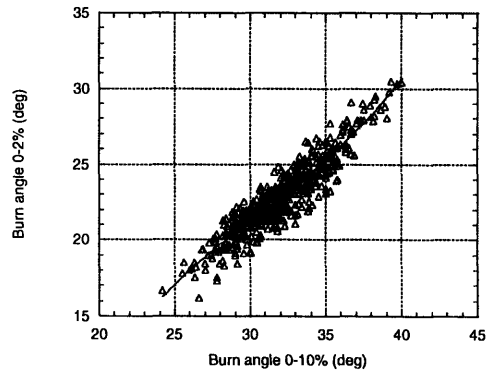
(e) Lean burn part (homogeneous)



(f) Lean burn part (stratified)

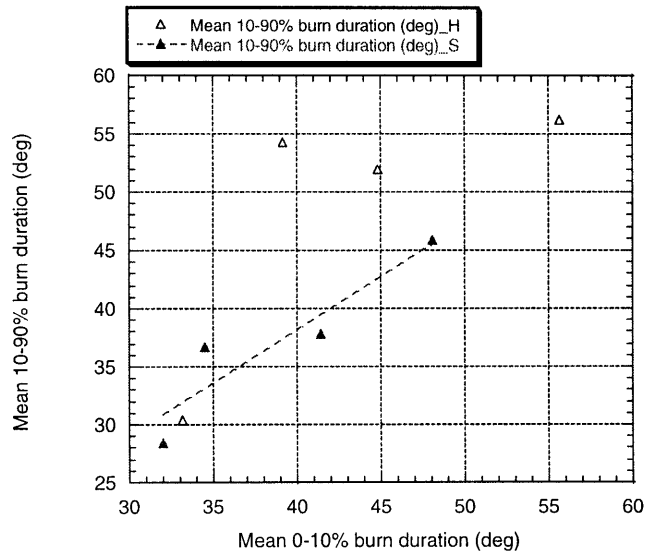


(g) Lean burn WOT (homogeneous)

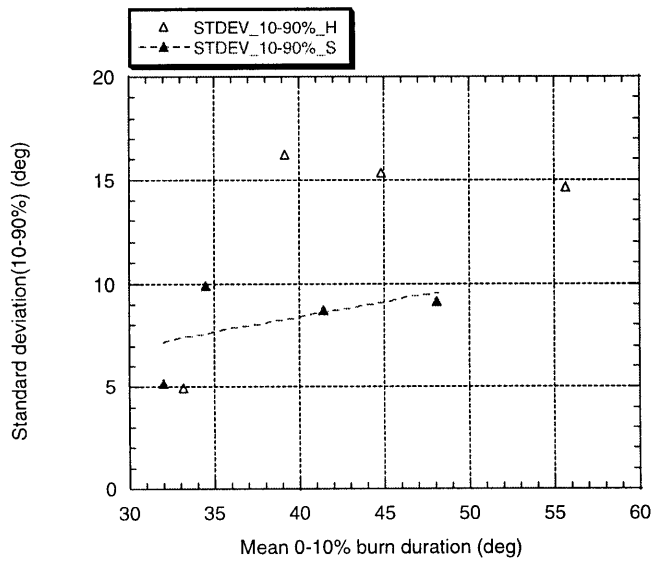


(h) Lean burn WOT

Figure 4.28 Effect of stratification strategy on variations in flame initiation $\theta_{0-2\%}$ and development angle $\theta_{0-10\%}$. Comparison between the homogeneous mixture and the stratified mixture in detail

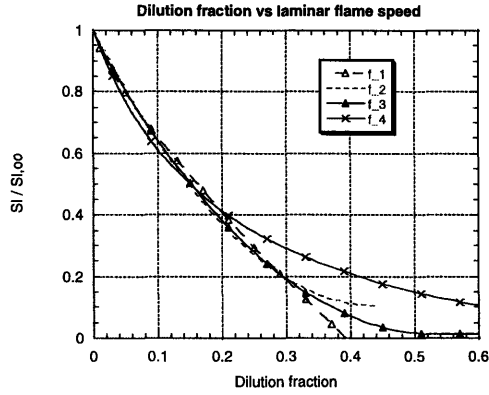


(a)



(b)

Figure 4.29 Effect of stratification strategy on variations in flame development angle $\theta_{10-90\%}$. Comparison between the homogeneous mixture and the stratified mixture in average value.



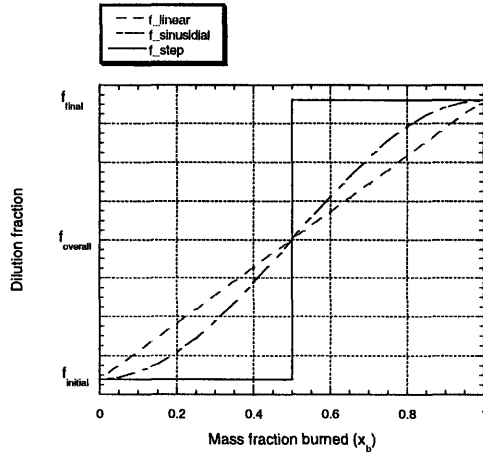
$$f_{-1} = 1 - 2.06f^{0.773}; \quad [28]$$

$$f_{-2} = 1 - 4.1f + 4.7f^2; \quad [29]$$

$$f_{-3} = \frac{1}{3}(1 - 2.06f^{0.773}) + \frac{2}{3}(1 - 4.1f + 4.7f^2); \text{ used for prediction}$$

$$f_{-4} = 1 - \frac{1.03f}{1.03 - 0.85(1 - f)}; \quad [36]$$

Figure 5.1 Fractional reduction in laminar flame speed as a function of EGR fraction.

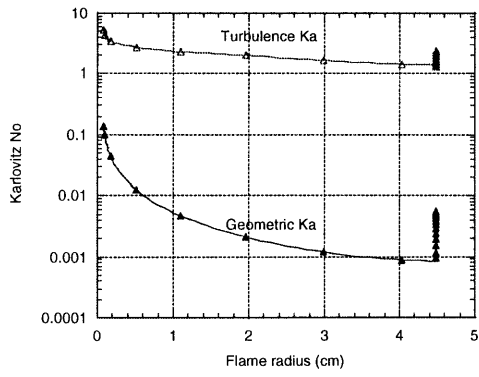


$$f_{-linear} = (f_{final} - f_{initial}) \cdot x_b + f_{initial}$$

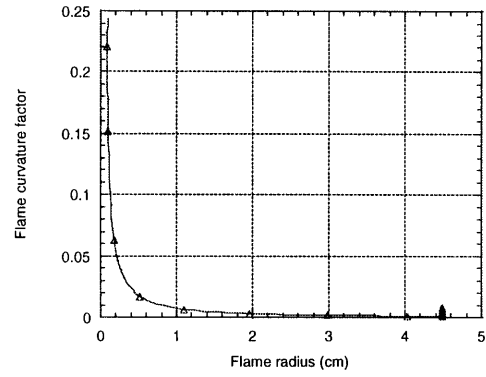
$$f_{-sinusoidal} = (f_{final} - f_{initial}) \cdot \sin(\pi(x_b - 0.5)) + f_{initial}$$

$$f_{-step} = \begin{cases} f_{initial} & x_b < 0.5 \\ f_{overall} & x_b = 0.5 \\ f_{final} & x_b > 0.5 \end{cases}, \quad f_{overall} = \frac{f_{initial} + f_{final}}{2}$$

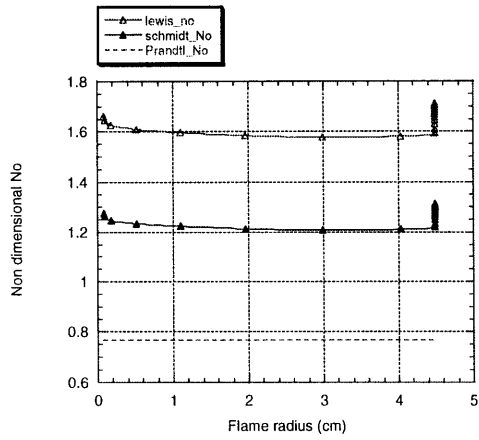
Figure 5.2 The comparison of the mixing function; linear mixing, sinusoidal mixing, step mixing



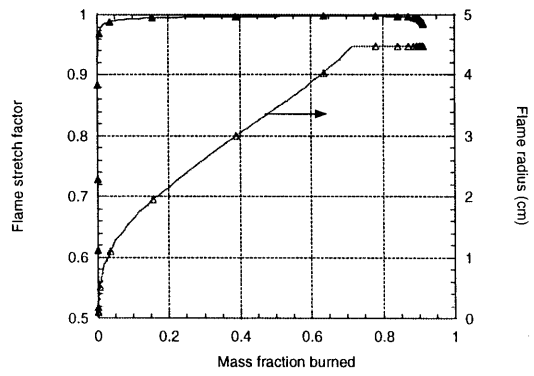
(a)



(b)

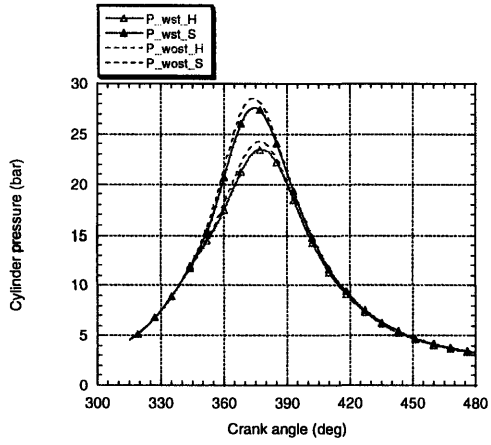


(c)

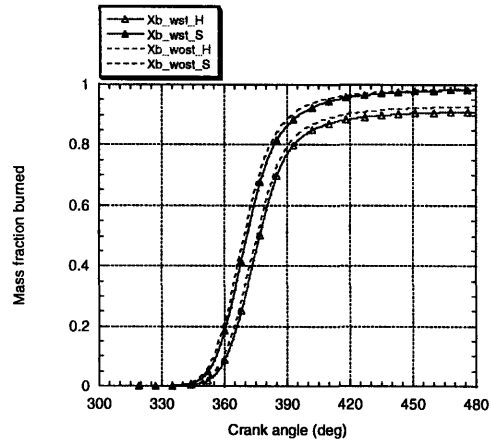


(d)

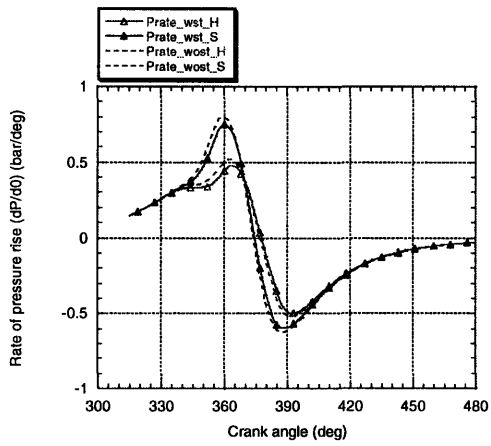
Figure 5.3 Non dimensional parameters affecting on the flame stretch factor.
 $\lambda=1$, EGR ratio = 31%, spark timing = 45 deg BTDC, homogeneous mixture



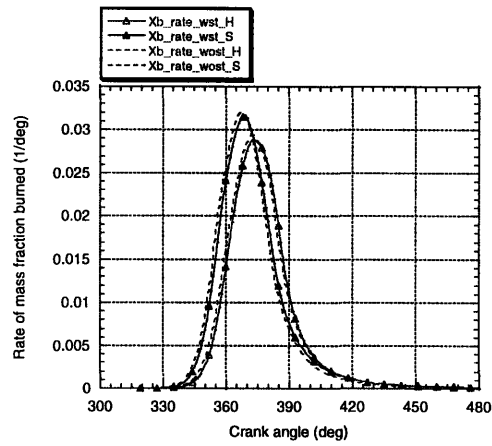
(a)



(b)

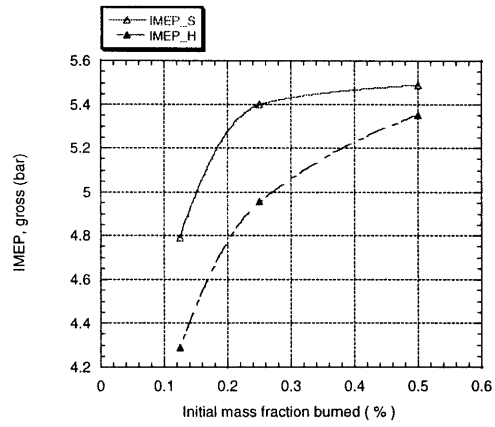


(c)

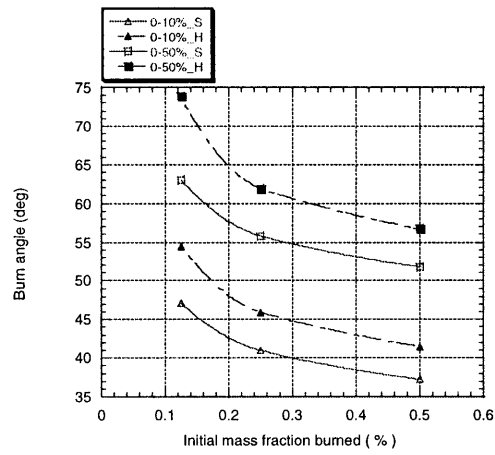


(d)

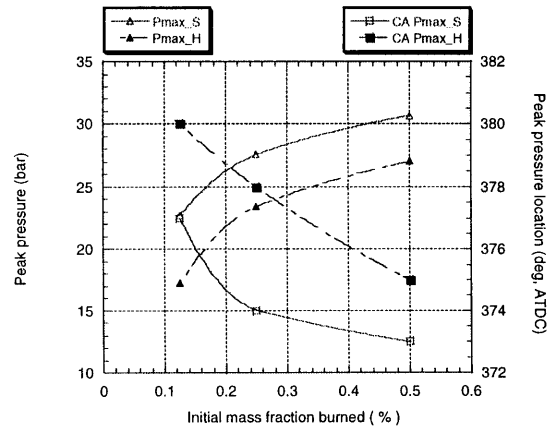
Figure 5.4 The effect of flame stretch factor on combustion.
 $\lambda = 1$, EGR ratio = 31%, spark timing = 45 deg BTDC



(a)



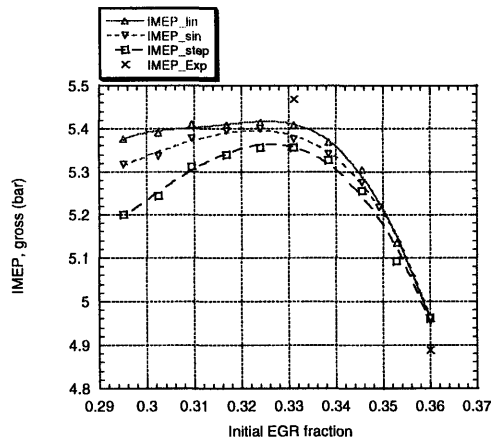
(b)



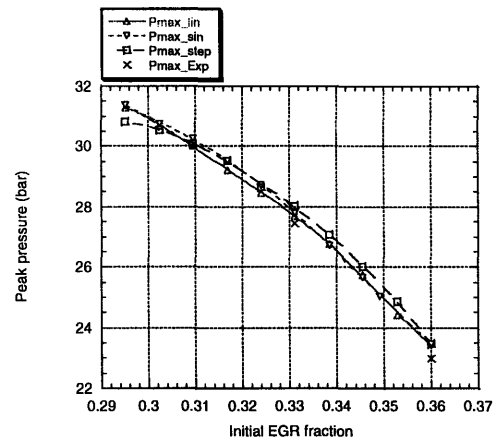
(c)

Figure 5.5

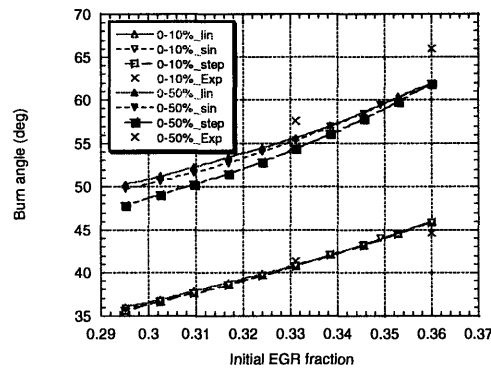
The effect of initial mass fraction burned on combustion.
 $\lambda = 1$, EGR ratio = 31%, Spark timing = 45 deg BTDC



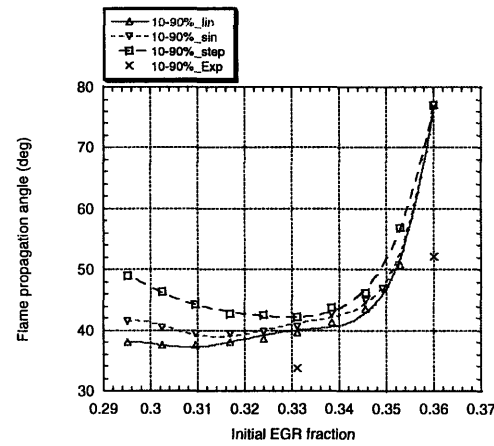
(a)



(b)

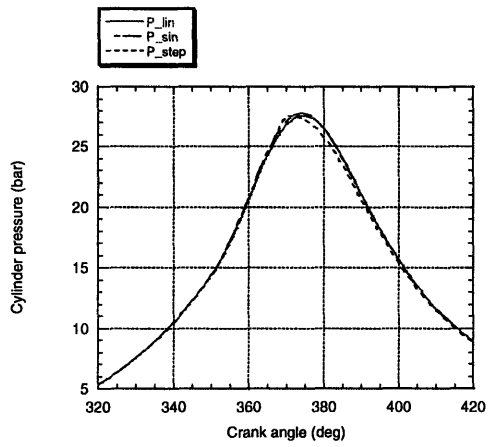


(c)

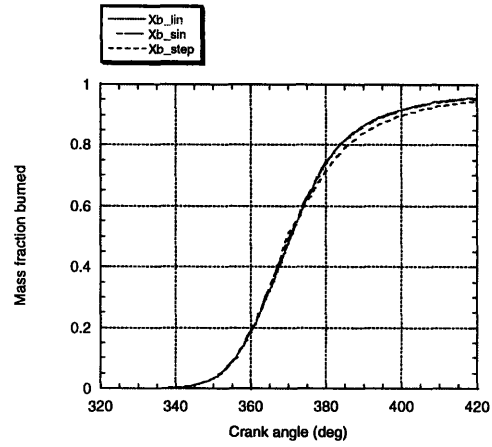


(d)

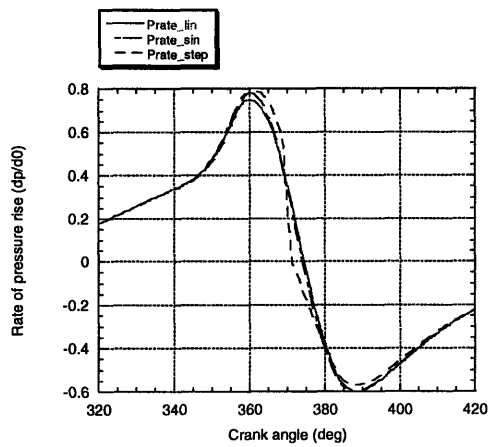
Figure 5.6 Computed engine performance as a function of initial residual fraction with the different mixing functions. $\lambda=1$, EGR in overall = 36. %, external EGR supplied = 31 %, spark timing = 45 deg BTDC, WOT



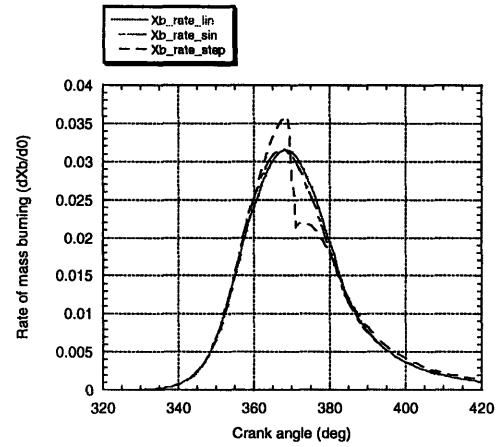
(a)



(b)

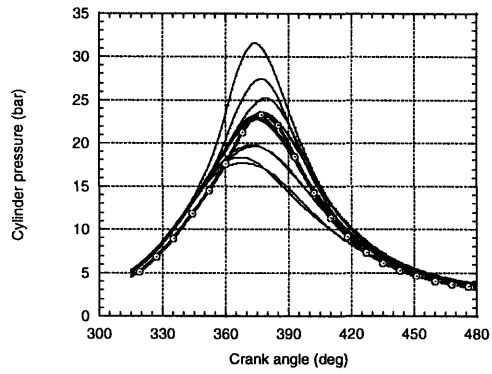


(c)

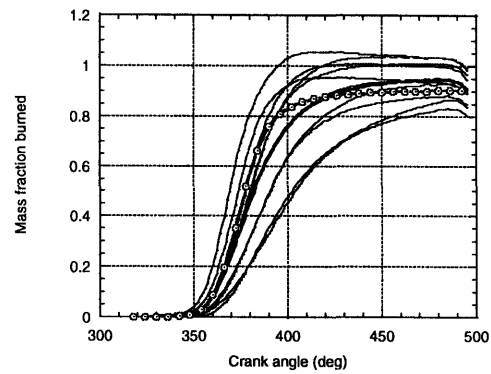


(d)

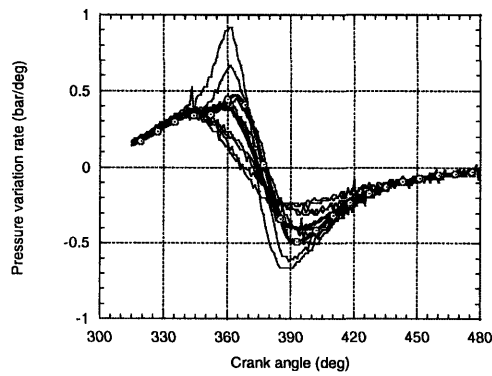
Figure 5.7 The effect of mixing function on combustion parameters. $\lambda=1$, Initial EGR gas fraction = 0.33, Overall EGR gas fraction = 0.36, spark timing = 45 deg BTDC.



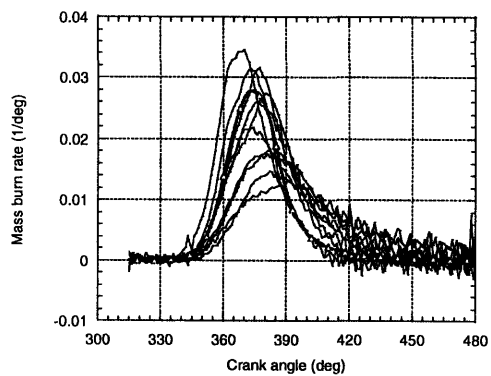
(a)



(b)



(c)



(d)

Figure 5.8 Engine performance comparison with the homogeneous mixture. Marked line for the simulation result of linear mixing model. $\lambda=1$, Initial EGR gas fraction=0.33, Overall EGR gas fraction=0.36, spark timing=45 deg BTDC.

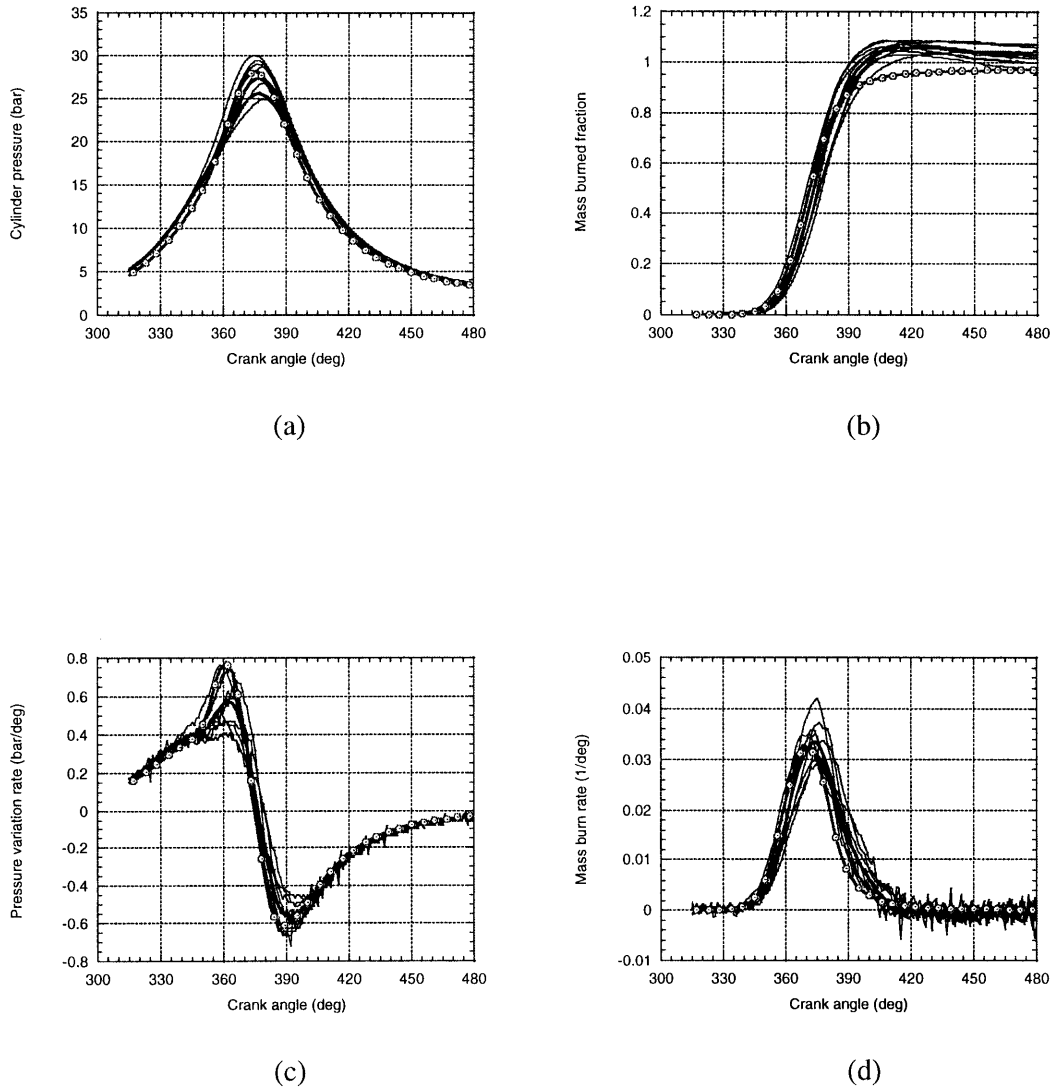
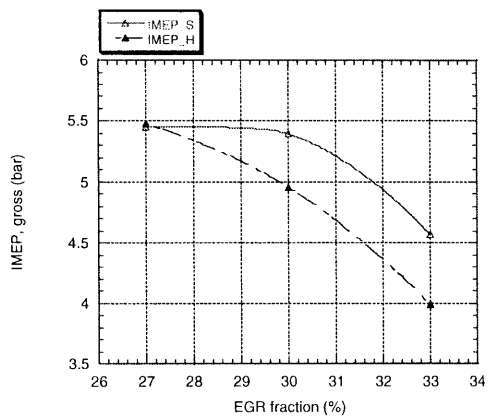
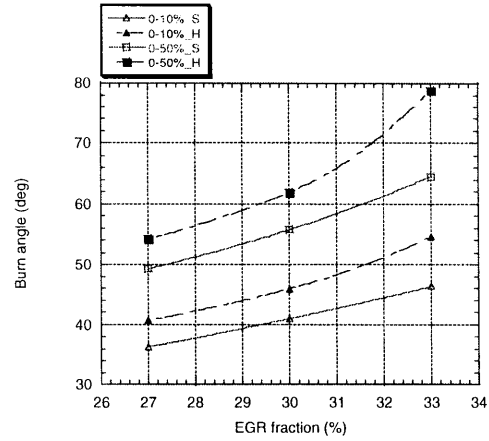


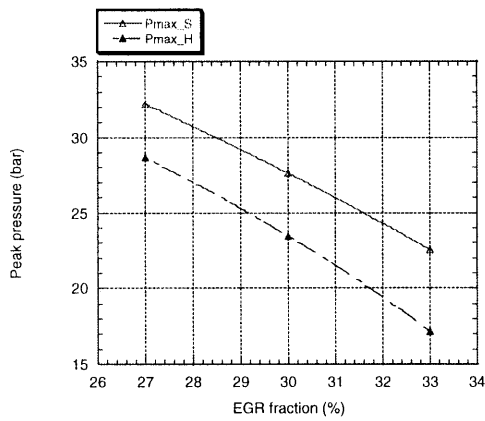
Figure 5.9 Engine performance comparison with the stratified mixture. Marked line for the simulation result of linear mixing model. $\lambda=1$, Initial EGR gas fraction = 0.33, Overall EGR gas fraction = 0.36, spark timing = 45 deg BTDC.



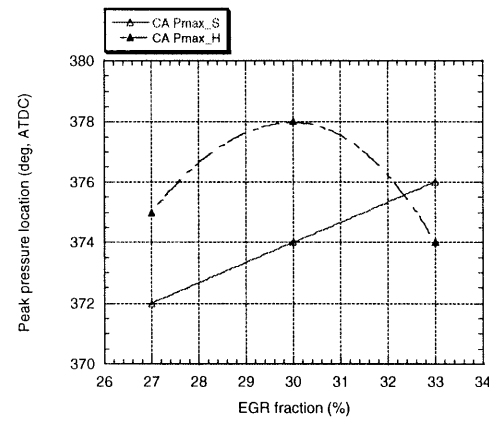
(a)



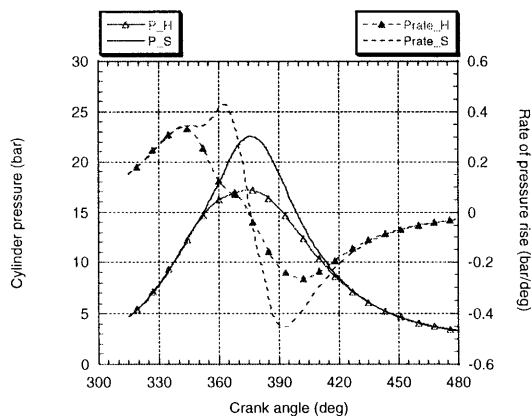
(b)



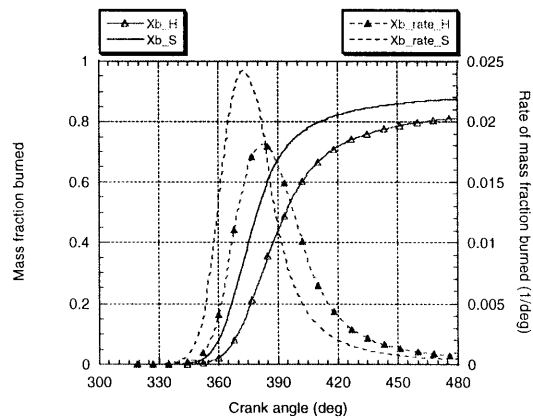
(c)



(d)

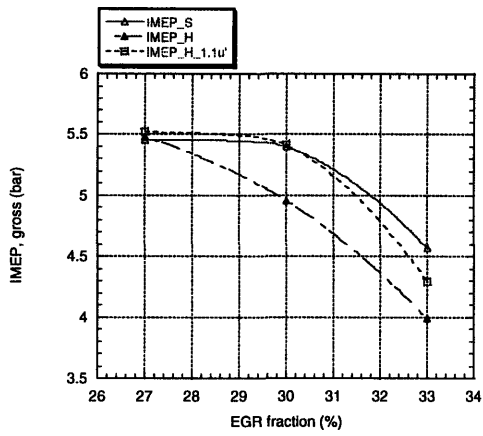


(e) 33% EGR

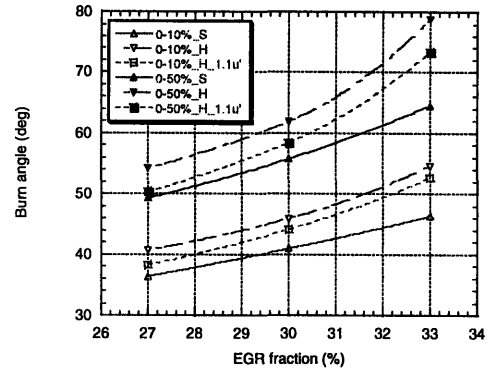


(f) 33% EGR

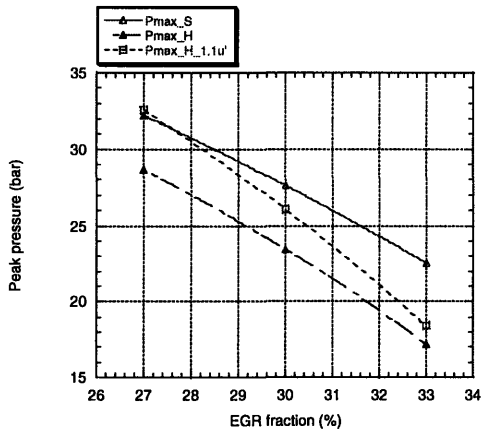
Figure 5.10 The effect of EGR fraction on engine performance. Engine performance variation as a function of EGR fraction. 1000 rpm, $\lambda = 1$, spark timing = 45 deg BTDC.



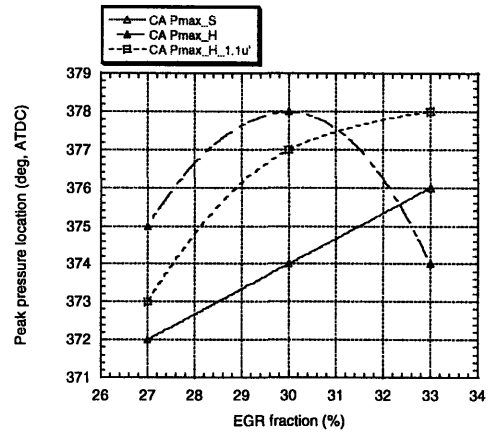
(a)



(b)

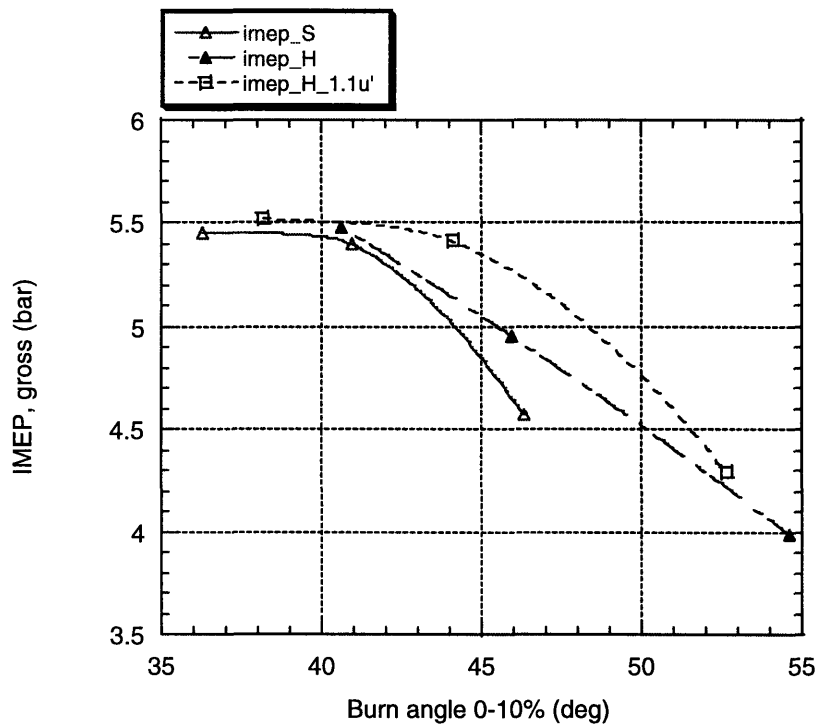


(c)



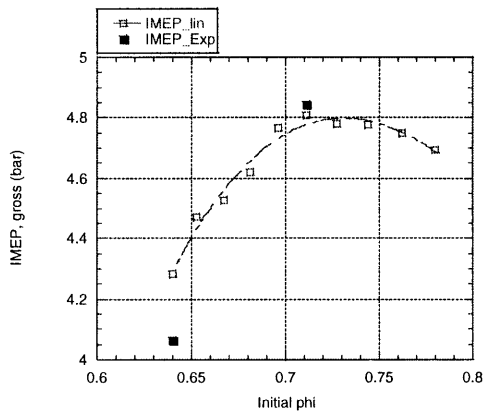
(d)

Figure 5.11 The engine performance comparison between mixture stratification and turbulence enhancement as a function of EGR fraction. 1000 rpm, $\lambda=1$, spark timing = 45 deg BTDC.

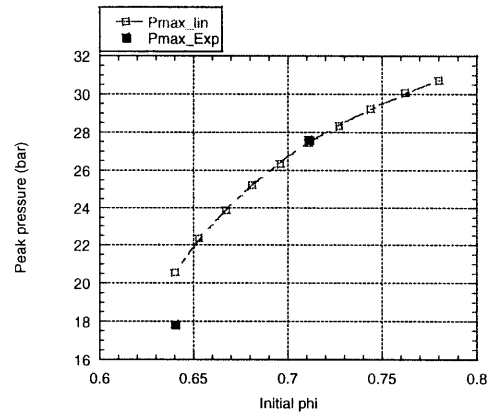


(g)

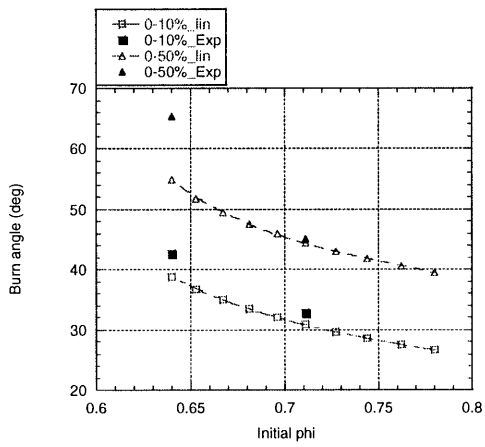
Figure 5.11 The engine performance comparison between mixture stratification and turbulence enhancement as a function of EGR fraction. 1000 rpm, $\lambda=1$, spark timing = 45 deg BTDC.



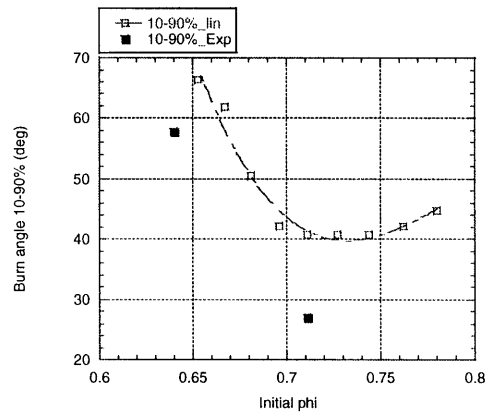
(a)



(b)

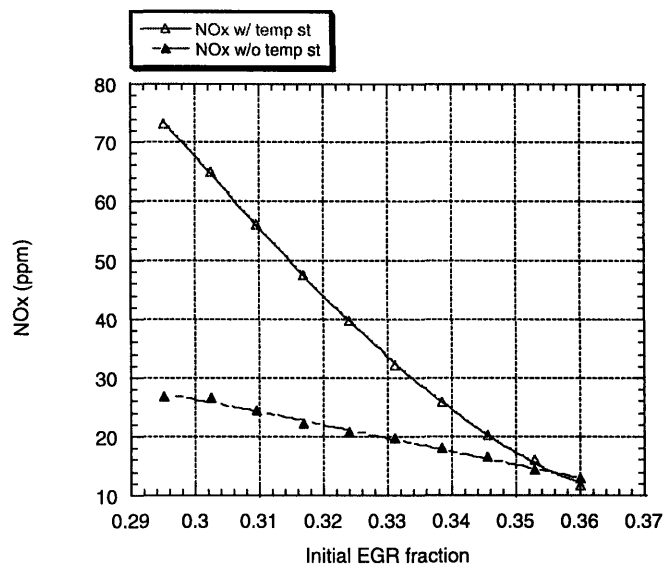


(c)

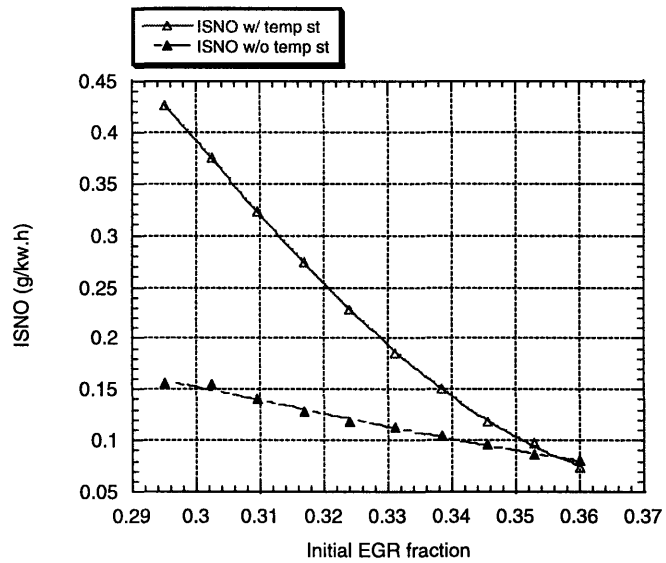


(d)

Figure 5.12 Computed engine performance as a function of initial fuel/air ratio. 1000 rpm, $\phi = 0.64$ ($\lambda = 1.56$) in overall, spark timing = 35 deg BTDC

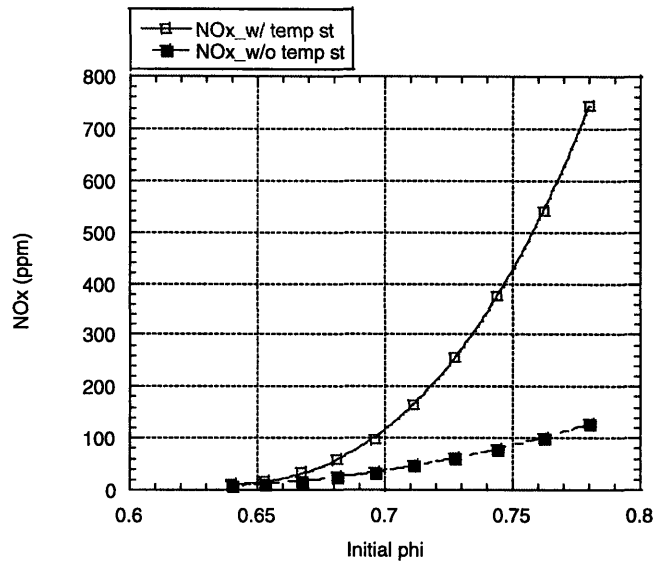


(a)

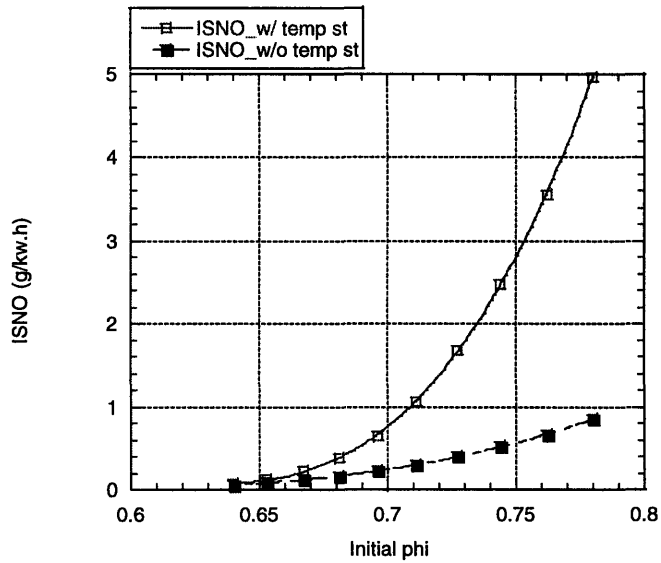


(b)

Figure 5.13 The effect of stratification of unburned gas mixture and burned gas temperature on NOx formation at EGR mixture. 1000 rpm, $\lambda = 1$, EGR ratio = 30%, spark timing = 45 deg BTDC.

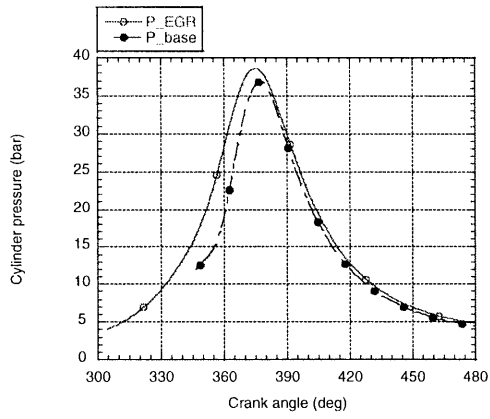


(a)

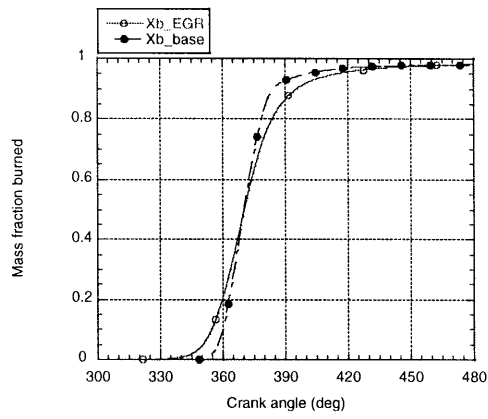


(b)

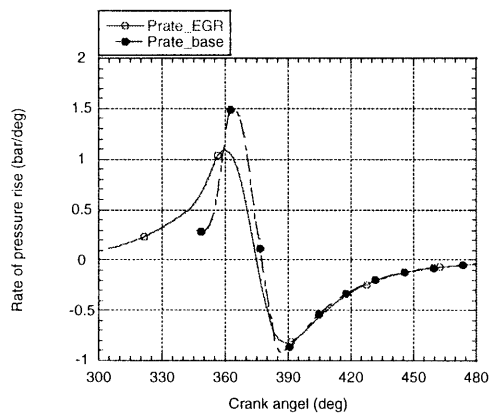
Figure 5.14 The effect of stratification of unburned gas mixture and burned gas temperature on NO_x formation at lean mixture. 1000 rpm, $\phi=0.64(\lambda=1.56)$ in overall, spark timing=35 deg BTDC



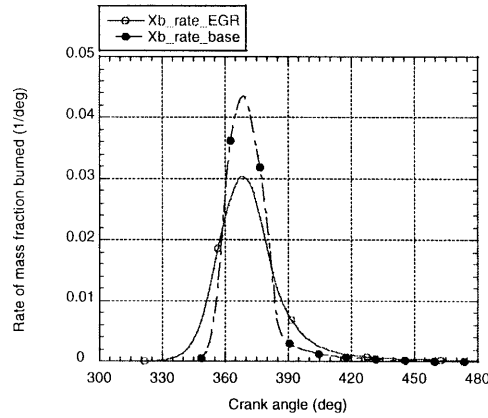
(a)



(b)



(c)



(d)

Figure 5.15 Comparison of combustion performance between with EGR and without EGR operation at constant BMEP. WOT for 30 % EGR and intake pressure = 0.79 bar for base w/o EGR. BMEP=695.5 Kpa, MBT spark timing, $\lambda=1$, 10% stratification effect of overall residual fraction with linear mixing model.

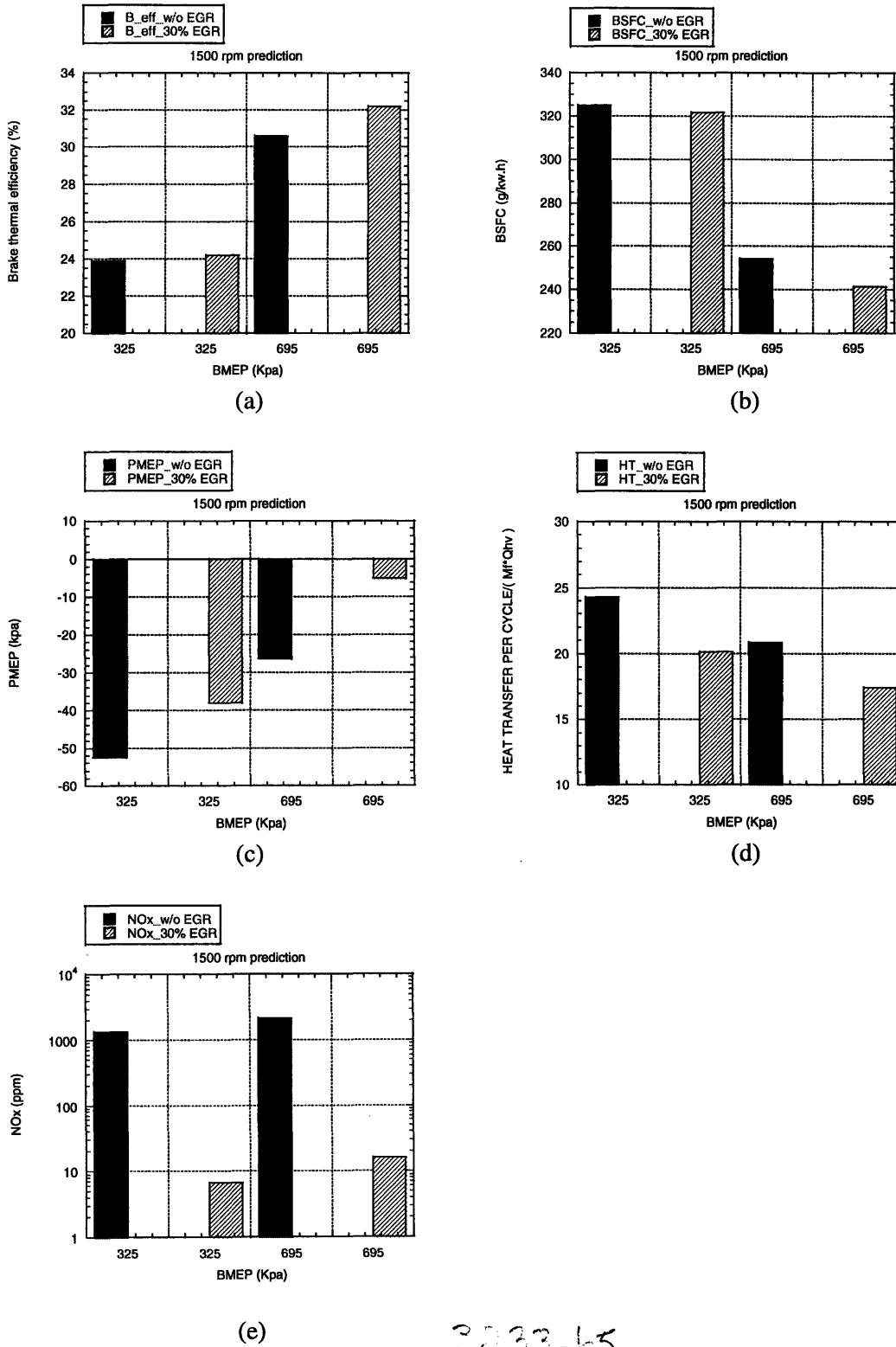


Figure 5.16 Engine performance improvement with the stratification strategy. 1500 rpm, MBT, $\lambda=1$, 10% stratification effect of overall residual fraction with linear mixing model